JANUARY 2020 Ph.D in Physics Engineering REYYAN KAVAK YÜRÜK

REPUBLIC OF TURKEY

GAZİANTEP UNIVERSITY

GRADUATE SCHOOL OF NATURAL & APPLIED SCIENCES

INVESTIGATION OF FACTORS INFLUENCING THE EFFICIENCY OF NUCLEAR BATTERIES

Ph.D THESIS

IN

PHYSICS ENGINEERING

BY

REYYAN KAVAK YÜRÜK

JANUARY 2020

INVESTIGATION OF FACTORS INFLUENCING THE EFFICIENCY OF NUCLEAR BATTERIES

Ph.D. Thesis

in

Physics Engineering

Gaziantep University

Supervisor

Prof. Dr. Hayriye TÜTÜNCÜLER

by

Reyyan KAVAK YÜRÜK

January 2020

©2020 [Reyyan KAVAK YÜRÜK]

REPUBLIC OF TURKEY
GAZİANTEP UNIVERSITY
GRADUATE SCHOOL OF NATURAL & APPLIED SCIENCES
PHYSICS ENGINEERING

Name of the Thesis : Investigation of Factors Influencing the Efficiency of Nuclear Batteries

Name of the Student : Reyyan KAVAK YÜRÜK

Exam Date : 17.01.2020

Approval of the Graduate School of Natural and Applied Sciences

Prof. Dr. A. Necmeddin YAZICI
Director

I certify that this thesis satisfies all the requirements as a thesis for the degree of Doctor of Philosophy.

Prof. Dr. Ramazan KOÇ
Head of Department

This is to certify that we have read this thesis and that in our consensus/majority opinion it is fully adequate, in scope and quality, as a thesis for the degree of Doctor of Philosophy.

Prof. Dr. Hayriye TÜTÜNCÜLER
Supervisor

Examining Committee Members:	Signature
Prof. Dr. Ramazan KOÇ	……..
Prof. Dr. Hayriye TÜTÜNCÜLER	……..
Prof. Dr. Hüseyin ZENGİN	……..
Prof. Dr. Gültekin ÇELİK	……..
Assoc. Prof. Dr. Osman Murat ÖZKENDİR	……..

I hereby declare that all information in this document has been obtained and presented in accordance with academic rules and ethical conduct. I also declare that, as required by these rules and conduct, I have fully cited and referenced all material and results that are not original to this work.

Reyyan KAVAK YÜRÜK

ABSTRACT

INVESTIGATION OF FACTORS INFLUENCING THE EFFICIENCY OF NUCLEAR BATTERIES

KAVAK YÜRÜK, Reyyan
Ph.D. in Physics Engineering
Supervisor: Prof. Dr. Hayriye TÜTÜNCÜLER
January 2020
110 pages

In this thesis, the conversion of the kinetic energy of beta particles emitted from a radioactive isotope to electricity is investigated by using the direct and indirect conversion methods. In the experimental part, analysis of the effects of low-activity radiation from Pm147 and Sr90 beta sources, two different phosphors and graphene on Si photovoltaic cell is performed. Phosphor layers with different mass thicknesses are prepared from ZnS:CuCl and $SrAl_2O_4:Eu^{2+},Dy^{3+}$ phosphor powders. The electrical performances of direct and indirect nuclear battery models are analyzed by measuring short-circuit current and open-circuit voltage. Furthermore, the time-dependent variation of the short-circuit current during the beta irradiation is researched. The most efficient battery model is determined as $Pm147/SrAl_2O_4:Eu^{2+},Dy^{3+}$/PV cell. In the theoretical part, betavoltaic battery designs are modeled using the p-n homojunctions, p-n heterojunctions, and Ni63, Pm147 beta sources by considering the parameters affecting the efficiency. A theoretical investigation of the electrical performances has been carried out on Si, GaP, GaN, GaP-Si, and GaN-Si betavoltaic batteries. In addition, the effects of doping concentration and junction depth on the maximum power are examined. The heterojunction photovoltaic cells are preferred to increase the collection efficiency and the power in the betavoltaic battery according to our calculations. By optimizing the doping concentration and junction depth, high-efficient heterojunction betavoltaic batteries are achieved.

Key Words: Nuclear battery, Energy conversion, Betavoltaic cell, Radioluminescence, Heterojunction semiconductor.

ÖZET

NÜKLEER BATARYALARIN VERİMLİLİĞİNİ ETKİLEYEN FAKTÖRLERİN ARAŞTIRILMASI

KAVAK YÜRÜK, Reyyan
Doktora Tezi, Fizik Mühendisliği
Danışman: Prof. Dr. Hayriye TÜTÜNCÜLER
Ocak 2020
110 sayfa

Bu tez çalışmasında bir radyoaktif izotoptan yayılan beta parçacıklarının kinetik enerjisinin elektriğe dönüşümü doğrudan ve dolaylı dönüşüm yöntemleri kullanılarak araştırılmıştır. Deneysel bölümde, Pm147 ve Sr90 beta kaynaklarından gelen düşük aktiviteli radyasyonun, iki farklı fosfor ve grafenin Si fotovoltaik hücre üzerindeki etkilerinin analizi yapılmıştır. Farklı kütle kalınlıklarına sahip fosfor tabakaları ZnS:CuCl ve $SrAl_2O_4:Eu^{2+},Dy^{3+}$ fosfor tozlarından hazırlanmıştır. Doğrudan ve dolaylı nükleer pil modellerinin elektriksel performansları kısa devre akımı ve açık devre gerilimi ölçülerek analiz edilmiştir. Ayrıca, beta radyasyonu sırasında kısa devre akımının zamana bağlı değişimi incelenmiştir. En verimli batarya modeli $Pm147/SrAl_2O_4:Eu^{2+},Dy^{3+}$/PV hücresi olarak belirlenmiştir. Teorik kısımda, betavoltaik pil tasarımları, p-n homoeklem ve p-n heteroeklem yarıiletkenler ve Ni63, Pm147 beta kaynakları kullanılarak ve verimliliği etkileyen parametreler göz önüne alınarak modellenmiştir. Si, GaP, GaN, GaP-Si ve GaN-Si betavoltaik bataryalarda elektriksel performansın teorik bir incelemesi yapılmıştır. Ek olarak, katkılama konsantrasyonunun ve eklem derinliğinin maksimum güç üzerindeki etkileri araştırılmıştır. Heteroeklem fotovoltaik hücreler, hesaplamalarımıza göre betavoltaik pilde toplama verimliliğini ve gücü artıracağı için tercih edilmiştir. Katkılama konsantrasyonu ve eklem derinliği optimize edilerek, yüksek verimli heteroeklem betavoltaik piller elde edilmiştir.

Anahtar Kelimeler: Nükleer batarya, Enerji dönüşümü, Betavoltaik hücre, Radyolüminesans, Heteroeklem yarıiletken.

“Dedicated to my family”

ACKNOWLEDGEMENTS

I would like to thank my supervisor, Prof. Dr. Hayriye TÜTÜNCÜLER for her inducement and support throughout this study. Her invaluable guidance and optimistic attitude was crucial to the completion of my PhD work. I also wish to express my sincere gratitude to Prof. Dr. Ramazan KOÇ for his guidance, criticism, and insight throughout the research. I would also like to thanks Prof. Dr. Eser OLĞAR, Research Assistant Seda ÖZKEÇECİ and all the staff at the Department of Physics Engineering, University of Gaziantep.

Moreover, I would like to express my appreciation to my husband M. Fatih, daughter Zeynep Serra, and son Hasan Erdem for their supports and patience in this exhausting PhD studies. I am grateful also to my dear mother and father, who taught me the value of knowledge, for their unconditional supports.

In addition, I would like to thank Gaziantep University Scientific Research Projects Governing Unit (BAPYB) for providing financial support to this study.

TABLE OF CONTENTS

Page

ABSTRACT ..... **v**
ÖZET ..... **vi**
ACKNOWLEDGEMENTS ..... **viii**
TABLE OF CONTENTS ..... **ix**
LIST OF TABLES ..... **xii**
LIST OF FIGURES ..... **xiii**
LIST OF SYMBOLS ..... **xvi**
LIST OF ABBREVIATIONS ..... **xix**
CHAPTER I: INTRODUCTION **1**
1.1 Basic Concepts of Nuclear Battery 1
1.2 Types of Nuclear Battery 3
1.2.1 Classification of Nuclear Batteries 3
1.2.2 Direct Conversion Nuclear Battery 5
1.2.3 Indirect Conversion Nuclear Battery 8
1.3 Historical Background of Nuclear Battery 10
1.4 Thesis Outline 14
CHAPTER II: THEORY OF DIRECT CONVERSION NUCLEAR BATTERY **16**
2.1 Beta Particles through Matter 16
2.1.1 Beta Decays 17
2.1.2 Behavior of Beta Particles 18
2.1.3 The Energy Spectrum of Beta Decay 19
2.1.4 Interaction of Beta Particles with Matter 21
2.1.4.1 Stopping power 23
2.1.4.2 Range 25
2.2 Principles of Direct Conversion Nuclear Battery 26
2.2.1 p-n Homojunction Betavoltaic Battery 27
2.2.1.1 Energy Loss and Rate of Electron–Hole Generation 28

2.2.1.2 Reflection Coefficient 29
2.2.1.3 Absorption Coefficient 30
2.2.1.4 Collection Efficiency 31
2.2.1.5 Leakage Current 32
2.2.1.6 Current-Voltage 33
2.2.1.7 Power 35
2.2.1.8 Fill Factor 35
2.2.1.9 Efficiency 36
2.2.2 p-n Heterojunction Betavoltaic Battery 36
2.2.2.1 Collection Efficiency 38
2.2.2.2 Leakage Current 39
2.3 Factors Affecting Efficiency of Direct Conversion Nuclear Battery 40
2.3.1 Effects of Radioisotope Selection 41
2.3.2 Effects of Semiconductor Selection 42
2.3.3 Effects of Semiconductor Thickness 45
2.3.4 Effects of Doping Concentration 46
2.3.5 Effects of Radiation Damage 47
CHAPTER III: THEORY OF INDIRECT CONVERSION NUCLEAR BATTERY 49
3.1 Radioluminescence and Radioluminescent Materials 50
3.2 Influence of Beta Irradiation on Phosphors 53
3.2.1 Mechanisms of Radioluminescence of Phosphors 53
3.2.2 Radiation-Induced Degradation of Phosphors 55
3.3 Indirect Conversion Nuclear Battery Designs 56
3.4 Energy Conversion Efficiency of Indirect Conversion Nuclear Battery 58
CHAPTER IV: EFFECT OF BETA SOURCE AND PHOSPHORS ON PHOTOVOLTAIC CELLS 61
4.1 Materials 61
4.1.1 Preparation of Phosphor Layers 63
4.2 Methods 65
4.3 Design and Structures 66
4.4 Results 68

CHAPTER V: MODELING AND SIMULATION OF DIRECT CONVERSION NUCLEAR BATTERIES 72
5.1 Simulation Calculations of Si, GaP and GaP-Si Betavoltaic Battery Models .. 74
5.1.1 GaP Betavoltaic Battery Model 74
5.1.2 Si Betavoltaic Battery Model 77
5.1.3 GaP-Si Heterojunction Betavoltaic Battery Model 79
5.1.4 Performance Comparison of these Models 81
5.2 Simulation Calculations of GaN and GaN-Si Betavoltaic Battery Models 83
5.2.1 GaN Betavoltaic Battery Model 83
5.2.2 GaN-Si Heterojunction Betavoltaic Battery Model 86
5.2.3 Performance Comparison of these Models 90
CHAPTER VI: CONCLUSIONS 92
REFERENCES 96
CURRICULUM VITAE 109

LIST OF TABLES

Page

Table 2.1 Reflection coefficient for some semiconductor materials [27]..... 30

Table 2.2 Linear absorption coefficients for Pm147 and Ni63 in some materials..... 30

Table 2.3 Radioactive properties of H3, Ni63, Pm147 and Sr90/Y90 beta sources for nuclear batteries [20]..... 41

Table 4.1 Parameters of inorganic crystalline powder phosphors used in the study..... 62

Table 4.2 Electrical performance datas of battery models. Assuming the fill factor (FF) is 0.5 for the photovoltaic cell..... 68

Table 5.1 Parameters used in the GaP n-p homojunction betavoltaic battery models..... 75

Table 5.2 Parameters used in Si n-p homojunction betavoltaic battery models..... 77

Table 5.3 Parameters used in GaP-Si n-p heterojunction betavoltaic battery models..... 80

Table 5.4 Electrical performance results for 1 mCi/cm^2 n-p betavoltaic battery models when junction depth values are optimum..... 82

Table 5.5 Collection efficiency (Q) results for Ni63/GaN p-n betavoltaic battery. Junction depths are taken as 1.5 μm..... 85

Table 5.6 Collection efficiency (Q) results for Ni63/GaN-Si p-n betavoltaic battery. Junction depths are taken as 0.5 μm..... 88

Table 5.7 Electrical performance results for 1 mCi/cm^2 Ni63/GaN and Ni63/GaN-Si p-n betavoltaic batteries when doping concentration and junction depth values are optimum..... 91

LIST OF FIGURES

Page

Figure 1.1 Types of nuclear radioisotope generators [20, 23]..... 5

Figure 1.2 Operating principle of betavoltaic battery [28]..... 7

Figure 1.3 Operating principle of an indirect conversion nuclear battery [36].. 10

Figure 1.4 Betacel battery design [30]..... 12

Figure 1.5 a) City Labs' NanoTritium^{TM} betavoltaic battery [43] b) Widetronix betavoltaic battery [44]..... 13

Figure 1.6 Design of different indirect conversion nuclear batteries: a) Phosphor+promethium oxide mixture–filled light source–based battery [48]. b) Battery with tritium aero gel composition [48]. c) Tritium gas-filled light source based battery [18]. d) Self-luminous microspheres containing light source-based battery [51]..... 14

Figure 2.1 Energy spectrum for β^- and β^+ decay [25]..... 19

Figure 2.2 Decay scheme for Sr90 + Y90 isotopes [53, 60]..... 20

Figure 2.3 Normalized energy spectrum of beta particles emitted by the decay of Sr90+Y90 [52]..... 21

Figure 2.4 Ranges of electrons (in mg/cm^2) in light materials [57]..... 25

Figure 2.5 Schematic of a p-n homojunction betavoltaic battery [69]..... 27

Figure 2.6 Schematic of the operation of a p-n junction betavoltaic battery [54]..... 28

Figure 2.7 Electron-hole pairs collection in the p-n junction betavoltaic battery..... 31

Figure 2.8 Betavoltaic circuit model [74]..... 33

Figure 2.9 I-V characteristics of a betavoltaic battery [54]..... 35

Figure 2.10 Energy band diagram of a typical heterojunction semiconductor in thermal equilibrium [81]..... 37

Figure 2.11 Schematic diagram of a heterojunction betavoltaic cell..... 38

Figure 2.12 Theoretical maximum of betavoltaic efficiency depending on semiconductor band gaps [18, 74]..... 44

Figure 2.13 The collection probability for a linearly scaled betavoltaic battery. The collection possibility is insignificant beyond the diffusion length of carriers [15]..... 46
Figure 3.1 Energy bands, excitations, scintillations, quenching and traps in the phosphor material [109]..... 53
Figure 3.2 Process of the luminescence [112]..... 55
Figure 3.3 Schematic diagram of the indirect conversion nuclear battery [99]..... 56
Figure 4.1 a) Optical image and b) SEM image of the graphene sheet [118].... 63
Figure 4.2 SEM image of $SrAl_2O_4:Eu^{2+},Dy^{3+}$ thin film on glass substrate made by spray pyrolysis method..... 63
Figure 4.3 a) Phosphor layer prepared with polypropylene. b) Phosphor layer prepared with PET carrier double-sided tape..... 64
Figure 4.4 Comparison of different mass thicknesses of phosphor layers for indirect conversion nuclear battery model..... 65
Figure 4.5 a) Direct conversion nuclear battery model, b) indirect conversion nuclear battery model, c) direct conversion nuclear battery model with graphene..... 67
Figure 4.6 a) Sr90/phosphor layer/photovoltaic cell battery model, b) Pm147/ phosphor layer/photovoltaic cell battery model, and c) Pm147/graphene layer/photovoltaic cell battery model..... 68
Figure 4.7 The graphs of the short-circuit current with respect to time for the battery models which are made with Pm147 beta source and ZnS:CuCl or $SrAl_2O_4:Eu^{2+},Dy^{3+}$ phosphors (interval 1 minute and the total time is 1 hour)..... 70
Figure 4.8 The graphs of the short-circuit current with respect to time for the battery models which are made with Sr90 beta source and ZnS:CuCl or $SrAl_2O_4:Eu^{2+},Dy^{3+}$ phosphors (interval 10 minute and the total time is 2 hours)..... 70
Figure 4.9 The graphs of the short-circuit current with respect to time for the battery models which are made with Pm147 beta source and graphene (interval 1 minute and the total time is 1 hour)..... 71
Figure 5.1 Schematic diagram of a GaP n-p homojunction betavoltaic battery 75

model.....

Figure 5.2 Collection efficiency versus the junction depth in the Ni63/GaP and Pm147/GaP n-p betavoltaic battery models..... 76

Figure 5.3 Maximum power versus the junction depth in the Ni63/GaP and Pm147/GaP n-p betavoltaic battery models..... 76

Figure 5.4 Collection efficiency versus the junction depth in the Ni63/Si and Pm147/Si n-p betavoltaic battery models..... 78

Figure 5.5 Maximum power versus the junction depth in the Ni63/Si and Pm147/Si n-p betavoltaic battery models..... 78

Figure 5.6 Designed 1 cm^2 area device structure of GaP-Si n-p heterojunction betavoltaic battery..... 79

Figure 5.7 Collection efficiency versus the junction depth in the Ni63/GaP-Si and Pm147/GaP-Si n-p betavoltaic battery models..... 80

Figure 5.8 Relationships between the maximum power and junction depth for Ni63/GaP-Si and Pm147/GaP-Si n-p betavoltaic battery models.... 81

Figure 5.9 Theoretical I–V characteristics of Si, GaP and GaP-Si betavoltaic batteries under 1 mCi/cm^2 Ni63 and Pm147 beta-radiation..... 83

Figure 5.10 Maximum power versus the junction depth and p-type doping concentration (N_a) in the Ni63/GaN p-n betavoltaic battery when N_d is $4x10^{17}$ cm^{-3}..... 84

Figure 5.11 Maximum power versus doping concentrations (N_a and N_d) for Ni63/GaN p-n betavoltaic battery..... 86

Figure 5.12 Designed 1 cm^2 area device structure of Ni63/GaN-Si p-n heterojunction betavoltaic battery..... 87

Figure 5.13 Relationships between the maximum power and p-type and n-type doping concentrations for Ni63/GaN-Si p-n betavoltaic battery..... 89

Figure 5.14 Relationships between the maximum power and p-type doping concentration and junction depth for Ni63/GaN-Si p-n betavoltaic battery when N_a is $5x10^{16}$ cm^{-3}..... 90

Figure 5.15 Theoretical I–V characteristics of GaN and GaN-Si battery under 1 mCi/cm^2 Ni63 beta-radiation..... 91

LIST OF SYMBOLS

$\boldsymbol{\alpha}$	Linear absorption coefficient
$\boldsymbol{\beta}$	Beta particle
$\boldsymbol{\Delta E_c}$	Conduction band discontinuity
$\boldsymbol{\Delta E_v}$	Valence band discontinuity
$\boldsymbol{\Delta m}$	Weight difference in the phosphor substrate
ε	Average energy for an electron-hole pair generation
$\boldsymbol{\epsilon}$	Absolute permittivity
$\boldsymbol{\eta}$	Efficiency of the battery
$\boldsymbol{\lambda}$	Probability of decay
$\boldsymbol{\mu_m}$	Mass attenuation coefficient
$\boldsymbol{\nu_e}$	Neutrino particle
$\boldsymbol{\bar{\nu}_e}$	Antinötrino particle
$\boldsymbol{\rho}$	Material density
$\boldsymbol{\tau_n}$	Minority carrier lifetime of the n-type semiconductor
$\boldsymbol{\tau_p}$	Minority carrier lifetime of the p-type semiconductor
$\boldsymbol{\varphi_0}$	Incident beta particle flux density
$\boldsymbol{A}$	Activity
$\boldsymbol{c}$	Speed of light
$\boldsymbol{d}$	Thickness of the phosphor layer
$\boldsymbol{D_n}$	Diffusion coefficient of the n-type semiconductor
$\boldsymbol{D_p}$	Diffusion coefficient of the p-type semiconductor
$\boldsymbol{d_n}$	Thickness of the n-type semiconductor
$\boldsymbol{d_p}$	Thickness of the p-type semiconductor
$\boldsymbol{E}$	Energy of the beta particle
$\boldsymbol{E_{avg}}$	Average energy of the beta particle
$\boldsymbol{E_g}$	Intrinsic band gap of the material

$\mathbf{E_i}$	Initial energy of the beta particle
$\mathbf{E_k}$	Average energy lost as heat
$\mathbf{E_{max}}$	Maximum energy of the beta particle
$\mathbf{E_R}$	Amount of energy converted into phonons
$\mathbf{k}$	Boltzmann constant
$\mathbf{L_n}$	Hole diffusion length
$\mathbf{L_p}$	Electron diffusion length
$\mathbf{m_e}$	Mass of electron
$\mathbf{m_0}$	Mass of the incident particle
$\mathbf{N}$	Number of the radionuclides
$\mathbf{N_\beta}$	Beta flux entering junction device
$\mathbf{N_a}$	Doping concentration in the p-type semiconductor
$\mathbf{N_d}$	Doping concentration in the n-type semiconductor
$\mathbf{N_{EHP}}$	Number of electron-hole pairs
$\mathbf{n}$	Ideality factor of the photovoltaic cell
$\mathbf{n_e}$	Multiplicative density of electrons
$\mathbf{n_i}$	Intrinsic carrier concentration in the semiconductor
$\mathbf{I_{ex}}$	Average excitation energy
$\mathbf{I}$	Current of the diode
$\mathbf{I_0}$	Leakage current
$\mathbf{I_{max}}$	Maximum current of the diode
$\mathbf{I_{sc}}$	Short-circuit current
$\mathbf{q}$	Electronic charge
$\mathbf{Q}$	Total collection coefficient
$\mathbf{Q_{max}}$	Maximum energy loss of the beta particle
$\mathbf{Q_{dr}}$	Collection efficiency of the depletion region
$\mathbf{Q_n}$	Collection efficiency of the n-type semiconductor
$\mathbf{Q_p}$	Collection efficiency of the p-type semiconductor
$\mathbf{P_{max}}$	Maximum power output
$\mathbf{r}$	Reflection coefficient
$\mathbf{R_{max}}$	Maximum range of the beta particle
$\mathbf{S}$	Cross-sectional area

$\mathbf{S_0}$	Surface recombination rate at the emitter semiconductor
$\mathbf{S_d}$	surface recombination rate at the back of the semiconductor
$\mathbf{S_n}$	Surface recombination velocity of the n-type
$\mathbf{S_p}$	Surface recombination velocity of the p-type
$\mathbf{S_{electronic}}$	Electronic stopping power
$\mathbf{S_{nuclear}}$	Nuclear stopping power
T	Temperature (K)
t	Life time of a radioisotope
W	Depletion region thickness of the p-n junction
x	Path length of the beta particle
v	Velocity of the beta particle
V	Applied voltage across the diode
$\mathbf{V_{bi}}$	Built-in voltage of the p-n junction
$\mathbf{V_{max}}$	Maximum voltage
$\mathbf{V_{oc}}$	Open-circuit voltage
Z	Atomic number of the absorber material

LIST OF ABBREVIATIONS

4H SiC	Four-hexagonal Silicon Carbide
AlGaAs	Aluminium Gallium Arsenide
CdSe	Cadmium Selenide
CPD	Contact Potential Difference
CsI (Tl)	Thallium doped Cesium Iodide
FEDs	Field Emission Displays
FF	Fill Factor
GaAs	Gallium Arsenide
GaN	Gallium Nitride
GaP	Gallium Phosphide
ICRU	The International Commission on Radiation Units and Measurements
IR	Infrared Radiation
MEMS	Micro-electromechanical Systems
MOCVD	Metal-Organic Chemical-Vapor Deposition
NaI (Tl)	Thallium doped Sodium Iodide
Ni63	Nickel 63
PDPs	Plasma Display Panels
PET	Polyethylene Terephthalate
Pm147	Promethium 147
PMMA	Polymethyl methacrylate
PS	Polystyrene
PV	Photovoltaic
RCA	American Radio Corporation
RTG	Radioisotope Thermoelectric Generator
SEM	Scanning Electron Microscopy
Si	Silicon

SiC	Silicon Carbide
Sr90	Strontium 90
$SrAl_2O_4:Eu^{2+},Dy^{3+}$	Eu^{2+} Dy^{3+} codoped Strontium Aluminate
TFEL	Thin Film Electroluminescent
UV	Ultraviolet Radiation
Y90	Yttrium 90
ZnS	Zinc Sulfide
ZnS:CuCl	Copper Chloride doped Zinc Sulfide
Zr90	Zirconium 90

CHAPTER 1

INTRODUCTION

1.1 Basic Concepts of Nuclear Battery

With the rapid improvement of micro-electromechanical systems (MEMS) technology, the need for low-power, small-scale, long-lasting, reliable, alternative energy production and storage systems is increasing in many areas such as medical devices, remote sensors, spacecraft and deep-sea probes.

The chemical batteries are less gratifying, mainly due to their low energy content, unit mass, instability under extreme ambient conditions, and short life [1]. In addition, if the power source can be rapidly depleted, the system requires frequent recharging for a continuous and long-life operation [2]. Nuclear batteries convert radioactive decay energy into electricity by thermal, ionization or charge collection methods using charged particles emitted from radioisotopes [1]. Radioisotope fuels have high energy densities of 1-100 MJ/cc and the energy density of radioactive material is nearly 10^4 times greater than the energy density of a conventional chemical battery [3]. Hence, nuclear batteries, which are suitable as alternatives to the chemical batteries, are very interesting for applications that require a small size, stable current and voltage, long lifetime without recharge or refuel [2].

Nuclear batteries, also called radioisotope generators or atomic batteries, are devices that convert nuclear energy of radioactive decay into electricity. Similar to nuclear reactors, nuclear batteries produce energy from radioactive source, but do not use chain reactions. In this respect, energy production with nuclear batteries is different from fission/fusion and chemical reaction energies [4]. These batteries which use the kinetic energy of natural radioactive-isotopes emitting alpha or beta ionizing radiation, generate power at the range of nW to kW according to the type of

conversion used and have very long life span from several tens of years to several hundreds of years [5].

In recent years, there has been an increasing attention in nuclear batteries. Regardless of the environmental conditions, they can be used in a wide range of temperatures and pressures, because of their low-power but long lifetime; they are preferred in some electronic accents. In addition, the rapid spread of low-power electronic devices and increase in the efficiency of the emergence of the methods and techniques is enhanced importance of these batteries [6-8]. Nuclear batteries could be a reliable micro-power source for scientific research of military equipment, space, the deep ocean and other special environment, because of their perfect characteristics such as long life time, high-energy density, and durability in extreme environments, management-free operation and anti-jamming properties [9].

Although it was discovered in 1913 [10], the research and development of nuclear batteries has been minimal for years because of limited low-power applications, rapid semiconductor degradation, limited availability and the high cost of suitable radioisotopes. Despite the positive developments and all the advantages that have been observed in recent years, the efficiency of nuclear batteries is still not at the desired level and efforts are underway to increase efficiency. Available developmental progress is encouraging and these resources can provide power for 20 years and potentially beyond military and commercial devices [11].

The only way to increase the efficiency of nuclear batteries is to realize a design that converts the kinetic energy of the resulting particles into electrical energy [12]. The kinetic energies of the particles that emerge from the isotopes degraded during the interaction with the substance are thrown out as light by turning them into more heat or by stimulating the electrons [4, 13]. In other words, the kinetic energies of the resulting radioactive particles can be slowed down before being converted to heat or light, and the substance can be ionized; the resulting loads can be collected on a surface and converted into static electricity.

In a nuclear battery, the capability of the medium through which the radioactive particle passes to carry an electric current is one of the main parameters determining the effectiveness of the battery. According to the function of the nuclear battery, the

most effective material type is semiconductor. The specific properties of the semiconductors allow the radioactive energy to utilize the decay of radioisotopes which enable the release of radioactive particles [14]. In a semiconductor the radiation energy will go into electron-hole pairs generation. Generating of electron-hole pairs indicate the most effective way for energy conversion. The interaction of ionizing radiation with semiconductors is used in alphavoltaics and betavoltaics technology [15]. All nuclear battery systems have many of the same design considerations, but efficiency enhancement and smaller size targets bring additional warnings and mechanical differences to the design process. The efficiency of any nuclear battery is eventually determined by the radioisotope source, radiation transport and energy conversion transducer physics [15]. The choice of suitable and practical radioisotope and semiconductor/capacitor also plays a critical role in the design of nuclear batteries. The maximum power and efficiency of the nuclear battery depends on the charging particle current and the performance of the external emission of radioactive sources [16].

There are more than ten kinds of energy conversion methods used in radioisotope batteries, including radioisotope thermoelectric generators, direct charge collection nuclear batteries, betavoltaic cells, reciprocating electromechanical cells and thermo photovoltaic cells [9]. Some of them are discussed in detail below.

1.2 Types of Nuclear Battery

1.2.1 Classification of Nuclear Batteries

The electrical energy of the radioisotopes generator is produced from radioactive materials that are decaying by an appropriate energy conversion technique. These batteries are divided into two main groups depending on the conversion technique [17]. In the first group, radioactive decay energy is generated by converting the kinetic energy of the particles formed in radioactive decay into thermal energy, and then converting the thermal energy into electrical energy. In the second group, electric energy is produced without a thermal cycle for various types of nuclear batteries (direct conversion, indirect conversion, and direct charge) [18].

Thermal converters energy outputs are functions of temperature differences of a certain element that constitute the energy transport mechanism. The thermal converters have been produced in the following forms: Radioisotope thermoelectric generator (RTG), thermionic converter, thermophotovoltaic cell, Stirling radioisotope generator and alkali-metal thermal to the electric converter. Thermoelectric devices primarily convert the kinetic energy of radioactive particles into heat by colliding them with the target particles and then convert the heat into electrical energy either by dynamic heat machines [19].

An amount of at least one gram of radioactive material is required to create a sufficient thermal gradient for an effective RTG. Alpha or beta radioactive isotopes with particle energy of hundreds or thousands of keVs (especially Pu238 and Sr90) are generally used for RTG to produce more than a few hundred milliwatts power. The efficiency of conversion for RTGs can achieve 8-10%. A modern type of RTG can achieve energy conversion efficiency of up to 20% and theoretical calculations advise that efficiency can be increased up to 30%. The use of large amounts of radioactive isotopes in RTGs limits the application of these devices due to high radiation and radiotoxic hazards [20]. For this reason, thermal generators are used in space and underwater vehicles where any external energy source is not accessible and generally has a life span of 5 to 50 years.

Non-thermal generators are classified under three groups. These are entitled as direct conversion nuclear batteries, also known as betavoltaic; indirect conversion nuclear batteries; and direct charge nuclear batteries based on the principles of capacitor. In the direct conversion nuclear batteries, the radioactivity can be directly converted into electrical energy via betavoltaics, in which the energy from a beta particle generates electron-hole pairs which are collected and used to produce power like a solar cell [21]. In the indirect nuclear battery, nuclear energy produces lights by means of a radioluminescence material, in the second stage the lights are converted into electricity by photon-electron transformation as in solar cell. The other non-thermal type, direct charge nuclear battery is in the form of a capacitor consisting of an electrode having a radioactive source on it and a metal foil in which an electrostatic charge is deposited. There may be dielectric or vacuum between the electrodes. Direct charged nuclear batteries provide high voltages (until hundreds of

kilovolts) at small currents (nano-amperes) depending on the rate of radionuclide decay. Electricity is discharged by switching off the circuit with a working load [18].

In the non-thermal converters, due to the fact that the power produced is generally at the ranges from micro- to milli-watt and the radioactive isotope is used in the amount of milligrams, they are mostly used in fields such as micro-electronics and health [20]. With the developments in recent years, these generators have been able to produce a higher level of power and become attractive [22].

The classification of radioisotope generators according to the conversion of radioactive decay to electrical energy is shown in Figure 1.1.

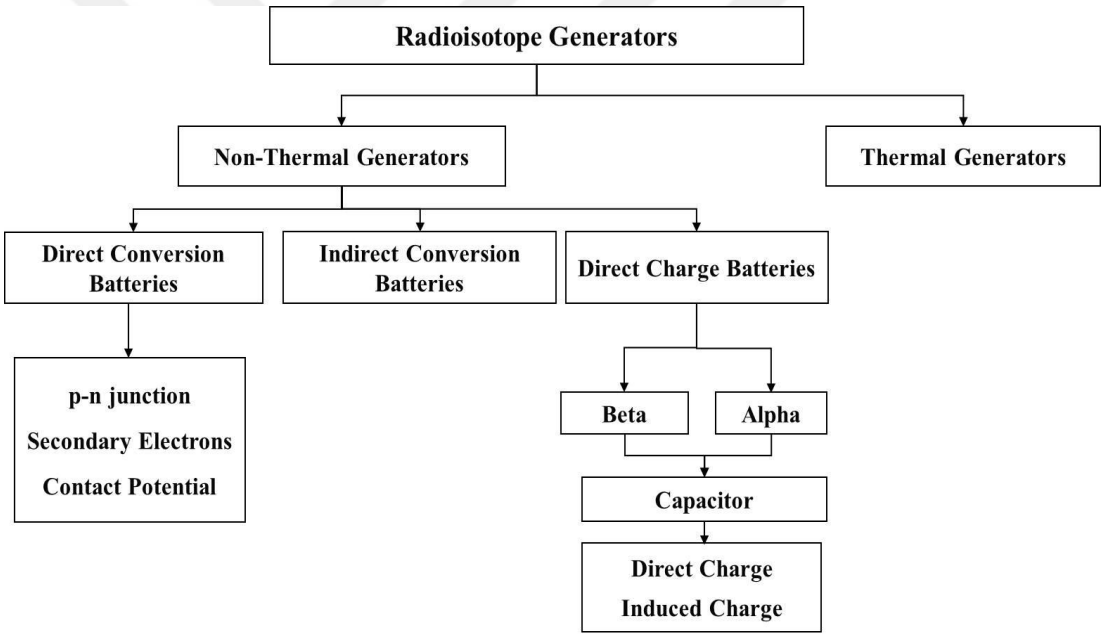

Figure 1.1 Types of nuclear radioisotope generators [20, 23].

1.2.2 Direct Conversion Nuclear Battery

In the direct conversion nuclear batteries, the current is improved from the charge on the beta or alpha particles which will generate potential differences [24]. These batteries operate using alpha or beta particles to ionize atoms in an environment between two electrodes, and the ionized charges are separated and collected using a voltage gradient between the electrodes. Each ionizing particle can ionize many

atoms depending on the average kinetic energy and the average ionization energy of the ambient atoms. The average ionization energy for most atoms is in the range of 1-100 eV, and most radioisotopes emit kinetic energy particles ranging from keV to MeV. The voltage gradient can be obtained in two different ways. First, the two electrodes in the battery can be formed from two different metals and the potential for contact between the two electrodes can be used to generate the voltage gradient. Such nuclear batteries are called the contact potential difference (CPD) battery [3].

In the second way the two electrodes may be along the p-n junctions, and the electric fields set-up through the depletion layer could be used to separate the charged particles [3]. In this method, beta or alpha particles enhance the electron-hole production across the p-n junction which will induce the flow of electrons through external circuit attached across junction and therefore electricity will be generated. Direct conversion nuclear batteries using beta particles for electrical energy production are known as betavoltaic batteries. In the direct conversion nuclear batteries there are also alphavoltaic devices which use alpha radiations to generate electricity from semiconductor p-n junctions [24].

Since alpha emitters contain a very powerful energetic alpha particle (usually greater than 1 MeV) that can quickly damage the micro device and shorten its life, betavoltaic conversion is preferred for micro-power sources according to the alphavoltaic conversion in the direct conversion nuclear battery [2]. Beta particles are electrons that are much smaller than 1 MeV and this kinetic energy is converted into electrical energy in betavoltaic batteries [25].

The mechanism of a betavoltaic battery is similar to that of a p-n junction diode for solar cell application. In these devices, the semiconductor is used as the p-n junction and basic operation of the device comprises two stages: First, absorption of the betas causing the formation of the electron-hole pairs, and the second step is the separation of the electron-hole pairs that cause a current in the external circuit. Figure 1.2 shows the operating mechanism of the betavoltaic battery. In particular, under the influence of the electric field generated by the p and n layers of a p-n junction, it is used to separate the pairs of electrons and holes formed in the depletion zone by the betas and constitute the accessible external potential of the betavoltaic device. In this way,

an electric current is switched on, depending on the intensity of ionized radiation without any extra power supply. It is desirable that the width of the depletion region be large enough to absorb most of the beta particles in the depletion region [17, 26].

In a betavoltaic battery, the short-circuit current depends on the number of electron-hole pairs generated at p-n junction. The open-circuit voltage varies depending on the energy band of the semiconductors used in the p-n junction. For silicon betavoltaics, this value can be up to several 100 mV. Larger voltages can be obtained by connecting a plurality of cells in series or using a wide band-gap semiconductor [3]. Only a fraction of the energy of the beta particles produces utilizable power. The remaining energy is lost in the semiconductor through the phonon interactions as heat [27]. Due to self-absorption and isotropic emission, the efficiency of the beta source is reduced. In addition, as a result of collisions of beta particles, the gaps and faults in the p-n junction reduce both the built-in potential and the charge carrier mobility. For these reasons, although beta radiation has high intensity energy and can supply energy for years, conversion efficiency in betavoltaic devices is at best 10 percent. The evaluation of the effects of interaction of beta particles with a p-n junction is the most important consideration in optimizing a betavoltaic battery design [28].

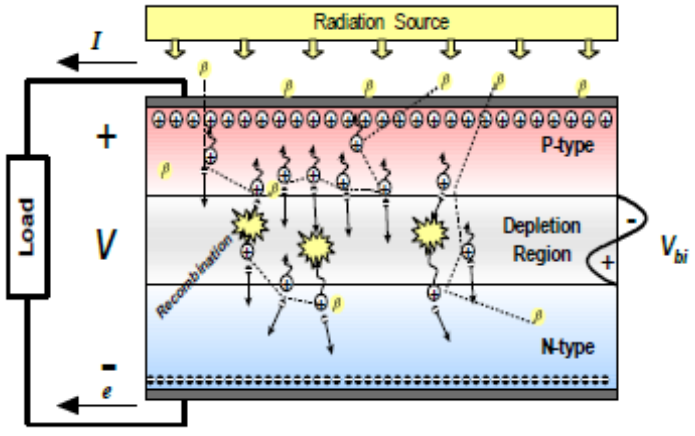

Figure 1.2 Operating principle of betavoltaic battery [28].

The devices that transform radioisotope sources via photovoltaic effect have been present since they were suggested by Rappaport in 1954 [29], two main issues hindering their more widespread use. The first one is the relatively low density of typical power densities due to a small amount of particle fluxes from radioisotope sources emitting beta particles [30]. A second key problem is that the disruption of performance in relatively short periods in previous devices is due to deterioration of the lattice structure in crystalline cells. Radiation harm has hampered the ability to access higher power devices when higher power radioisotope sources reason faster deterioration of the material [21]. Further development of betavoltaic cells has been hampered by the tightening of laws related to the use of radioactive sources, due to material issues. With the advances made in material technology in recent years, it can be seen that by using these developments, the efficiency, performance and radioactive fuel requirements of betavoltaic cells can be increased. Furthermore, the reduction in power demand in the remote sensing and calculation applications provided by the nano-scale revolution can lead to an expansion of the applicability of these power sources [27].

Betavoltaic battery is promising for micro electronics devices, implantable biomedical devices and military intelligence applications. In addition, these batteries can be used in space, remote sensing devices, mobile phones, etc.. Betavoltaic is very small and lightweight because of its high energy density, and its integration into MEMS is easy because its main component is semiconductor [9, 31].

1.2.3 Indirect Conversion Nuclear Battery

Indirect conversion consists mainly of a two-stage process. In the first stage, alpha or beta radioactive decay energy is converted to electromagnetic/light radiation (photons). In the second stage, the conversion of light to electricity is carried out. In this method, firstly, alpha or beta particles are dropped onto some radioluminescent materials, such as phosphorus from which light is produced. The radioactive particles collide with the atom of the radioluminescent material, causing an increase in the energy level of the electron. In order to maintain stability, this energy is released by the electron in the form of photons. The photons produced as in the solar cell are then converted into electrical energy by a photovoltaic [24].

In the indirect conversion nuclear battery, absorbing kinetic energy of radioactive particle and the visible luminescence-emitting phosphorus layer is placed between the source and the semiconductor adjacent to the radioactive source. The indirect conversion nuclear battery mechanism is shown in Figure 1.3. Such a battery has advantages such as tolerance to the use of high-energy ionizing particles [15, 32] and can be applied to minimize radiation damage seen in betavoltaics. Because the semiconductor is not directly exposed to ionizing radiation and phosphorus materials are more stable than photovoltaic devices. Therefore, the indirect conversion nuclear battery may use a radioisotope that emits higher energy particles. Although the first overall efficiency is lower, the long-term indirect power output is higher and the service life is longer than the betavoltaics [18, 33, 34].

However, this method is more complex than direct conversion because it requires two operations to generate electricity, and the efficiency of each operation must be relatively high for good whole energy conversion efficiency. The efficiency of the first stage can be improved by achieving high absorption of the particles emitted in the radioluminescence material and by minimizing the light absorption in the radioluminescence agent. The efficiency of the second stage depends on the absorbable fraction of the sunlight in the depletion region and the compatibility of the semiconductor material with the energy band gap [3]. In other words, the maximum value of the spectral response curve of the PV device depends on how well the luminescent material matches the emission wavelength [18, 20].

The spectral response of the radioluminescence source must be matched with the response of the absorbing collector's material to ensure the highest efficiency. Nano tubular or micro spherical structures filled with tritium, thin films and nano size powders can be used to optimize the efficiency of the radioluminescence material. When the spectra are matched and the power conversion is optimal, a 2% overall efficiency of 3.5 V open-circuit voltage can be obtained [20, 35]. Theoretically, the productivity can increase to 25%. The life of the battery depends on the half-life of the radioisotope and the extent to which the radioluminescence material is damaged by high energy radiation [35].

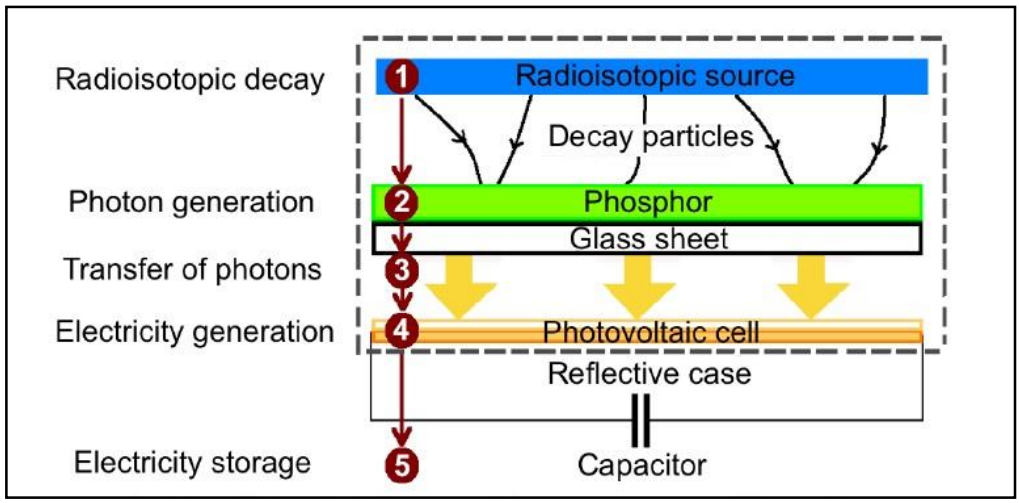

Figure 1.3 Operating principle of an indirect conversion nuclear battery [36].

1.3 Historical Background of Nuclear Battery

Various methods have been developed in order to convert the radioactive energy emitted during the decay of natural radioactive elements into electrical energy. According to this principle, the oldest working nuclear battery was proposed by Moseley in 1913 [10]. Moseley used a thin-walled spherical bulb filled with radium as a radioactive source. The device consisted of two electrodes with a potential of 150 kV and a vacuum between the electrodes; beta particles from a source of 20 mCi radium produced a 10^{-11} A current that led to a power of 1.5 μW [8]. After Henry Moseley's nuclear battery, a lot of research and development was carried out and this technology was developed over a century. There have been many international patent applications and numerous publications.

In 1947, a vacuum nuclear battery developed by Linder by the Sr90 beta source was a thin-walled tubular structure with a spherical tip, emitting beta particles. The open-circuit voltage of this battery was 365 kV and the short-circuit current was about 1 nA. The efficiency of the use of Linder beta radiation was about 75%, while the efficiency of the Moseley battery was 8% [18]. In 1953, Rappaport developed a direct charge nuclear battery using Sr90 and solid polystyrene dielectric. The Radiation Research Corporation has designed and produced different types of direct charge nuclear batteries using tritium and Sr90. In addition, The Russian Corporation "Majak" produced the direct charger nuclear batteries using Pm147 [20].

Since 1961, radioisotope power systems provide electrical and thermal power for many spacecraft. A grapefruit-sized radioisotope thermo-electric generator using heat generated from alpha particles emitted as a result of natural decay of Plutonium238 radioisotope fuel to produce electrical energy in the spacecraft was developed in the early 1950s [37]. The power systems were early used by the U.S. in 1961 in space. Since then, the U.S. has used 41 RTG as a power source for 26 space systems on 25 missions. These implementations have included the Earthorbital air and communication satellites, the robotic traveling spacecraft on Mars, the scientific stations on the Moon, and the deep alien planets across Jupiter, Saturn and beyond [38]. Since the 1970s, thermoelectric generators are known as an alternative source of energy used in applications that have a primary and greatest concern for life and reliability such as space missions, medical devices, military usage, etc... [39].

Semiconductor p-n junctions were first proposed in the 1950s to convert nuclear radiation into electricity. However, the conversion efficiency was low due to non-optimal isotopes and poor quality of the semiconductor [26]. In 1951, Ehrenberg et al. first introduced the concept of Betavoltaic Impact [40]. Ehrenberg et al. have identified the betavoltaic effect by observing the current magnification of the selenium photocells when bombed with electron beam. Again in these years, Ohmart, Linder and Christian also worked on the production of electricity with radioactive material [11]. In 1953, Rappaport made a betavoltaic cell using Sr90 and Y90 with semiconductor junction. This battery has a efficiency of 0.2%, but it has broken down pretty quickly due to radiation damage [28]. American Radio Corporation (RCA) has taken important steps in the development of betavoltaics since the early work of Rappaport [26]. In 1956, further studies on the betavoltaic effect of Sr90-Y90 beta sources in silicon and germanium p-n junctions have been developed by Rappaport and colleagues in RCA [11]. In 1960, the Radiation Research Corporation built betavoltaic batteries with Pm147 supply on silicon with 0.4% and 0.77% overall efficiency [20].

In the 1960s, small-scale methods for radioisotope batteries were further investigated. Until the 1970s, more than 100 articles were published in medical journals describing betavoltaic approaches for isotopic-powered pacemakers. Several companies in the U.S. (Medtronic, Cordis) have developed products in this field. The

first versions used Pu238 and Pm147 as an isotope source. The first successful long-term pacemaker was implanted in a patient aged 34 years by Dr. Otrestes Fiandra and Dr. Robert Rubio in Uruguay in 1960 [41].

Extensive studies have been carried out at Donald W. Douglas Laboratory from 1968 to 1974 to produce a sustainable betavoltaic power supply [28]. As a result of these studies, Donald W. Douglas Laboratory presented betavoltaic devices using planar silicon working with Pm147 with efficiency ranging from 0.7 to 2%. This battery, called Betacel, was used as a power source for pacemakers and its design is as shown in Figure 1.4. [26].

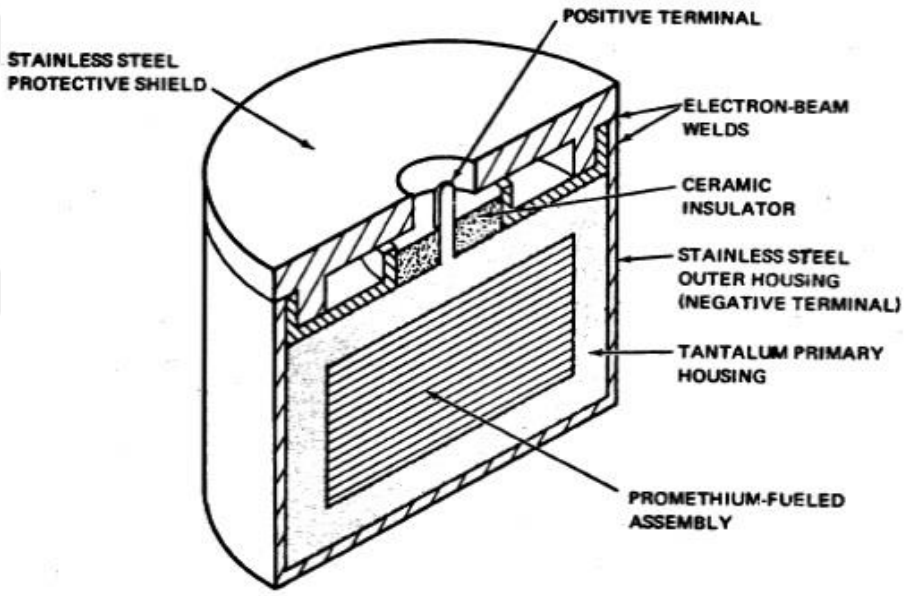

Figure 1.4 Betacel battery design [30].

In the first studies on the betavoltaic battery, experimental and theoretical analyzes were performed using silicon, germanium and gallium arsenide with Pm147 and Sr90-Y90 beta sources. The band-gap dependence of the electron-hole pair creation with ionization radiation was experimentally presented by Klein [42] and the theoretical operation of betavoltaics for various semiconductor materials was explained by Olsen [30]. In recent years, betavoltaic devices have been renewed in order to increase efficiency by using the new materials and micro and nano technologies [26]. Particularly, the use of tritium and Ni63 beta sources and

amorphous silicon (a-Si) and wide band-gap such as silicon carbide (SiC) and gallium nitride (GaN) p-n junction designs have been increased. In 2006, Qynergy developed a krypton-85 betavoltaic Qyncell™. The energy density was high, but it was distorted due to radiation damage and a large amount of defects in silicon carbide. Betabatt developed a three-dimensional porous silicon diode tritium design but failed to achieve a sufficiently high current density. Widetronix developed Ni63-4HSiC betavoltaic cells with energy conversion efficiency of up to 6% shown in Figure 1.5 (b). In 2008, City Labs successfully produced the tritium betavoltaic prototypes shown in Figure 1.5 (a) [11].

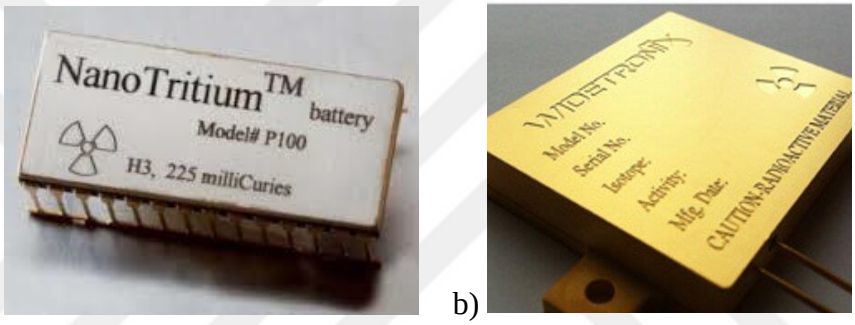

Figure 1.5 a) City Labs' NanoTritium™ betavoltaic battery [43]. b) Widetronix betavoltaic battery [44].

Besides studies on the direct conversion of radioactive decay energy into electrical energy, research has also been carried out for indirect energy conversion since the 1950s and some different designs are shown in Figure 1.6 (a-d) [18]. Walko et al. [48] fabricated radioluminescence nuclear battery based on the H3/ZnS aerogel composite light source and different photovoltaic cells. Prelas et al. [46, 47] studied optoelectronic betavoltaics based on Kr85 and the diamond, and this study showed that the use of wide band gap photovoltaics in nuclear batteries increased efficiency. Sims et al. [49] showed that the gallium phosphide (GaP) semiconductor had an efficiency of 23.54% and 14.59% in the blue light of 968 μWcm^{-2} and 2.85 μWcm^{-2} by indirect nuclear battery application using ZnS:Ag phosphor with GaP. Sychov et al. [45] produced an indirect conversion nuclear battery based on Pu238/ZnS/AlGaAs with a power output of 21 μW. Hong et al. [34] optimized the

parameters of a beta radioluminescence nuclear battery and theoretically showed 2.5% energy conversion efficiency [50].

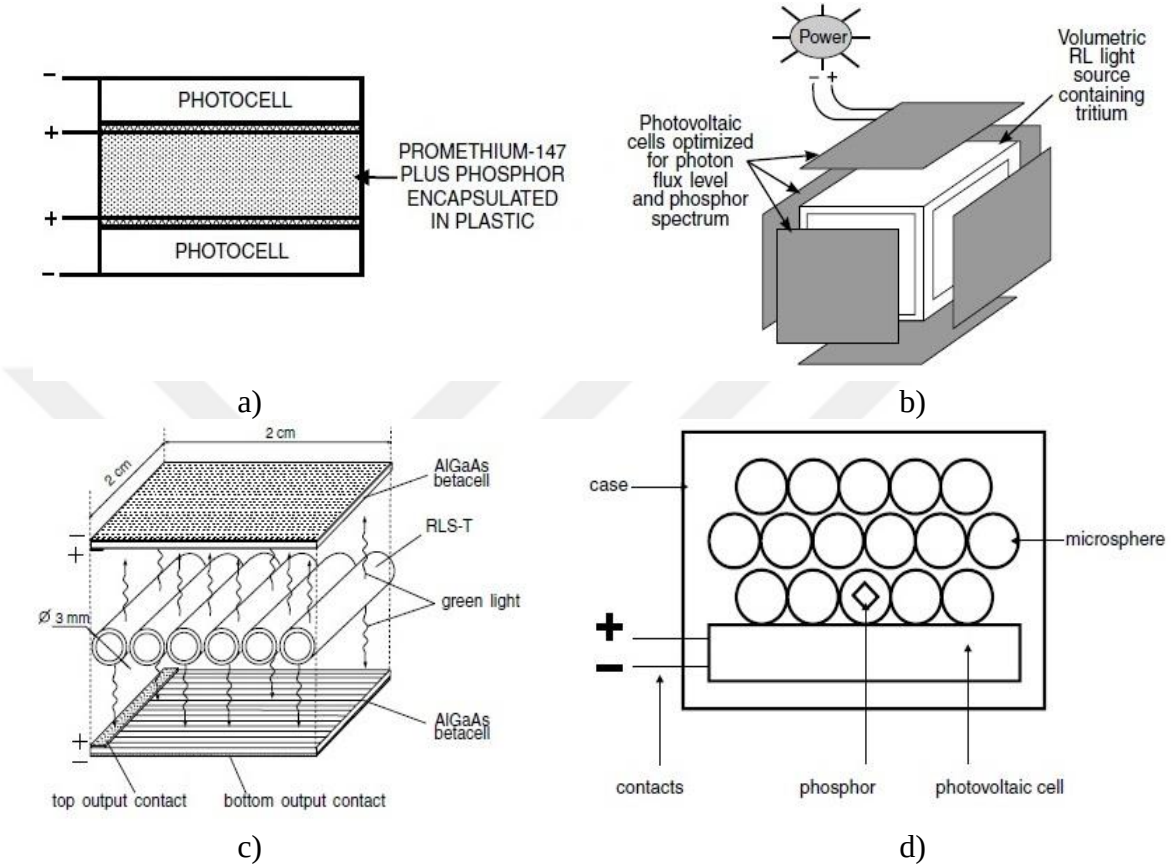

Figure 1.6 Design of different indirect conversion nuclear batteries: a) Phosphor + promethium oxide mixture–filled light source–based battery [48]. b) Battery with tritium aero gel composition [48]. c) Tritium gas-filled light source based battery [18]. d) Self-luminous microspheres containing light source-based battery [51].

1.4 Thesis Outline

In this thesis, non-thermal radioisotope generators that respond to the power supply needs of micro-scale devices, especially direct conversion and indirect conversion nuclear batteries and factors affecting the efficiency of these batteries were investigated by experimental and theoretical analyzes.

The subject of nuclear batteries discussed is an interdisciplinary field related to the fields of physics, electricity and nuclear engineering, including energy harvesting, semiconductor theory, and radiation transport in materials. This thesis includes the theory of operation for betavoltaic and radioluminescence nuclear batteries a discussion on factors affecting efficiency, the analysis of beta-emitting radioisotope sources, radiation transport in semiconductors, semiconductor theory, the design and simulation of battery models, a critical review of battery output results, and a highlight of battery efficiency parameters.

Researches on nuclear batteries are still in progress due to the presence of radioactive isotopes at low prices in the market and the increase of new technological materials. The work in the nuclear battery field is practical and feasible, and efforts to increase efficiency are noteworthy. In recent years, energy conversion and storage techniques have gained importance. For this reason, nuclear batteries are chosen as the subject of the thesis. Currently, the efficiency of all commercial and laboratory-produced betavoltaic batteries is less than 3% [52]. In this study, we aimed to increase the efficiency by analyzing with different ways in the design and materials of the direct and indirect nuclear battery.

In Chapter 1, the classification, introduction, short history and current status of nuclear batteries are described. In Chapter 2, direct conversion nuclear batteries are discussed theoretically with the behavior of the beta particle and the characteristic analysis of homojunction and heterojunction betavoltaic batteries. In particular, the factors affecting the efficiency of the batteries are examined step by step. In Chapter 3, indirect conversion nuclear batteries are discussed theoretically. Chapter 4 covers the experimental part of this study. This section focuses on the design, manufacture, and characterization of battery models. In chapter 5, theoretical research is performed to obtain more efficient betavoltaic battery models using Si, GaN, GaP, GaP-Si, or GaN-Si semiconductors, and Ni63 or Pm147 beta sources. In addition, the effects of doping concentration and junction depth on maximum power have been investigated and optimized. Finally, a summary of the thesis work is provided in Chapter 6.

CHAPTER 2

THEORY OF DIRECT CONVERSION NUCLEAR BATTERY

2.1 Beta Particles through Matter

Ionizing radiation emitted in radioactive decay is charged particles and electromagnetic waves. Beta particles are high-energy electrons and positrons, thrown by weak nuclei of an unstable radioactive atom, released in weak nuclear decays. When beta particles enter a substance, they interact with electrons and nuclei in the material through the electromagnetic force. In this interaction, it creates various effects on the atoms of the substance by making elastic or non-elastic scattering and it can provide the possibility of generating electrical energy by providing electron flow [18].

In elastic scattering, the first particles do not lose, new particles do not appear and the particles involved in the interaction do not change their inner energies. The total kinetic energy of the particles involved in the elastic interaction remains unchanged and is redistributed between these particles by changing the interactive particle motion directions. In the case of non-elastic interaction, the kinetic energy of the moving particle is converted to other forms, such as the excitation energy of the nucleus or atom, the resting energy of the newly formed particles, and the radiation energy [18].

When beta particles enter the substance they lose energy in four ways: direct ionization, formation of delta rays by ionization, Cerenkov radiation and bremsstrahlung production. The most common of these is direct ionization and bremsstrahlung production [53]. The events that take place vary depending on the type of interaction and material properties of the substance with the charged particle [3]. It is important to examine the behavior of beta particles in materials to optimize

nuclear battery design. It is also necessary to understand how beta particles behave in a semiconductor differently from other materials [54]. For this reason, the interaction of beta particles with matter is discussed in this section and the principles of electrical current produced after the interaction are examined theoretically.

2.1.1 Beta Decays

Atoms emit beta particles during their beta decay process. Beta decay happens when there are too many protons or too many neutrons in the nucleus of an atom. There are three different kinds of beta decay:

1. β^+ decay: proton $\rightarrow$ neutron + $e^+ + \nu_e$

A positive charged electron (positron) is emitted from the core of the atom. In this case, the number of protons in the atomic nucleus decreases, the number of neutrons increases by one and the mass number remains unchanged. Here, ν_e is called neutrino. Accordingly, in β^+ decay, a proton transforms into a neutron, a positron, and a neutrino.

2. β^- decay: neutron $\rightarrow$ proton + $e^- + \bar{\nu}_e$

A minus charged electron is emitted from the core of the atom. In this case, the number of protons in the atomic nucleus increases by one, the number of neutrons decreases. Here, $\bar{\nu}_e$ is called antinötrino. According to this, a neutron decays into a proton, an electron, and an antineutrino.

3. Electron capture: proton + e^- $\rightarrow$ neutron + ν_e

Instead of emitting positron, some nuclei can capture one of the planetary electrons. This is often referred to as "inverse beta transition" or electron capture [55]. In the electron capture, the core captures one of the closest electrons.

Antineutrino and neutrino are high energy basic particles with little or no mass and are released to protect energy during the beta decay process. Negative beta decay is much more common than positive beta decay.

The rate at which a beta radioisotope decays is proportional to the number of radionuclides, N, present and the probability of decay, λ:

$$\frac{dN}{dt} = -\lambda N \tag{2.1}$$

The number of decays per second (activity), from a sample of nuclei is measured in Becquerel (Bq). One decay per second equals one Becquerel. The one curie, the older decay unit, is the activity of approximately 1 gram of radium and equals $3.7x10^{10}$ Becquerel [56]. Using the activity, $A_0 \equiv N_0\lambda$, where N_0 is the initial number of radionuclides, the activity of a radioisotope sample as a function of time is given by:

$$A = A_0\, e^{-\lambda t} \tag{2.2}$$

The parameter used to characterize the life time of a radioisotope is its half-life, $t_{1/2} = \ln(2)/\lambda$, which corresponds to the time it takes half of a given sample to decay [32].

2.1.2 Behavior of Beta Particles

Beta particles are physically identical to atomic electrons. But, while electrons are negatively charged, beta particles which are called as negatrons or positrons respectively can be negative or positively charged [57]. The difference between beta particles and electrons is their energy. Beta particles have a very small mass and a high energy. Although the speed varies depending on the source and the medium, beta particles can go almost at the speed of light. Due to their light mass and high speed they are deflected in a much curved way and affected by electric and magnetic fields [53].

Beta particles cause ionization, such as primary electrons produced by photons. These particles are charged alone, lighter and much faster than alpha particles. Beta particles lose their energies, as in the alpha particles, by ionization and excitation. They interact more frequently because they have smaller mass (1/7300 alpha particle mass) and have lower electrical load than alpha particles. Beta particles have moderate penetration power and need energy greater than 70 keV to exceed human

skin. They can penetrate water or human meat up to 1-2 centimeters. They can be stopped by a few millimeters thick aluminum plate [58].

Several hundred beta sources are known; some occur naturally and others are made artificially in the laboratory. The energies of the beta sources range from a few keV to 15 MeV and their half-life ranges from about one second to hundreds of years [25]. The maximum energy of a single beta particle emission is equal to the difference in the resting energies between the main and the side atoms. To preserve the momentum, most of this energy is given to the beta particle because its mass is much smaller than that of the nucleus [32].

2.1.3 The Energy Spectrum of Beta Decay

While alpha particles and gamma rays published by radioisotopes are published in a single energy corresponding to the differences between the energy levels in the nucleus, beta particles show a continuous energy distribution starting just over 0 MeV and extending to a maximum value present for a given radionuclide [53]. A small number of beta particles are released with this maximum energy. The average energy of the beta spectrum is approximately one-third of the maximum of the published beta.

In interacting with matter, it is necessary to know what the energy of beta particles is to determine the extent to which the electron is receiving in the semiconductor and to what extent it creates spot defects, such as spaces and interstitials in the cage. Figure 2.1 shows the energy spectrum of beta minus and beta plus decay operations [25].

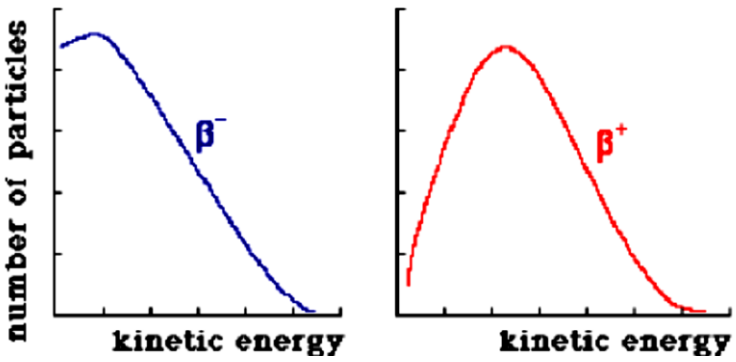

Figure 2.1 Energy spectrum for β^- and β^+ decay [25].

As an example, Sr90 beta source which we used in our experiment has a short-lived daughter isotope of Y90. Each of these radioactive isotopes has maximum beta decay energy, 0.546 and 2.280 MeV respectively. Shown in Figure 2.2 is the decay of Sr90 along with the second and tertiary products [59]. Sr90 is abundant long-lived fission product and Sr90 decays with half-life of 28.90 years into short-lived daughter Y90, which in turn decays with half-life of 64 hours into stable Zr90 [53, 60].

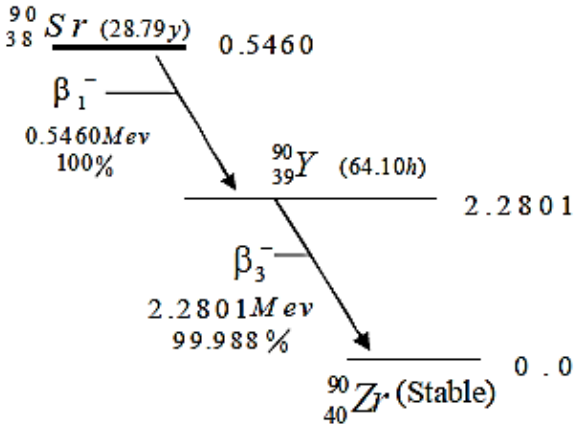

Figure 2.2 Decay scheme for Sr90 + Y90 isotopes [53, 60].

Hence, when the beta energy spectrum is classified as the intensity of radiation in different particle energies, the emission probability distribution is normalized to two, representative of the two beta particles emitted in the Sr90+Y90 decay. As illustrated in Figure 2.3, the maximum energy of the beta particle is ~2.2 MeV, which corresponds to the end-point energy of the beta decay of Y90; the average energy of the beta particle is ~0.3 MeV [52].

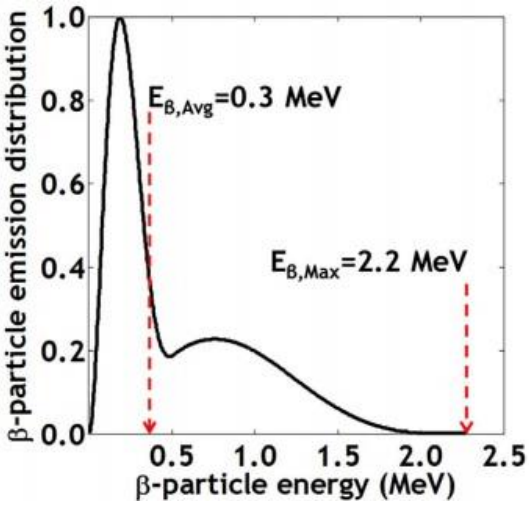

Figure 2.3 Normalized energy spectrum of beta particles emitted by the decay of Sr90+Y90 [52].

2.1.4 Interaction of Beta Particles with Matter

In colliding with an atom, an electron may

- Scatter elastically without loss of energy and leave the atom intact.
- Radiate a photon when scattering from the atomic nucleus; the electron continues with reduced energy (Bremsstrahlung).
- Continue to travel with reduced energy in a non-elastic collision, while the atomic electron spreads to a state of excitement (excitation).
- Remove one atomic electron and ionize the atom. Two electrons exit from the interaction zone (ionization).
- Create Cherenkov radiation when its velocity reaches a speed higher than the phase speed of light in a dielectric environment. However, this is not very common [61].

Bremsstrahlung, ionization and excitation processes contribute to the energy loss of the electron. Loss of energy by excitation and ionization is called collective energy loss. The loss of energy that occurs in the Bremsstrahlung photons is called the radiation energy loss [61].

Beta particles that penetrate the matter lose their kinetic energies by loss of ionization and loss of radiation, and are separated from their original flow. Low

kinetic energy electrons (<0.5MeV) lose their energies due to the loss of ionization in which the beta electrons are subjected to elastic and inelastic collisions with the atoms in the irradiated matter. Through Coulombic interactions, beta particles transfer their energies to an electron that is connected to an atom in the absorber material. This electron is then ejected from the orbit through energy transfer. It has sufficient energy to generate additional ionizations along the path in the absorber material through the formation of secondary electrons. Secondary electrons are born with sufficient energy to form tertiary electrons, and the tertiary electrons have enough energy to form quadruplets and so a large number of electrons are generated [62]. Beta particle with high kinetic energy may lose a significant portion of their energy with radiation loss; here, the slowing of the beta particle in the Coulombic field of a core within the substance causes the formation of Bremsstrahlung or soft electromagnetic radiation. In both types of interaction, the change in the energy of the beta particles can be significant and the deviations in the direction of movement can be quite large [3].

In the interacting matter the following changes occur: the atoms formed are excited or ionized, and the dissociation of the molecules, changes in the lattice structure of the crystals, changes in conductivity, and many other secondary processes have been observed. In this study, the discussion of the radioactive beta transmitter regions of the electrons in the 10^4-10^7 eV energy range is limited. For these energies, the deviation of the electrons is almost completely due to elastic collisions with the atomic nucleus and the loss of energy is the result of interaction with atomic electrons due to the practical neglect of the effect of the bremsstrahlung [63].

The penetration range of beta electrons increases with the increasing initial energy of beta electrons [3]. In addition, the slowing of the beta electrons in matter depends on the density of electrons in the substance [62]. The dissolution of the electrons at large angles during penetration into the material causes each electron to follow a tortuous path. Thus, the range of one electron is not as constant as those of the heavily charged particles, and obtaining the range distribution is problematic. It is also possible that the primary and secondary electrons are emitted by the backward scattering of the substance [64].

2.1.4.1 Stopping power

Beta particles transfer kinetic energy to the electrons of the absorber material through Coulomb scattering and Bremsstrahlung radiation when interacting with the substance and this can be calculated with the Bethe-Bloch formula [62]. The deposited energy can be calculated by integrating the stopping power over the entire path length of the charged particle when it moves within the solid. The rate at which the charged particles lose energy as they pass through a certain material is called the stopping power of this material.

It is important to know the total stopping power of the electron and positron in understanding the mechanisms of interaction with matter. The total stopping power of positrons and electrons is defined as the average energy loss per unit path length because of ionization, excitation and radiation losses.

The stopping powers depend on the mass, charge, speed of the charged particle and the atomic number and density of the medium. The total rate of energy loss of the beta particle as it traverses matter is the sum of the Coulombic and radiative losses. Elastic and inelastic electronic collisions with beta particles are much more probable making this the primary form of energy loss [32]. Thus, the stopping power consists of two parts; electronic stopping power because of the interaction with the atomic electrons of the absorber material and nuclear stopping power because of the interaction with the atomic nucleus [64]:

$$-\frac{dE}{dx} = S_{electronic} + S_{nuclear} \approx S_{electronic} \tag{2.3}$$

where E is energy of the beta particle, $S_{electronic}$ and $S_{nuclear}$ are the electronic and nuclear stopping power or energy loss, respectively. Electronic (collision) stopping power is every time much larger than nuclear (radiation) stopping power. The minus sign in the equation indicates that charged particles lose kinetic energy [64].

The ratio of beta particle energy loss through bremsstrahlung radiation to kinetic energy loss through excitation and ionization can be estimated as [64]

$$\left(-\frac{dE}{dx}\right)_{rad} / \left(-\frac{dE}{dx}\right)_{col} = \frac{Z\,E}{800} \tag{2.4}$$

where Z is the atomic number of the absorber material and E is the energy of the beta particle in MeV. According to this equation, the energy loss caused by radiation is very low when the particle energy is less than about 1 MeV [7]. This equation shows that the loss of radiation for particles with high kinetic energy (over 0.5 MeV) in materials with high atomic number is close to the loss of ionization. Relatively low-energetic electrons, such as tritium beta particles, lose relatively little loss of energy compared to the loss of ionization [18].

A charged particle with mass m_0 interacts primarily with the electrons (mass m_e) of the atom and then loss of the kinetic energy with inelastic collision. The amount of energy lost by the particle depends on distance of approach to the electron and its the kinetic energy. Maximum energy loss (Q_{max}) is given by [65]:

$$Q_{max} = \frac{2\, m_e\, c^2\, \beta^2\, \gamma^2}{1+\frac{2\gamma m_e}{m_0}+(m_e/m_0)^2} \tag{2.5}$$

where m_e is the mass of atomic electron; c is speed of light; m_0 is the mass of particle; $\beta = v/c$; v is the velocity of particle; $\gamma = 1/\sqrt{1-\beta^2}$ is the relativistic factor. When $m_0 = m_e$, Eqn. (2.5) is written as: $Q_{max} = (\gamma - 1)m_e c^2$.

The collisional stopping power above 10 keV energies is theoretically well described in ICRU 37 Report [66]. The average energy loss (collisional stopping power) for a beta particle was also computed by Bethe in the first Born approximation [65]:

$$\left(-\frac{dE}{dx}\right)_{col} = \frac{2\pi k_0^2 q^4 n_e}{m_0 v^2}\left[\ln\frac{m_0 v^2 E_{kin}}{2I_{ex}^2(1-\beta^2)} - \left(2\sqrt{1-\beta^2}-1+\beta^2\right)\ln 2 + 1 - \beta^2 + \frac{1}{8}(2 - 2\sqrt{1-\beta^2}-\beta^2)\right] \tag{2.6}$$

where $k_0 = 8.9876 \times 10^9$ Nm^2C^{-2}, q is electronic charge, n_e is the multiplicative density of electrons, E_{kin} is the kinetic energy that can be given to a free electron in a single collision and I_{ex} is the average excitation energy.

The collisional energy loss of low energy beta particles can be expressed approximately with the formula given below [7]:

$$\left(-\frac{dE}{dx}\right)_{col} = \frac{4\pi q^4 NZ}{m_0 v^2}\left[\ln\left(\frac{2m_0 v^2}{I_{ex}}\right) + 1.2329\right] \text{ MeV/ (g/cm}^2\text{)} \tag{2.7}$$

The energy loss from the Bremsstrahlung radiation can be computed by the following formula [7]:

$$\left(-\frac{dE}{dx}\right)_{rad} = \frac{NEZ(Z+1)q^4}{137m_0^2c^4}\left[4\ln\left(\frac{2E}{m_0c^2}\right) - \frac{4}{3}\right] \text{ MeV/ (g/cm}^2\text{)} \quad (2.8)$$

where E is the beta particle energy, Z is atomic number of target atoms, N is number of target atoms per unit volume [7].

2.1.4.2 Range

When an electron (beta particle) passes through the substance, it loses all its energy with its average energy loss rate and stops after a trace length called the (mean) range. Range is the amount of absorption thickness material required to stop the maximum energy particle from exiting the material. Figure 2.4 shows the required absorption thickness in mg/cm^2 relative to the maximum energy of the electron in light materials. While the absorption thickness would be a fixed value for a source the thickness require would vary upon the type of material used.

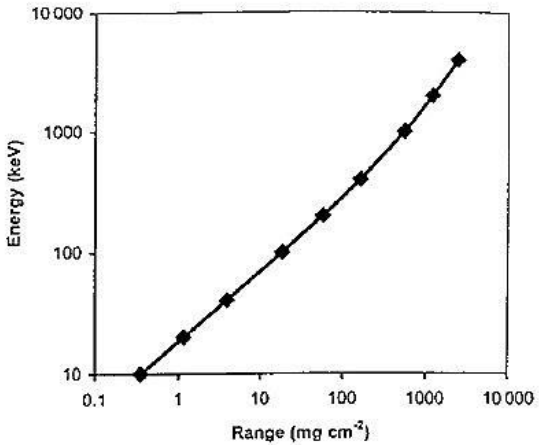

Figure 2.4 Ranges of electrons (in mg/cm^2) in light materials [57].

Theoretical calculation of range is based on the assumption that electrons traverse the material with energy losses at a continual rate. The average range can be computed by integrating the stopping power over energy [67]:

$$R(E_i) = \int_{E_i}^{0} \frac{-1}{dE/dx} dE \quad (2.9)$$

where E_i is the initial energy of beta particle. Maximum range, R_{max}, (material independent) can be calculated from a formula given by Katz and Penfold [68]:

$$R_{max}[g/cm^2] = \begin{cases} 0.412\ E_{max}^{1.265-0.0954\ln(E_{max})}, & 0.01 \leq E_{max} \leq 2.5\ MeV \\ 0.530\ E_{max} - 0.106, & E_{max} > 2.5\ MeV \end{cases} \quad (2.10)$$

where E_{max} is the maximum energy of the beta particle emitted.

2.2 Principles of Direct Conversion Nuclear Battery

The direct conversion nuclear battery transforms the kinetic energy of particles emitted from a radioisotope into power directly similar to a photovoltaic diode that converts light into power.

Semiconductor elements in different conductivity types (p-n junction, p-i-n junction, etc.) are more widely used in converting beta radiation into electricity [18]. Alphavoltaic and betavoltaic batteries are typical of semiconductor based direct energy conversion. In a semiconductor, kinetic energy of the beta particle is consumed in the electron-hole pair and heat production. Direct energy conversion nuclear batteries use electron-hole pairs produced in the material. If no mechanism uses the generated electron-hole pairs, the energy from the ions will also turn into heat. In the interaction of ionizing radiation with matter, about 40-50% of kinetic energy goes to ionization and the rest directly into heat. Therefore, if the energy conversion system does not use the produced heat, the maximum theoretical efficiency for the production of the ion pair will be limited to 40% to 50%. The maximum theoretical efficiency of the conversion mechanism will be further reduced by process inefficiencies in the system [15].

Ionizing radiation forms e-h pairs in the p-n junctions of semiconductor materials. By balancing the p- and n-type regions, a local potential occurs and this leads to the separation of connected e-h pairs. Eventually, the n-type side is charged negatively and the p-type side is charged positively. Since each beta particle forms tens of thousands of e-h pairs, p-n junction diode convert a small number of high-energy beta particles into a much larger low-energy electron current [18].

2.2.1 p-n Homojunction Betavoltaic Battery

The direct conversion nuclear battery (betavoltaic cell) is the power source that electron-hole pairs that are generated in the semiconductor by high-energy beta particles from the decay of radioactive isotopes convert to electrical current. A betavoltaic device is similar to a photovoltaic device. As illustrated in Figure 2.5, a typical design of a betavoltaic device consists of a layer of beta-emitting material and a front and back contact located adjacent to a semiconductor p-n junction.

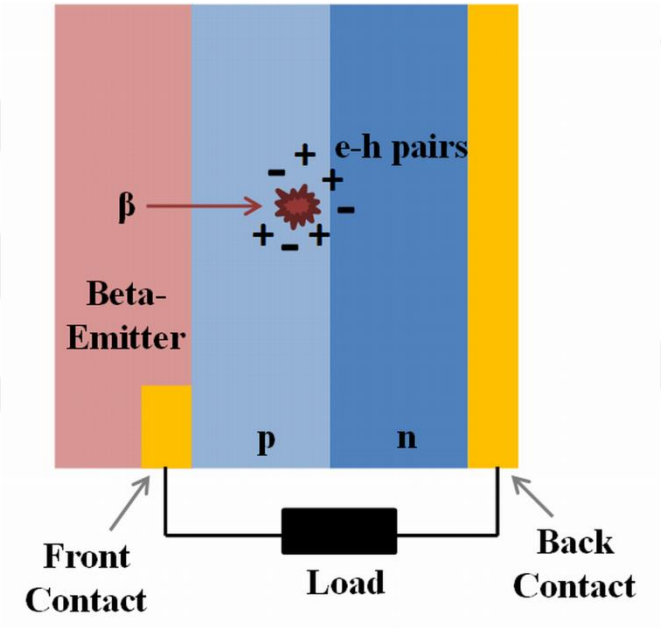

Figure 2.5 Schematic of a p-n homojunction betavoltaic battery [69].

It is important to figure out the production process of electron-hole pairs in semiconductor materials that are the basis of the betavoltaic battery operating principle. Energetic particles emitted from the beta source enter the semiconductor. It then produces e-h pairs that are collected in and around the depletion region of the semiconductor p-n junction through collisions, stimulations and ionization, leading to usable power. The number of e-h pairs produced depends on the kinetic energy of the beta particles. Each beta particle produces tens of thousands of e-h pairs. However, only a portion of the energy of the beta particle produces usable power. The rest is lost as heat due to phonon interactions in the semiconductor [70].

In order to obtain maximum power from a betavoltaic battery, it is very important to minimize the recombination, that is, to separate the generated electron-hole pairs. The generated electron-hole pairs in both the p-type and the n-type regions must reach the depletion region by diffusion to be collected. In a minority carrier diffusion length, the produced e-h pairs are spread along the edge of the depletion region, and along with the e-h pairs produced in the depletion region, are swept across the junction by the depletion electric field to produce electrical power [71]. Figure 2.6 is a schematic view illustrating the mechanism of the battery, and shows a cross-section of the battery. Only e-h pairs generated within a diffusion length from the depletion region or inside the depletion region are collected and produce current [25].

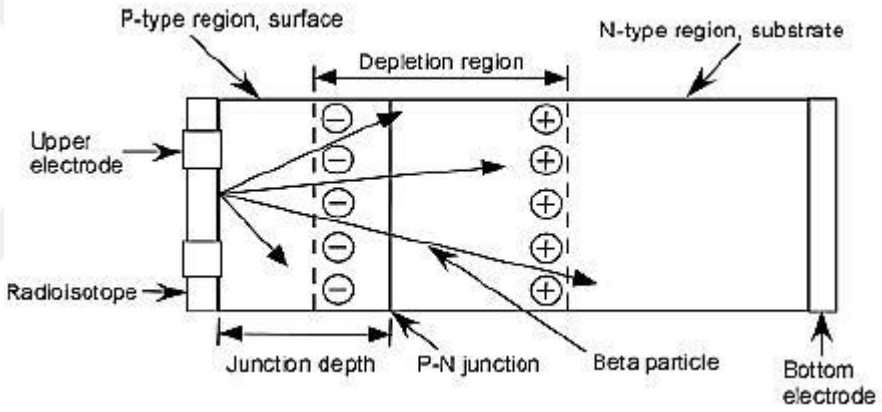

Figure 2.6 Schematic of the operation of a p-n junction betavoltaic battery [54].

As seen from Figure 2.6, this device, which is irradiated with beta radiation, acts as a battery and powers the load when a load is applied to its ends due to a change in carrier concentration near the junction, in the p-n junction consisting of a n-type region (electrons are the majority carriers) and a p-type region (the majority carriers are holes) [72].

2.2.1.1 Energy Loss and Rate of Electron–Hole Generation

When beta particles move inside the semiconductor, they lose their energies by interacting with the lattice. The e-h pairs are generated gradually until the energy of the particle falls below the threshold energy [26]. Thus, a single beta particle is

responsible for the production of many e-h pairs [30]. Part of the energy is lost in unwanted processes characterized as optical phonon losses, band gap losses, and heat losses caused by energy transfer to lattice. Klein experimentally determined that the beta radiation ionization energy needed to form an e-h pair is linearly bound to the semiconductor band gap [26]. Accordingly, the radiation ionization energy (ε) required for the electron-hole pair production is given as follows [42]:

$$\varepsilon = E_g + \langle E_k \rangle + \langle E_R \rangle = 2.8\, E_g + 0.5 \quad \text{eV} \tag{2.11}$$

where E_g is the intrinsic band gap and the amount of energy required to pass electrons from the valence band to the conduction band, E_R is the amount of energy converted into phonons, and E_k is the average energy lost as heat [73]. Accordingly, on average, an e-h pairs generating energy is approximately three times the band gap of the band [54].

The number of e-h pairs in idealized case can be estimated as follows [74]:

$$N_{EHP} = N_\beta \frac{E_{avg}}{\varepsilon} \tag{2.12}$$

where E_{avg} is average energy of beta particle, N_β is beta flux entering junction device and ε is the average energy for an e-h pair generation. Actually, the number of generated e-h pairs is proportional to the number of defects or traps where recombination occurs, the band gap energy of the semiconductor material, and the minimum energy for an electron to move to the conduction band [11].

2.2.1.2 Reflection Coefficient

When a high-energy electron strikes the semiconductor, it is exposed to elastic and inelastic scattering forms. Elastic scattering occurs on the semiconductor surface and the electron is scattered back. This situation can be called the electron "reflection" from the surface. This is undesirable; energy is not transferred to the semiconductor lattice and cannot contribute to the formation of power generation. The fraction of back-scattered electrons is called the reflection coefficient (r), and can be calculated depending on the Z-number of the target material [27]:

$$r = -0.0254 + 0.016Z - 1.86\text{x}10^{-4}Z^2 + 8.3\text{x}10^{-7}Z^3 \tag{2.13}$$

In this equation, it is seen that the back scattering is independent of the initial energy of the electron and when the atomic number (Z) of the target material is reduced, the back-scattered electrons are less. For a compound, r can be calculated from the relative weight fraction for each element [27]. According to this formula, the reflection coefficient for some semiconductors is calculated and given in Table 2.1.

Table 2.1 Reflection coefficient for some semiconductor materials [27].

	Si	**GaP**	**GaN**	**GaAs**	**4H SiC**
r	0.16	0.27	0.28	0.32	0.13

2.2.1.3 Absorption Coefficient

The linear absorption coefficient (α) how far into a material particle can penetrate before it is absorbed. The absorption coefficient depends on the material and on the wavelength of the absorbed particle [75]:

$$\alpha = \mu_m \, x \, \rho \quad (cm^{-1}) \tag{2.14}$$

Here ρ is the material density and μ_m, the mass attenuation coefficient is given by [76]

$$\mu_m = 0.017/E_{max}^{1.43} \tag{2.15}$$

where μ_m is in cm^2g^{-1} and E_{max} (MeV), the maximum energy of beta particle.

The factor α in describes the decay of excess concentration of e-h pairs generated by beta particles. For Pm147 and Ni63 beta sources, linear absorption coefficients of some materials are calculated in Table 2.2.

Table 2.2 Linear absorption coefficients for Pm147 and Ni63 in some materials.

	Beta source	**Si**	**GaP**	**GaN**
α	Pm147	336	596	886
	Ni63	1886	3352	4982

2.2.1.4 Collection Efficiency

The collection efficiency is defined as the fraction of generated e-h pairs that is collected by the p-n junction for a number of particles absorbed. This efficiency, which is described as the number of collected carriers, does not include any losses from phonons [27]. The collection efficiency depends on minority carrier diffusion lengths, junction and depletion region thickness and also very weakly on the surface recombination rate [77]. Figure 2.7 shows e-h pairs collection in the p-n junction betavoltaic battery.

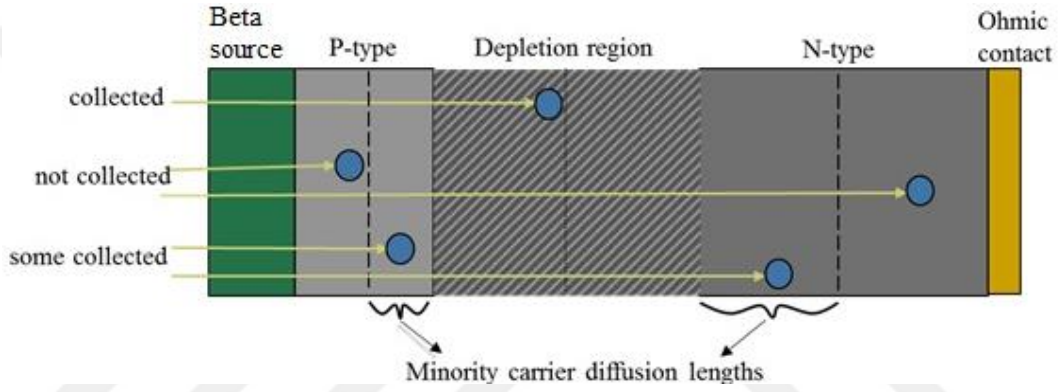

Figure 2.7 Electron-hole pairs collection in the p-n junction betavoltaic battery.

To calculate the collection efficiency of a betavoltaic battery, a formulation must be obtained for the current-voltage characteristics. Sufficiently expressions for collection efficiency are given in [78-80], while the most general one is derived in [81]. It has the following formula:

$$Q_p = \frac{\alpha L_p}{(\alpha L_p)^2 - 1}\left(\frac{S_0 + \alpha L_p - e^{-\alpha d_p}\left(S_0 \cosh\left(\frac{d_p}{L_p}\right) + \sinh\left(\frac{d_p}{L_p}\right)\right)}{S_0 \sinh\left(\frac{d_p}{L_p}\right) + \cosh\left(\frac{d_p}{L_p}\right)} - \alpha L_p e^{-\alpha d_p}\right) \quad (2.16)$$

$$Q_n = \frac{\alpha L_n e^{-\alpha(d_n + W)}}{(\alpha L_n)^2 - 1}\left(\alpha L_n - \frac{S_d\left(\cosh\left(\frac{d_n}{L_n}\right) - e^{-\alpha d_n}\right) + \sinh\left(\frac{d_n}{L_n}\right) + \alpha L_n e^{-\alpha d_n}}{S_d \sinh\left(\frac{d_n}{L_n}\right) + \cosh\left(\frac{d_n}{L_n}\right)}\right) \quad (2.17)$$

$$Q_{dr} = e^{-\alpha d_p}(1 - e^{-\alpha W}) \quad (2.18)$$

$$Q = Q_p + Q_n + Q_{dr} \quad (2.19)$$

Where Q, Q_p, Q_n, Q_{dr} are the collection coefficients of e-h pairs in the total, emitter, base and the depletion region, respectively, α is the absorption coefficient, $L_p = \sqrt{D_p \tau_p}$ is the electron diffusion length in p-type material, d_p is the thickness of the p-type, $L_n = \sqrt{D_n \tau_n}$ is the hole diffusion length in n-type material, τ_p, τ_n are the minority carrier lifetime of p- and n-type, respectively, d_n is the thickness of the n-type, $S_0 = \frac{S_p L_p}{D_p}$ is the surface recombination rate at the p-type, and $S_d = \frac{S_n L_n}{D_n}$ is the surface recombination rate at the back of the n-type, S_p and S_n are the surface recombination velocity at the p- and n-type surface, respectively, D_p and D_n are the p-type diffusion coefficient and n-type diffusion coefficient, respectively.

Here depletion region thickness (W) and built-in voltage (V_{bi}) of junction given by

$$W = \sqrt{\frac{2\,\epsilon\,(N_a + N_d) V_{bi}}{q N_a N_d}} \tag{2.20}$$

$$V_{bi} = \frac{k\,T}{q} \ln\left(\frac{N_a N_d}{{n_i}^2}\right) \tag{2.21}$$

where k is the Boltzmann constant, T is the temperature (K), q is the electronic charge, ϵ is the absolute permittivity ($\epsilon = \epsilon_r \epsilon_0$; ϵ_r and ϵ_0 are the dielectric constants in the region and in vacuum, respectively) (Farad/cm^{-1}), N_a, N_d are the acceptor and donor concentrations (cm^{-3}), respectively, n_i is the intrinsic carrier concentration (cm^{-3}).

2.2.1.5 Leakage Current

The leakage current (I_0) is a portion of the reverse current in the diode resulting from the diffusion of minority carriers from neutral regions to the depletion region. In case of the ideality factor (n)=1, the leakage current can be written by [82]:

$$I_0 = S\,q\left(\frac{n_i^2 D_n}{N_a L_n} + \frac{n_i^2 D_p}{N_d L_p}\right) \tag{2.22}$$

where S is the cross-sectional area, q is elementary charge, $D_{p,n}$ are the diffusion coefficients of holes and electrons, respectively, $N_{a,d}$ are the acceptor and donor concentrations at the p side and n side, respectively, n_i is the intrinsic carrier concentration in the semiconductor material, $L_{p,n}$ are the diffusion length of holes and electrons, respectively.

2.2.1.6 Current-Voltage

As shown in Figure 2.8, an equivalent circuit for a betavoltaic battery is fundamentally the same as that for a solar cell, except that the current source is due to collection of e-h pairs produced by beta particles [74]. The current-voltage characteristic of an equivalent circuit can be determined by cell voltage, external current and power. Maximum power and ideal efficiency can be specified in terms of I_{sc} and V_{oc}.

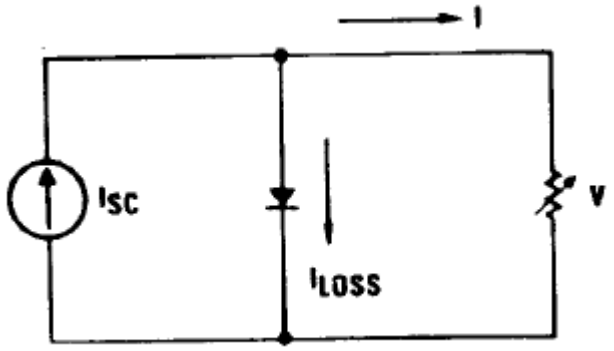

Figure 2.8 Betavoltaic circuit model [74].

The power generation in a p-n junction betavoltaic cell is characterized by the current-voltage (I-V) characteristics of the beta-particle illuminated and non-illuminated diode. A betavoltaic battery displays the same behavior as a simple p-n junction diode since its mechanism is based on p-n junction. Therefore, the dark current of a betavoltaic battery is given by [70]

$$I = I_0 \left[\exp\left(\frac{qV}{nkT}\right) - 1\right] \tag{2.23}$$

where I is the current, I_0 the reverse leakage current of the diode, V the applied voltage across the diode, q the electronic charge, k Boltzmann's constant, T the temperature in Kelvin (K) and n is the ideality factor (n=1 corresponds to an ideal junction).

Just like a solar cell, under beta-particle illumination, assuming that the series resistance is zero and the shunt resistance is infinite, the current-voltage characteristic of the diode is changed by adding a generation current term [83]:

$$I = I_0 \left[\exp\left(\frac{qV}{nkT}\right) - 1\right] - I_{sc} \tag{2.24}$$

where I_{sc}, which originates from the e-h pairs created from the beta particle in the semiconductor, is short-circuit current.

Maximum possible current I_{max} that can be collected under short-circuit condition is given by [84]

$$I_{max} = Sq\,\varphi_0 \frac{E_{avg}}{\varepsilon}(1 - r) \tag{2.25}$$

where φ_0 is the incident beta particle flux density (is approximately equal to activity), E_{avg} is average energy of beta particle, ε is the average energy for an e-h pair production, S is area of the beta source, and r is the reflection coefficient for beta particles from the semiconductor surface. The flux density (φ_0) is the total particle track length per unit volume and per unit time. Theoretically short-circuit current is given by [78]

$$I_{SC} = Q\,I_{max} \tag{2.26}$$

where Q, which is a function of the beta particle, the semiconductor and the device properties, is the collection efficiency of the devices. If all the created e-h pairs are collected by the battery, then Q is equal to 1 [84].

In a betavoltaic battery, the generated e-h pairs are driven by the junction voltage. The maximum voltage is the open-circuit voltage (V_{oc}). When I = 0, the open-circuit voltage can be given as follows [15, 85]:

$$V_{oc} = \frac{n\,k\,T}{q} \ln\left(\frac{I_{sc}}{I_0} + 1\right) \tag{2.27}$$

where k is the Boltzmann constant, n is the ideal factor, T is the temperature (K) and q is the electronic charge.

2.2.1.7 Power

The power produced by the battery is related to the open-circuit voltage and the short-circuit current. The maximum power is the product of short-circuit current (I_{sc}), open-circuit voltage (V_{oc}), and fill factor (FF). According to this, maximum power output a p-n junction betavoltaic battery can produce is given by the following equation:

$$P_{max} = V_{max}\, I_{max} = V_{oc}\, I_{sc}\, FF \tag{2.28}$$

where P_{max} is the maximum power output, V_{max} is the maximum voltage and I_{max} is the maximum current. Traditionally, the I-V characteristic curve of the betavoltaic battery is given in Figure 2.9. Under beta irradiation, the curve is shifting in the direction of negative voltage. Maximum power output can be defined from the I-V characteristics under beta radiation.

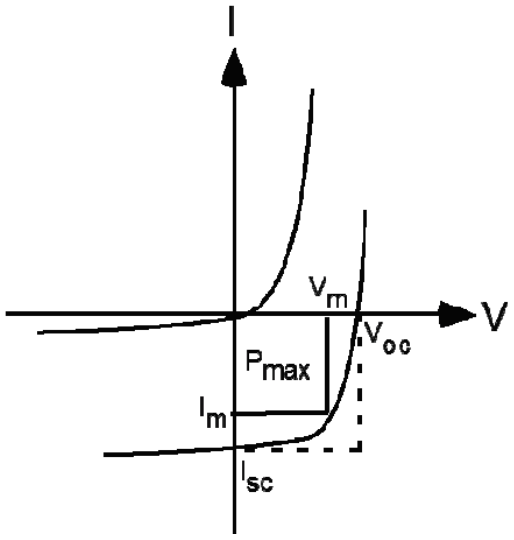

Figure 2.9 I-V characteristics of a betavoltaic battery [54].

2.2.1.8 Fill Factor

The fill factor (FF) is basically a measure of battery quality. It is calculated by comparing the maximum power to the theoretical power that would be output at both the short-circuit current and the open-circuit voltage together:

$$FF = \frac{V_{max}\, I_{max}}{V_{oc}\, I_{sc}} \tag{2.29}$$

The fill factor can be precisely calculated as follows [86]

$$FF = [\vartheta_{oc} - \ln(\vartheta_{oc} + 0.72)] / [\vartheta_{oc} + 1]; \quad \vartheta_{oc} = q V_{oc}/kT \tag{2.30}$$

where k is the Boltzmann constant, n is the ideal factor, T is the temperature (K) and q is the electronic charge.

2.2.1.9 Efficiency

In the direct nuclear energy conversion efficiency, the energy of the e-h pair production and the band gap width are important parameters. The e-h pair generation energy affects the short-circuit current and the band gap affects the open-circuit voltage. The principal energy conversion parameter is efficiency. In the direct conversion nuclear batteries, the magnitude of η is defined as follows [18, 54, 87]:

$$\eta = \frac{P_{max}}{P_{theory}} = \frac{V_{oc}\, I_{sc}\, FF}{q\, A\, E_{avg}} \tag{2.31}$$

where A is activity of the beta source, E_{avg} is average energy of beta particle, and q the electronic charge. In general, conversion efficiency is used to assess the performance of betavoltaic batteries. As seen in the above equation, short-circuit current and open-circuit voltage play an important role in increasing the conversion efficiency [85].

2.2.2 p-n Heterojunction Betavoltaic Battery

A semiconductor heterojunction is produced by combining different semiconductors which have different band gap energy. Since the materials used to form a heterojunction have different energy band gaps, the energy band have discontinuity at the junction interface. For example, as in Figure 2.10, a junction can be formed in which the semiconductor changes suddenly from a wide bandage material to a narrow bandage material.

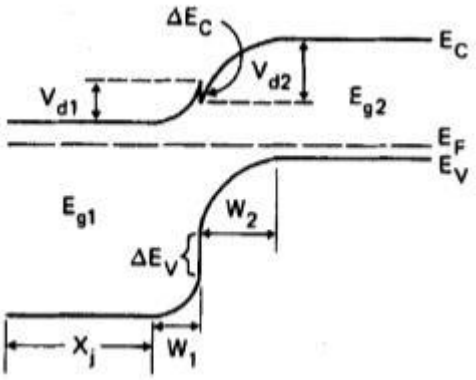

Figure 2.10 Energy band diagram of a typical heterojunction semiconductor in thermal equilibrium [81].

The most important advantage that the heterojunction can have over normal p-n homojunction is in the short wavelength response; if the band gap energy of first semiconductor is large, high energy particles will also be absorbed in the depletion region [81]. The p-n heterojunction cell generally has a better short wavelength response, better radiation tolerance, and lower serial resistance than a normal p-n junction cell. In order to obtain maximum electrical performance, it is essential that the materials selected for manufacturing heterojunction have good lattice matching and coherent thermal expansion coefficients [82].

There are convenient applications of heterojunction structures for a large variety of devices such as laser diode**s,** solar cells, LEDs, photodetectors. Heterojunction cells have many similarities and several differences to Schottky barrier cells. The most important similarity is that short wavelength particles can be absorbed in most cases and this leads to a good high particle energy response. The most important difference is that the open-circuit voltage can be quite high without the need for interface layers as in a p-n junction [81].

The properties and formulas given for p-n junction in the previous section also apply to heterojunction. However, there are some changes in the leakage current and collection efficiency calculations. They are discussed below.

2.2.2.1 Collection Efficiency

The collection mechanism for a p-n heterojunction photovoltaic cell is similar to that of a p-n homojunction photovoltaic cell. The main contribution to the photocurrent comes from the base region of p-n junction, with smaller contribution coming from the emitter layer and the depletion region [88]. Schematic diagrams of heterojunction betavoltaic cell which have two different semiconductors and the coordinates assumed in the analysis have been shown in Figure 2.11.

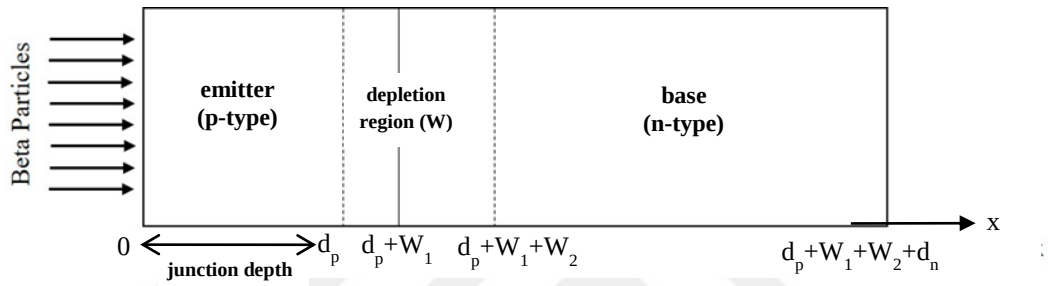

Figure 2.11 Schematic diagram of a heterojunction betavoltaic cell.

The built-in voltage of a heterojunction can be larger than in a homojunction [81]. For heterojunction semiconductor, built-in voltages and thickness of depletion region values at semiconductor 1 and 2 are calculated by [89]

$$V_{bi1} = \frac{kT}{q} \ln\left(\frac{N_a}{n_{i1}}\right) \tag{2.32}$$

$$V_{bi2} = \frac{kT}{q} \ln\left(\frac{N_d}{n_{i2}}\right) \tag{2.33}$$

$$V_{biTotal} = V_{bi1} + V_{bi2} \tag{2.34}$$

$$W_1 = \sqrt{\frac{2\,\epsilon_1\epsilon_2\,N_d}{qN_a(\epsilon_2 N_d+\epsilon_1 N_a)}\,V_{biTotal}} \tag{2.35}$$

$$W_2 = \sqrt{\frac{2\,\epsilon_1\epsilon_2\,N_a}{qN_d(\epsilon_2 N_d+\epsilon_1 N_a)}\,V_{biTotal}} \tag{2.36}$$

where k is the Boltzman constant, T is the temperature (K), q is the electronic charge, ϵ_1 (Farad/cm^{-1}) is the absolute permittivities of semiconductor 1, ϵ_2 (Farad/cm^{-1}) is the absolute permittivities of semiconductor 2, N_a, N_d are the acceptor and donor concentrations for semiconductor 1 and semiconductor 2, respectively, n_{i1} is the

intrinsic carrier concentration of semiconductor 1 and n_{i2} is the intrinsic carrier concentration of semiconductor 2.

Collection efficiency for heterojunction semiconductor is given by [81]

$$Q_p = \frac{\alpha_1 L_p}{(\alpha_1 L_p)^2 - 1}\left(\frac{S_0 + \alpha_1 L_p - e^{-\alpha_1 d_p}\left(S_0 \cosh\left(\frac{d_p}{L_p}\right) + \sinh\left(\frac{d_p}{L_p}\right)\right)}{S_0 \sinh\left(\frac{d_p}{L_p}\right) + \cosh\left(\frac{d_p}{L_p}\right)} - \alpha_1 L_p e^{-\alpha_1 d_p}\right) \quad (2.37)$$

$$Q_n = \frac{\alpha_2 L_n e^{-\alpha_1 (d_p + W_1)} e^{-\alpha_2 W_2}}{(\alpha_2 L_n)^2 - 1}\left(\alpha_2 L_n - \frac{S_d\left(\cosh\left(\frac{d_n}{L_n}\right) - e^{-\alpha_2 d_n}\right) + \sinh\left(\frac{d_n}{L_n}\right) + \alpha_2 L_n e^{-\alpha_2 d_n}}{S_d \sinh\left(\frac{d_n}{L_n}\right) + \cosh\left(\frac{d_n}{L_n}\right)}\right) \quad (2.38)$$

$$Q_{dr1} = e^{-\alpha_1 d_p}(1 - e^{-\alpha_1 W_1}) \quad (2.39)$$

$$Q_{dr2} = e^{-\alpha_1 (d_p + W_1)}(1 - e^{-\alpha_2 W_2}) \quad (2.40)$$

$$Q = Q_p + Q_n + Q_{dr1} + Q_{dr2} \quad (2.41)$$

where $Q, Q_p, Q_n, Q_{dr1}, Q_{dr2}$ are the collection coefficients of electron–hole pairs in the total, emitter, base, the depletion region 1 and the depletion region 2, respectively, α_1 and α_2 is the absorption coefficients for semiconductor 1 and 2, respectively, L_p is the electron diffusion length in emitter material, d_p is the thickness of the emitter, L_n is the hole diffusion length in base material, d_n is the thickness of the base, $S_0 = \frac{S_p L_p}{D_p}$ is the effective surface recombination rate at the emitter surface, and $S_d = \frac{S_n L_n}{D_n}$ is the effective surface recombination rate at the back surface of the base, D_p and D_n are the emitter diffusion coefficient and the base diffusion coefficient, respectively, S_p and S_n are the surface recombination velocity at the emitter and the base surface, respectively [81].

2.2.2.2 Leakage Current

In case of the ideality factor (n)=1, the leakage current of heterojunction p-n diode can be written by [90]

$$I_0 = S\,q\left(\frac{N_d D_n \exp[-q(V_{bi} - \Delta E_c)/kT]}{L_n \tanh(d_n/L_n)} + \frac{N_a D_p \exp[-q(V_{bi} + \Delta E_v)/kT]}{L_p \coth(\frac{d_p}{L_p} + \phi)}\right) \quad (2.42)$$

where V_{bi} is the built-in potential of the diode, ΔE_c is the conduction band discontinuity expressed in volts, ΔE_v is the valence band discontinuity expressed in volts, d_p is the thickness of the p side, d_n is the thickness of the n side, ϕ is given by

$\tanh\phi = \frac{S_p L_p}{D_p}$ where S_p is the surface recombination velocity for the window semiconductor.

2.3 Factors Affecting Efficiency of Direct Conversion Nuclear Battery

Nuclear batteries can be seen as a source of radiation from a variety of materials, one of which is a converter. The purpose of the nuclear batteries design is to deposit most of the power generated by the source into the converter. The efficiency of nuclear batteries varies depending on the source, the converter, and the method of interface of the source and the converter. The matching between the length of the transducer scale and the range of ionizing radiation is one of the most important parameters affecting the efficiency of nuclear batteries [62].

The energy accumulation in the semiconductors of the beta particles, the penetration depths and the amount of e-h pairs in the semiconductors are of great importance in the efficiency of the betavoltaic battery. Therefore, the parameters determining the semiconductor design, such as junction depth or top layer thickness, doping concentrations and thickness, are important to increase e-h pairs production. The efficiency of the battery also varies depending on how the beta particle energy is selected, the angular emission of beta particles such as isotropic or non-isotropic emissions, and the self-absorbing effects [62]. Therefore, charging particle current and the external emission of ionizing radiation sources are other important parameters that affect efficiency. Three factors determine density of the beta particle flux: specific activity of the radioactive isotope, mass thickness of the source layer and absorption of beta particles in the protective layer [20]. The half-life, specific activity, toxicity, purity and reliability of radioactive source, and also radiation damage are among other parameters that affect the performance of the nuclear battery [17].

In summary, the efficiency of betavoltaic batteries is controlled by the following main processes: self-absorption in beta source; the collection efficiency of electron-hole pairs produced in the space-charge region of the semiconductor part of the converter; secondary X-ray radiation, which occurs when electrons interact with the

semiconductor structure [62]. Below, important parameters that affect the efficiency of the betavoltaic batteries are discussed separately.

2.3.1 Effects of Radioisotope Selection

Radioisotopes can emit alpha particles, beta particles and gamma rays. In theory, any kind of radiation can be used to produce electricity in nuclear batteries. But in practice, beta-emitting sources are more suitable as a source of power for the direct conversion nuclear batteries. Alpha particles can cause damage to the junction regions due to their high energies, which will quickly degrade the structure. Gamma rays are difficult to absorb in small junctions because of their strong penetration ability. Both beta and alpha-emitter radioisotopes are used in the direct conversion nuclear battery studies. Beta sources, however, are more preferred than alpha sources [91]. Important parameters to be considered in the selection of beta source; reliability, cost, safety, efficiency, size, half-life and maximum energy [2]. A few beta-emitting radioisotopes most commonly used in betavoltaic batteries and their properties are given in Table 2.3.

The most important reason limiting the use of all radioisotope power and its conversion to useful electrical power is self-absorption. In applications, only a small portion of the power in the source can be used, and the majority of them are absorbed by the source itself. Therefore, it is necessary to use thin radioactive films to effectively transform the radiation [27].

Table 2.3 Radioactive properties of tritium (H3), Ni63, Pm147 and Sr90/Y90 beta sources for nuclear batteries [20].

Isotope	**Half-Life (year)**	**Average Decay Energy (keV)**	**Maximum Decay Energy (keV)**	**Specific Activity of the Chemical Compound (Ci/g)**
Tritium (H3)	12.32	5.7	18	1100
Ni63	100.1	17.4	67	57
Pm147	2.62	62	225	800
Sr90/Y90	28.9	198/930	540/2240	116

The radioisotope beta sources used in experimental and theoretical studies in the thesis are as follows:

Nickel 63 (Ni63):

As shown in the Table 2.3, Ni63 is a beta emitter with a half-life of 100.1 years, an average energy of about 17 keV and a maximum energy of 67 keV. Therefore, power supplies can extend the operating life of a system by almost a century. The beta spectrum of Ni63 is below the radiation damage threshold of semiconductors such as Si and SiC (about 200 keV for Si). In addition, Ni63 is easier to use than other beta particles such as H3, Pm147 and Sr90 due to its low energy spectrum and solid metal form [92].

Promethium 147 (Pm147):

Promethium 147 (Pm147) is a soft beta emitter with 99.9% abundance; it has an average energy of 62 keV and a maximum energy of 225 keV. It has a half-life of 2.62 years. Pm147, which is deposited on surfaces by irradiation in Promethium oxide (Pm_2O_3) chemical form, has been widely used in low-power betavoltaic micro-batteries produced for cardiac pacemaker applications in the past.

Strontium 90 (Sr90):

Strontium90 (Sr90) is a pure beta emitter with average decay energy of 196 keV and maximum decay energy of 546 keV. It has only a beta decay mode and has a long half-life of 28.9 years. It has Yttrium90 (Y90) daughter with a negative beta emission. The Y90 emits a negative beta radiation (E_{max} = 2.283 MeV) with a half-life of almost 64 hours and then decays into stable Zirconium90. Sr90 is a by-product of the fission reaction of Uranium and Plutonium in a nuclear reactor.

2.3.2 Effects of Semiconductor Selection

Direct conversion nuclear batteries generally use semiconductor p-n junction as a converter with materials such as Si, GaN, SiC and GaP [93]. The semiconductor p-n junction is the key part of the electrical performance of the betavoltaic battery, so the efficiency depends on the quality of the semiconductor material of the diode. The diode also affects the open-circuit voltage of the battery [9].

In general, wide-band gap semiconductors have the advantage of higher radiation resistance, allowing the use of higher-energy radioisotope sources [25]. To achieve higher power conversion efficiencies, it is important to use wide-band gap materials that provide low leakage currents [27]. In a silicon betavoltaic battery, the diffusion length remains longer than the depth at which electrons are generated, but lifetime deterioration causes a significant change in open-circuit voltage. But, in a wide-band gap semiconductor, such as GaN, there are several factors that provide higher efficiency. Most importantly, the voltage of the betavoltaic battery is higher due to higher band gap [21]. Furthermore, the use of wide-band gap semiconductors increases radiation tolerance in betavoltaic batteries. The maximum energy of the beta particles should not be higher than the threshold energy of the semiconductor for radiation damage. In addition, the penetration depth is a function of the material density; a more dense material requires shorter distances. For this reason, a thicker material is needed for less dense material to absorb beta radiation. For example, Si, which has about half the GaN density, will require two times the thickness according to GaN [17].

According to the operation principle of the betavoltaic battery developed by Olsen [74], the effectiveness of betavoltaic conversion increases with the band gap (E_g) of semiconductor converters. The graph of the maximum efficiency of betavoltaic battery depending on semiconductor band gaps is given in Figure 2.12. Betavoltaic efficiency is about 22% for semiconductors with E_g ~ 2 eV and about 15% for silicon.

Although wide band gap materials have advantages in terms of power conversion efficiency and radiation tolerance, there are still weaknesses in terms of costs and difficulties in the production process, especially in SiCs. In addition, due to the small diffusion lengths in wide-band gap semiconductors, the efficiency of collection is low. If the diffusion length for cell thickness is too small, the aggregation efficiency is low (L<<d). This criterion means the loss of a high minority carrier in a collective manner. For example, the efficiency of the wide-band SiC-Pm147 betavoltaic battery is smaller than the efficiency of the high-quality silicon-Pm147 betavoltaic battery [77].

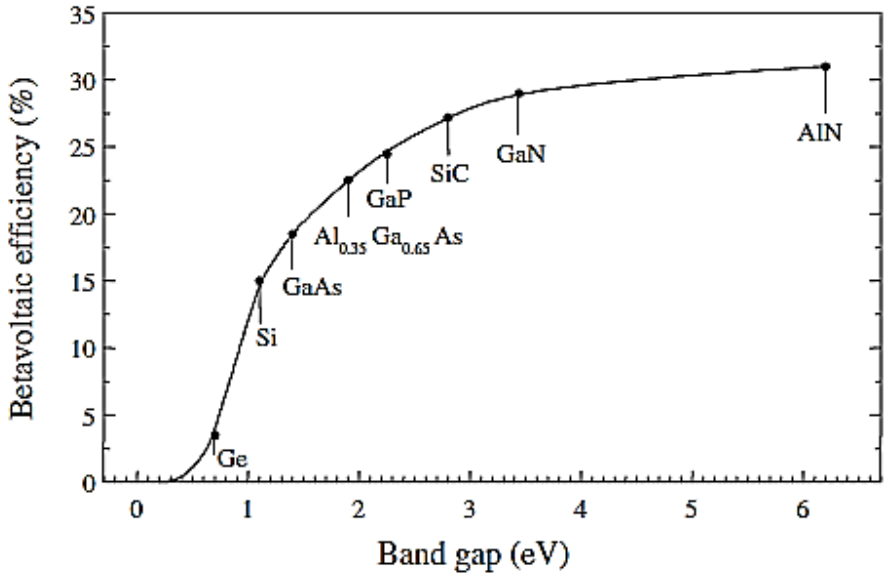

Figure 2.12 Theoretical maximum of betavoltaic efficiency depending on semiconductor band gaps [18, 74].

In recent years, big progress has been made in developing the quality of silicon and new classes of semiconductor materials have arisen with wider band gaps than silicon. Many types such as crystalline silicon, patterned silicon, amorphous silicon, silicon carbide, porous silicon have been formed. The traditional semiconductors used in betavoltaic batteries have planar surfaces. Porous silicon can be used to maximize the event flow and growth of the active surface area of the semiconductor junction. This significantly increases the surface area of the material to absorb the beta particles and provides higher efficiency. The fact that the radioactive material is in the immediate vicinity of the pores makes it possible to convert the maximum amount of energy [14]. However, the desired level of success in the production stage has not been achieved yet. Artificial manipulations on the material surface increase errors and limit conversion efficiency. In order to solve this problem, the use of vertical p-n junction silicone in the betavoltaic cell without damaging the semiconductor surface was emphasized [94]. A new development in betavoltaic batteries is the idea of using amorphous or liquid semiconductor. High-energy emissions from radioactive isotopes can slowly disrupt semiconductors in solid

crystal or lattice structures. This results in decreased efficiency over time. Liquid semiconductors have also been used to overcome this result [14].

2.3.3 Effects of Semiconductor Thickness

The thickness of the emitter, base and depletion zones of the photovoltaic cell should be consistent with the range calculated by taking into account the average energy of the beta particle [15]. One of the most important issues affecting the efficiency of betavoltaic battery design is the thickness of the top layer (junction depth) [95]. The thicknesses of the layers affect the collection efficiency and accordingly short-circuit current, also seen in the equations given in Section 2.2.

If the e-h pair is produced at a diffusible distance to the depletion zone of the p-n junction, the natural electro-static potential can separate the e-h pair before recombination. Otherwise, e-h pairs that are not produced near the depletion zone undergo recombination. The thickness of the material (in particular the top layer thickness) must be adjusted to match the beta-radiation penetration of the semiconductor material in order to increase the collection of the e-h pair and to achieve high conversion efficiencies. That is, the range of beta particles in the material must match the length scale of the device and this is the first guiding principle. The p-n junction structure in which the radiation-dependent current is generated and the e-h pairs formed by the radiation are separated and disposed by the built-in electric field is important for the betavoltaic batteries. The collection efficiency of e-h pairs in the depletion zone is higher than in the n-type and p-type regions, as shown in Figure 2.13. So, for highly efficient p-n junction betavoltaic cell, the depletion region should be designed at a suitable thickness and depth to significantly improve the output power [7]. However, the depletion zone is limited to the thickness micrometer range (~1 μm) [15]. The junction thickness of the n-type region is very large and deep; therefore, the number of e-h pairs formed in the n-type region is high and makes a significant contribution to the current [7].

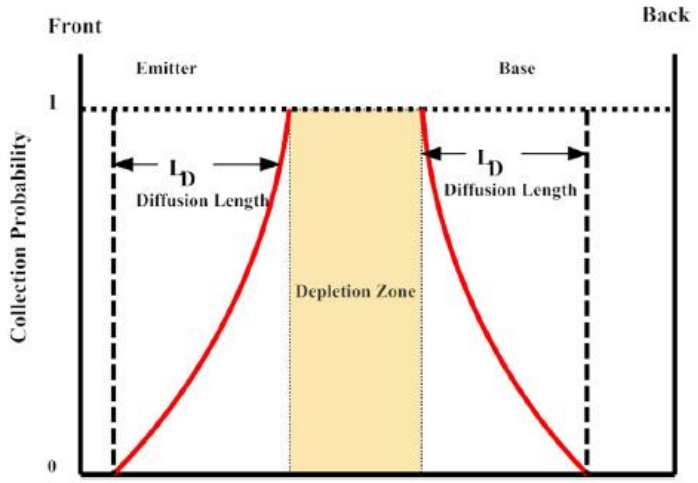

Figure 2.13 The collection probability for a linearly scaled betavoltaic battery. The collection possibility is insignificant beyond the diffusion length of carriers [15].

In a betavoltaic cell, the minority carriers in the n-type region and the p-type region can be collected by diffusion transfer to the depletion zone, so the minority carrier diffusion length is a critical parameter affecting the electrical performance and collection efficiency of the device. If the diffusion transfer length is greater than a diffusion length of a minority carrier, almost all of the e-h pairs produced are recombined prior to spreading to the depletion site [40]. In other words, if the diffusion length exceeds the upper layer and depletion zone thickness, the collection of e-h pairs produced by the electron flow will be highly effective [96]. Therefore, in semiconductor selection, materials with high diffusion length and diffusion lifetime should be selected and layer thicknesses should be adjusted according to these values.

2.3.4 Effects of Doping Concentration

An intrinsic semiconductor refers to a pure semiconductor with no impurities in the crystal lattice. The operation of adding impurities atoms through diffusion is called doping. Doping is a method for creating excess holes and electrons in semiconductors and allows the use of semiconductors in the construction of electronic devices [54]. The p-type semiconductor has a great number of positive charge carriers (holes) and the n-type semiconductor has a great number of negative

charge carriers (electrons). Placing these two types of material together will allow charge movement to cause an electrical current to be generated when a potential is applied. This is known as a p-n junction [14].

In the p-n junction betavoltaic batteries, the doping concentration has direct effects on the collection efficiency, the leakage current, the depletion region width and the minority carrier diffusion length. A low doping concentration expands the width of depletion region, which increases the amount of charge collected and short-circuit current. However, a low doping concentration also increases the leakage current, which reduces the open-circuit voltage. The leakage current increases inversely with the decrease in the doping concentration. A low doping concentration increases the minority carrier diffusion length, which increases the charge collection efficiency [54]. In addition to those produced in the depletion region, e-h pairs produced within a diffusion length adjacent to the depletion region may also contribute to the generation of electricity. Therefore, the minority carrier diffusion length is a key factor affecting the short-circuit current and conversion efficiency in the betavoltaic cell. Minority carrier diffusion length decreases as doping concentrations of the emitter and base regions increase. Therefore, a lower doping concentration generally leads to a greater collection efficiency and short-circuit current [95].

As a result, doping concentrations in the emitter and base regions in the p-n junction should be optimized to achieve a high conversion efficiency of the betavoltaic battery. Because it has a direct effect on the important parameters affecting the efficiency such as leakage current, depletion region width, diffusion coefficient, carrier lifetime and the diffusion length of the carriers [73, 95].

2.3.5 Effects of Radiation Damage

Due to the deterioration of the semiconductor materials when it is exposed to beta radiation, the performance of betavoltaic battery may decrease over time, the power output may deteriorate and the battery may fail prematurely. Some measurements and calculations can be used to determine radiation damage. These measurement parameters include power output deterioration, capacitance voltage, carrier concentration, minority carrier diffusion length, radiation damage factor, and open-circuit voltage. Radiation damage in betavoltaic batteries depends on both the

particle energy emitted by the radioisotope and the radiation hardness of the semiconductor material [54]. Higher energy particles penetrate the semiconductor material more so that they form more e-h pairs, but damage the material lattice faster. [11]. The radiation resistance of the semiconductor material depends on the strength of the atomic bond, the size of the atoms in the crystal lattice and the migration barriers of vacancy and interstitial of the semiconductor. The possibility of radiation damage to the battery can be minimized by reducing beta particle energy and selecting appropriate materials [54].

Radiation damage often limits the efficiency of nuclear batteries and adversely affects them and worsens over time. Ionizing radiation has effects such as displacement of the atoms that cause damage in the semiconductor material, localized heating, ionization, and core transformation. When exposed to ionizing radiation, there is a possibility that a solid may be damaged by a gas or liquid due to collisions [62].

The effects of radiation damage to the semiconductor material should be considered in the design of betavoltaic batteries. At best, the maximum kinetic energy of beta particles should be smaller than the radiation damage threshold of the semiconductor material [84]. If not, the energy of the emitted beta particles will be sufficient to displace the atoms in the semiconductor lattice. Defects in the material due to radiation damage, increased leakage currents, shortened minority carrier diffusion lengths, shortening the life of the device and generally lead to reduced battery performance. Wide band gap semiconductor materials such as GaN and SiC have higher atomic bond and radiation damage resistance, and have the potential to achieve greater betavoltaic conversion efficiency [54, 84]. For example, GaN has a damage threshold of 440 keV [97] with a high radiation resistance when silicon has a damage threshold of 200 keV [92, 97]. However, wide band gap semiconductor materials are generally characterized by lower mobility and carrier lifetime, which adversely affect diffusion lengths. To keep radiation damage at low levels, appropriate beta sources such as H3, Ni63 and Pm147 should be used for betavoltaic batteries [98]. Another solution method may be to place the appropriate material between the semiconductor and the beta source using the indirect conversion method.

CHAPTER 3

THEORY OF INDIRECT CONVERSION NUCLEAR BATTERY

The performance of a betavoltaic battery containing a semiconductor exposed to high energy electrons is limited by radiation damage in the semiconductor. Therefore, as an alternative, research has been conducted since the 1950s on the indirect conversion of ionizing radiation energy into electrical energy. Numerous indirect conversion nuclear battery designs have been developed. These designs have differences in terms of battery designs and other properties, as well as the radionuclide and phosphor used [18]. Basically, in the battery design, a phosphor layer that absorbs energetic beta particles emitted from the radioisotope source and then re-emits energy in luminescence is placed between the radioisotope and the semiconductor diode. The luminescence is then converted to electricity by means of semiconductor materials [99]. There are two stages of energy conversion: the radiation energy emitted from the radioisotope is first converted into light and then into electrical energy [32].

The indirect conversion nuclear battery is advantageous in that the semiconductor is not exposed to direct ionizing radiation, thereby minimizing or eliminating radiation damage. Because phosphor layers are more stable than photovoltaic devices [45]. Therefore, indirect conversion can use a radioisotope in nuclear batteries that emits charged particles of higher energy. Although the initial overall efficiency is lower, the power output is higher in the long run and the battery life is longer than betavoltaics due to its resistance to radiation damage. Indirect conversion nuclear battery stands out as autonomous devices that are practical and require no power supply. The spectral composition of these batteries has a wide range from UV to near-IR. They also have a long service life [18].

Although indirect conversion nuclear batteries have such advantages, there is still a limited power output in applications [99]. The efficiency of electrical power generation for the indirect conversion nuclear battery depends on the matching of the emission spectra of the light source and the photovoltaic sensitivity [18]. However, it is difficult to achieve good overall energy conversion efficiency because two-step process is required to generate electricity and separate losses occur at each step. The efficiency of the first step can be enhanced by performing high absorption of charged particles reaching the phosphor layer and minimizing light self-absorption in phosphor. The efficiency of the second step is mainly determined by the amount of incident light that can be absorbed in the depletion region and the compatibility with the energy band gap of the semiconductor used in the photovoltaic [3].

3.1 Radioluminescence and Radioluminescent Materials

Radioluminescence is the photon emission of the substance during the electron transition while returning from the excited state to the steady-state after absorbing the ionizing radiation. The substances can be excited by irradiating with high-energy photons or electrons. In this context, the photon emission resulting from the excitation of high energy electrons is called cathodoluminescence, and the photon emission resulting from the excitation of high energy photons is called photoluminescence [100, 101]. Luminescence, i.e. photon emission, usually occurs within the visible range of the electromagnetic spectrum but is not limited to this region. The luminescence can be divided into two categories, fluorescence, and phosphorescence, depending on the duration of the emission. Fluorescence is an instantaneous incident light emission when applying an external energy source. Phosphorescence is the condition that the light emission continues for a certain time even after the external energy source is removed [102].

Much of the success in the design of a high-efficiency indirect energy conversion battery depends on the choice of luminescent material that converts radiation energy into light. Luminescent material, which is usually phosphor, must be resistant to radiation damage, have high energy conversion efficiency, and emit photons at a maximum precision range for the photovoltaic device. Many materials have been used for photon emission by absorbing nuclear radiation. In general, phosphor

materials can be divided into two main categories: organic and inorganic. Inorganic phosphors are more effective than organic phosphors for nuclear excitation since organic phosphors are less preferred due to instability at high temperatures and low absorption power for high energy charged particles [103].

Phosphor is a wide band gap semiconductor doped with impurities to change the energy gap for photon emission at a given wavelength emitted when it absorbs external energy. It is usually in powder form but is converted to thin-film form because it has more practical use in applications [104]. Phosphor substances are crystals with at least two major physical components. They consist of a host lattice and an impurity atom, usually an activator ion. Occasionally, an additional impurity ion is added which transfers energy to the activator, increasing the emission intensity of the activator. The host cage may be selected for physical conditions such as high operating temperature, whereas the activator may be selected to emit a desired light color by producing deep receiver levels at different depths [105]. Radioluminescence in inorganic phosphors occurs through donor-acceptor pair recombination or rare-earth dopant ion-center recombination. In the latter, rare-earth dopant ions are introduced into the inorganic phosphor crystal, thereby placing electronic energy levels within the wide band gap (usually 3.5 - 6.5 eV) of the inorganic crystal. Luminescence occurs when excited electrons switch between these dopant energy levels [32].

The zinc sulfide group of inorganic phosphors is more practical, durable and efficient for light sources induced by nuclear radiation. An energy conversion efficiency of about 25 percent has been reported for ZnS type phosphors under nuclear radiation stimulation [103]. The most effective known radioluminescent materials include phosphors based on A2B6. Another class of efficient radioluminescence materials is alkali halides such as NaI (Tl) and CsI (Tl) [18]. $ZnS:Cu^{+},Co^{2+}$, used in clocks, was the most well-known phosphor material until very recently. However, this phosphor has short deterioration time and moisture sensitivity. In the 1990s, a number of new phosphor materials such as $SrAl_2O_4:Eu^{2+}$ and derivative $SrAl_2O_4:Eu^{2+},Dy^{3+},B^{3+}$ were discovered. At present, phosphor materials can be classified into six groups: 1. Aluminates, 2. Silicates, 3. Aluminosilicates, 4. Oxides, 5. Oxysulfides, 6. Sulfides [106].

Phosphors are often used as radiation sensors because they emit light when exposed to ionizing radiation [105]. Since 1930, radioluminescent dyes, which are mostly used in the watch industries, have had commercial applications. A pure beta emitter has been found to cause relatively little radiation damage to phosphor [101]. In addition, thin film phosphors having a thickness equal to the beta particle spacing have the advantage of reducing self-absorption light emission. They are widely used in thin film electroluminescent (TFEL) devices. The most common phosphor material used here is ZnS:Mn, but CaS, SrS, gallates and thiogallates have recently been developed. Thin cathodoluminescence films are highly popular for use in field emission displays (FEDs) and plasma display panels (PDPs) [18]. Phosphors can be dispersed on any surface and can eliminate an operator's exposure to harmful radiation. Phosphor powders are chemically inert and resistant to various harsh environments [102]. Also inorganic phosphors that have emission in the visible spectrum have also attracted attention in recent years due to their potential applications in optoelectronics such as lightning systems. With the help of phosphor, higher energy efficiency can be achieved than conventional lighting systems. Likewise, in the context of energy saving, phosphor films can be used in highway or railway signaling systems, in utilitarian or emergency lighting of buildings. In addition, phosphor powders are embedded in polymer matrices to obtain new materials adapted to specific applications as well as to maintain the integrity of the crystalline structure of the phosphor by separating it from the external environment. Today the phosphor composites are obtained by embedding copper doped zinc sulfide (ZnS:Cu) or strontium aluminate phosphors in polymer-matrices such as polystyrene (PS) or polymethylmethacrylate (PMMA) [107].

In summary, doped inorganic phosphors have been used extensively in areas such as radiation detection, lamp industry, cathode ray tube indicators, and nuclear light efficiency of approximately 25% have been achieved for some phosphor species. The rate of degradation of phosphor materials is expected to be slower than that of photovoltaic cells used to convert radioluminescent emission [32].

3.2 Influence of Beta Irradiation on Phosphors

3.2.1 Mechanisms of Radioluminescence of Phosphors

When exposed to radiation, phosphor materials store radiation energy, emit energy as light, and continue to emit light for a long time after the radiation stops [18, 108]. In this process, the emission of photons during the transition of the excited electrons from the conductivity band to the ground state is called radioluminescence.

The mechanism of radioluminescence is based on the interaction of ionizing radiation with matter. Radiation interacts with matter by producing electrons, holes, and excitation in the medium. A series of physical processes take place in the phosphor material, including emissions of secondary electrons, back-scattered radiation ions and Auger electrons [100]. The high-energy secondary electrons are further stimulated by collisions and rise to the conductivity band. These energetic electrons transmit energy to the luminescence centers (activation centers). Most of the energetic electrons continue in the solid phosphor layer and form electron-hole pairs; a small part of the electrons are dispersed and reflected. Electron-hole pairs can perform radiationless recombination and transfer their energy to activator ions and then emit light. This process is called radiation recombination. As illustrated in Figure 3.1, the recombination of electrons and holes occurs at the center of the luminescence and makes it excited and causes light emission.

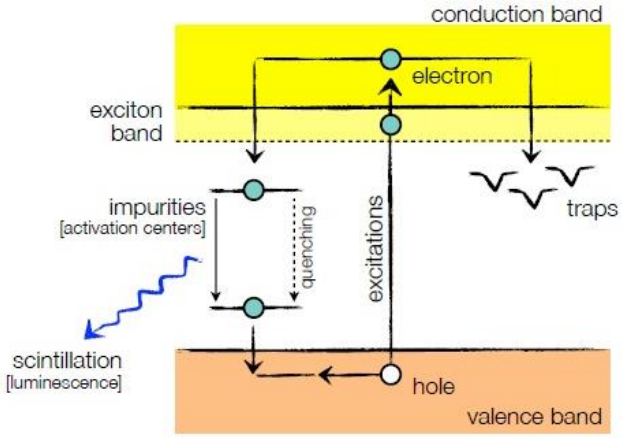

Figure 3.1 Energy bands, excitations, scintillations, quenching and traps in the phosphor material [109].

Most phosphors consist of a transparent micro-crystalline host and one or more activators, i.e. a small amount of purposely added impurities ions dispersed in the host lattice, to allow transfer of visible light to the surface of the phosphor [110]. The activators are added to the phosphor materials for the transport of energy. The luminescence spectrum is independent of the characteristics of the exciting radiation and depends on the nature of the activator [18]. Furthermore, the color of the photon emission can be adjusted by selecting the activator ion without changing the host cage [111]. The luminescence properties of a phosphor can be characterized by emission spectrum, decay time and brightness [100].

The luminescence of commonly used phosphors such as ZnS:Cu,Cl and $SrAl_2O_4$: Eu^{2+},Dy^{3+} is explained by the donor-acceptor recombination model. In this model, as described above, phosphor substances emit light caused by the relaxation (radiation recombination) of electrons induced by radiation energy. There are also many alternative relaxation paths that do not result in recombination, such as energy discharges from lattice vibrations or carrier thermalization. To increase the amount of radiation recombination, dopant ions (activator and co-activator) are introduced into the host lattice of the material. These ions, which are usually metals or rare-earth elements, have energy states that remain within the range of band gap of the material. As a result of excitation, the electrons of the host lattice are excited beyond the band gap and relax in one of the excited states of the dopant atom. The excited electron relaxes further to a lower energy state associated with the dopant and emitting a photon in the process. The luminescence is obtained directly from the host or from activators/additives intentionally added to the host lattice. One activator tends to absorb energy from the primary excitation and transfer it to the other activator to increase the light intensity [100]. The energy transfer processes in the phosphor material are shown in Figure 3.2.

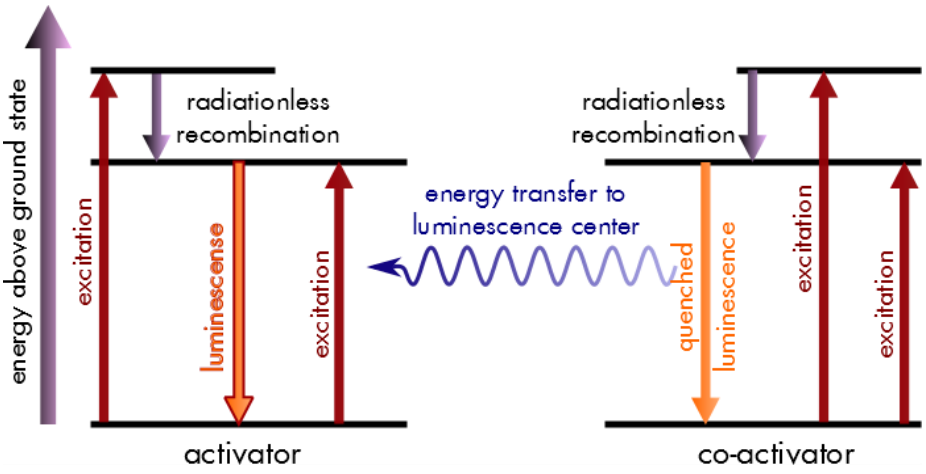

Figure 3.2 Process of the luminescence [112].

3.2.2 Radiation-Induced Degradation of Phosphors

Phosphor degradation is a decrease in the efficiency of a phosphor material due to prolonged exposure to ionizing radiation. Exposure of phosphor material to radioactive particle bombardment may cause crystal structure damage. In irradiated crystals, especially in semiconductors (including most phosphor materials), atoms (ions) pass from normal lattice regions to irregular regions. Therefore, point defects occur in the phosphor crystal. Displacement energy is required for the displacement of an atom. The size of this parameter varies depending on the nature of the material and the mass of the displaced atom and is between 5 and 80 eV. Radiation defects can produce energy levels at various depths in the forbidden band of the phosphor crystal. These levels have different functions in the electron and hole traps and the quenching sites. Point defects can interact with radiative recombination centers, thereby altering their energies and radiation properties accordingly. At the same time, point defects can act as color centers in the crystals and have absorption bands in the luminescence region of the radiated recombination centers [18]. Since most of the color centers usually absorb ultraviolet light, the phosphor crystals emitting light in the visible region are expected to be less damaged from radiation [113].

Radiation defects usually lead to a decrease in brightness intensity over time [18, 114]. In the design of radioluminescent nuclear batteries, a binder is often used to fix phosphor. Since the binder is also exposed to the radiation field, radiation-induced transformations can occur. Due to radiation damage to the phosphor material, the

energy conversion efficiency generally decreases after irradiation, depending on the type and energy of radiation, the absorbed dose rate, the type of phosphor and the binder [18]. In order to increase radiation tolerance, it is beneficial to develop and use quantum dot nanophosphor. It has also been reported in studies that radioluminescent nanoparticles exhibit greater radiation tolerance than their bulk counterpart [32].

3.3 Indirect Conversion Nuclear Battery Designs

In the design of the indirect conversion nuclear battery, the two-stage conversion process should be considered. In a generally preferred composition, a layer of phosphor that absorbs energetic particles emitted from the radioisotope source and then re-emits luminescence energy is placed between the radioactive source and the semiconductor transducer. The resulting luminescence is absorbed by the semiconductor material and converted into electricity [99]. The laminated design of a typical indirect conversion nuclear battery consisting of a radioactive beta source, phosphor layer acting as an intermediate product, and photovoltaic (PV) devices is shown in Figure 3.3.

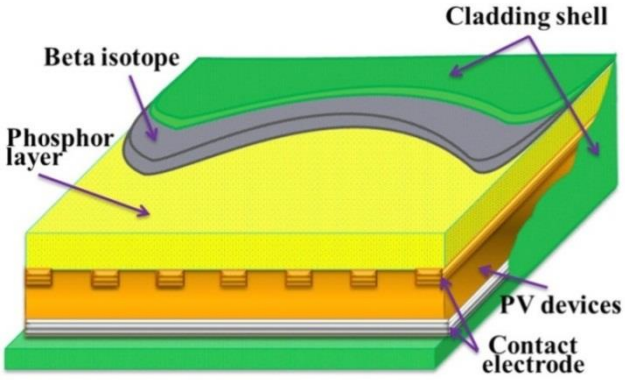

Figure 3.3 Schematic diagram of the indirect conversion nuclear battery [99].

The radioluminescence phosphor layer, which acts as an inter-absorbent, may consist of semiconductor or insulator materials that emit visible light when excited by high energy photons or ionizing radiation. This layer protects the photodiode from radiation. As the phosphor material is less affected by radiation, radiation-related

damage in the battery is reduced [32]. Some of the structures that can be used as radioluminescence material in battery design are nanotubes or micro spherical structures filled with tritium, thin-film phosphor, and nano-sized phosphor powders. In the selection of radioluminescent materials, it has been reported that it uses a variety of inorganic phosphors such as ZnS and strontium aluminate, as well as CdSe-based phosphors, tritium in micro or nano-sized particles and aerogel phosphor composition containing tritium or organic luminophores [35].

The radioisotope layer must be thin enough to allow isotropic beta emission to leave the radioisotope source and enter the phosphor layer. Beta emission spectrum and emission angle should be considered for optimization of thickness. The thickness should be less than the range of beta particles scattered from the radioisotope layer. Some of the beta particles symmetrically having both up and down vector components are likely to enter the phosphor layer. Therefore, placing a reflective aluminum layer on the outer side of the weld may prevent beta particle losses [62]. The maximum range of radioisotopes can be calculated with Eqn. (2.10).

The phosphor layer which interacts with the beta particles must be thick enough to absorb all of the energy of the beta particles. After the interaction, photons with isotropic emission in phosphor are produced. The phosphor layer must be sufficiently thin to avoid self-absorption of these photons. Therefore, the thickness of the phosphor layer should be greater than a range of beta particles in phosphor, but less than the average free path of a produced photon. Thickness of the phosphor layer is calculated using the empirical formula [33]:

$$d = \Delta m/(S\rho) \tag{3.1}$$

where, d is thickness of the phosphor layer, Δm is the weight difference between the starting and final substrate, S is the surface area, and ρ is the density [33].

The photons produced must pass through the binding layer, if any, before reaching the photovoltaic cell. So the binder must be sufficiently transparent and thin. However, double losses occur due to total internal reflection at both the phosphor-binder and binder-air interfaces. When the phosphor is deposited directly on the semiconductor surface, the total internal reflection at the phosphor-photovoltaic

interface is reduced, since the photovoltaic cells generally have an equal or higher refractive index [18].

The photovoltaic cell used in a nuclear battery is essentially the same type as the cell used in a solar battery. The photovoltaic cell has an energy band gap that must be matched as closely as possible with the emission spectrum of phosphor [62]. In order to optimize the performance of an indirect energy conversion battery, the response spectrum of the photovoltaic cell must first be matched to the emission spectrum of radiophosphors [18]. The emission spectrum of the phosphor layers can be considered between visible light, that is, about 400 to 750 nm wavelengths. The corresponding photon energy range is from 1.65 to 3.1 eV. If the photovoltaic cell energy band matches the emission energy of the phosphor used, the battery efficiency will increase. Therefore, wide band gap semiconductor photovoltaic cells should be preferred in the design.

Nowadays, considering current studies, indirect conversion nuclear batteries produce relatively low power output [62]. In order to increase power generation, particular attention should be adjusted to the following aspects in the designs: The thickness of the radioactive source should be optimized, the reflective layer should be used, the phosphor composition should be improved according to the radioluminescence efficiency and the self-absorption of the photon should be reduced [18].

3.4 Energy Conversion Efficiency of Indirect Conversion Nuclear Battery

The indirect conversion of radioactive decay energy to electrical energy seems less efficient than direct conversion. This two-stage conversion can be less efficient as losses will occur in both steps. The efficiency of each energy conversion stage is assessed separately [41]. The loss of kinetic energy of betas before reaching the phosphor layer and the loss of photons due to configuration geometry are among the most important losses. The advantage of indirect conversion is that the radiation tolerance of phosphor is higher than that of the semiconductor device, and the indirect conversion power output may be higher than direct conversion when evaluated in the long term [26]. Therefore, analysis and testing are required in design for optimum energy conversion efficiency [18].

In theory, the efficiency of indirect conversion nuclear batteries is around 25% [35]. At the same time, the photo- and radioluminescence efficiency of phosphor and semiconductor materials is in the range of 20% to 25% [18, 32]. However, these values have not yet been achieved in practice. The life of the battery depends on the half-life of the radioisotope and how fast the radioluminescent material decays with high-energy radiation [35]. Extensive studies have focused on improving energy conversion efficiency by using a variety of radiation sources, different types of phosphor and semiconductor materials such as single-crystalline silicon, GaP, and AlGaAs [99].

Critical targets in indirect energy conversion nuclear battery design are high tolerance to ionizing radiation, high radioluminescence efficiency, and proper matching of emission wavelength to the spectral response of the semiconductor device [34, 50, 99]. Therefore, the efficiency of the indirect conversion nuclear battery generating electric energy depends on the emission power of the phosphor material and the matching of the maximum spectral response curve of the photovoltaic cell [18, 62]. The radiation tolerance, thickness, homogeneity, particle size, and band spacing, efficiency, spectral sensitivity of the phosphor layer can be optimized to improve battery performance and conversion efficiency [32]. In addition, the correct connection between the radiation source, phosphor, and photovoltaic cell is required to achieve maximum nuclear-electric conversion efficiency. Therefore, designs that maximize radioluminescence transmission should be realized. Assuming a planar geometry, the phosphor layer must be thick enough to absorb most of the radiation, but allow the transmission of emitted light to avoid self-absorption. The thickness and homogeneity of the films in which the nanocrystalline phosphors are deposited can be better adjusted [115].

Energy efficiency in the conversion of radiation to luminescence is the ratio of luminescence energy to absorbed radiation energy. That is, the internal efficiency is equal to the ratio of the number of radiation emitted from the source to the number of recombination of electron-hole pairs in the phosphor material [116]. Theoretically, phosphors can produce highly effective emissions. In practice, however, the efficiency of phosphors is lower due to non-radiation recombination mechanisms [49]. Since recombination radiation is spread in all directions, most of it is reflected

back from the crystal surface and absorbed in the device [116]. Furthermore, most of the energy of the beta particles penetrating the phosphor layer is lost as a result of inelastic interactions with lattice ions. These interactions result in Auger electrons, x-rays, phonons, secondary electrons, and electron-hole pairs. Thus, only part of the energy transferred to phosphor is converted to light emission [18]. It should be noted that by increasing the thickness of the phosphor layer, the produced phosphor light cannot be intensified. Optical effects such as scattering, absorption, and light capture determine the optimum thickness for the maximum brightness of the phosphor [49]. Another important problem affecting phosphor performance is surface charge. Since phosphor is generally a wide-band gap material, a negative charge resulting from a low secondary electron emission coefficient can accumulate on the surface. The accumulated charge changes the surface potential and therefore the kinetic energy of the primary electrons. It also increases the possibility of e-h pairs separating before they come together to emit light [104].

Developing an appropriate phosphor layer structure is an important opportunity to improve the efficiency of indirect conversion nuclear battery [99]. In addition, in recent years for the selection of phosphor material, persistent luminescent phosphors have attracted attention because of their high quantum efficiency, long phosphorescence, and good stability. Persistent luminescent phosphors such as $SrAl_2O_4:Eu^{2+},Dy^{3+}$ have both a higher initial density and a longer life than ZnS-type phosphors [117].

CHAPTER 4

EFFECT OF BETA SOURCE AND PHOSPHORS ON PHOTOVOLTAIC CELLS

In this chapter, conversion of kinetic energy from the decay of a radioactive isotope to electricity is investigated experimentally by using the direct and indirect conversion methods. In this context, simple nuclear battery models are designed. Analysis of the effect of low-activity radiation from Pm147 and Sr90 beta sources on crystalline silicon photovoltaic cell is performed. Phosphor layers with different mass thicknesses are prepared from crystal powders of copper chloride doped zinc sulfide (ZnS:CuCl) and Eu^{2+} Dy^{3+} codoped strontium aluminate ($SrAl_2O_4$:Eu^{2+},Dy^{3+}) phosphors. In addition, a planar geometry used is formed by combining a thin film beta source, phosphor layer, and photovoltaic cell without a gap. Both the influence of beta sources and the phosphor layers on battery performance is analyzed separately. Moreover, the effect of graphene usage on the battery models is investigated. Effect of beta sources and phosphors is observed on the photovoltaic cell by measuring short-circuit current and open-circuit voltage. The efficiency of the battery models is determined with the obtained results. Furthermore, short-circuit current values are examined at various times during the irradiation.

4.1 Materials

In this study, Strontium-90 (Sr90) and Promethium-147 (Pm147) are preferred as radioactive beta sources. The intense presence in the nuclear reactor wastes and the long half-life make the choice of Sr90 as the radioactive source attractive. In other words, nuclear reactor wastes such as Sr90 may be considered as nuclear batteries or mini nuclear fuel in the future. Pm147 is used frequently in betavoltaic battery studies because it produces high energy and reduces radiation damage due to its

kinetic energy which is lower than Sr90. Liquid Pm147 and Sr90 radioactive sources are obtained from Eckert & Ziegler Isotope Products. 3.7 MBq Pm147 liquid beta source poured between plastic thin films and dried is made ready to use. Activity value of this film of size 3.5 cm×4.5 cm is approximately 4400 Bq/cm^2 is measured. Also, 3.7 MBq liquid Sr90 beta source is used in the glass tube. The activity of the Sr90 beta source emitted from the glass tube is measured as 20 kBq/cm^2.

ZnS:CuCl and $SrAl_2O_4:Eu^{2+},Dy^{3+}$ phosphor materials given in Table 4.1 are preferred as a luminescent material for the indirect conversion method because it has a widespread application in the literature. For many decades, zinc sulfide (ZnS) is the most famous and widely used persistent phosphor. ZnS is proper for usage as the phosphor layer in an indirect conversion nuclear battery. It has a wide band gap (3.5–3.7 eV), a high light transmittance, and low dispersion in the infrared and visible regions [99]. On the other hand, in recent years the $SrAl_2O_4:Eu^{2+}$, Dy^{3+} phosphor has attracted a lot of attention because of its high quantum efficiency, good stability, and long afterglow. Its long afterglow features have resulted in its utilization in a wide variety of light-emitting devices [100].

Table 4.1 Parameters of inorganic crystalline powder phosphors used in the study.

Phosphor	**Luminescence color**	**Density (g/cm^3)**	**Grain diameter (µm)**	**Afterglow (hour)**
ZnS:CuCl	Green	1.78	~20	~ 4½
$SrAl_2O_4:Eu^{2+}$, Dy^{3+}	Green	3.56	20-40	~ 10-12

In this study, commercial mono-crystalline silicon 1.5 V and 100 mA photovoltaic cell with an area of 2.5x5 cm^2 is used as a photovoltaic converter. In addition, 25 µm thick conductive graphene sheets are provided on Graphene-Supermarket. Optimal and SEM images of graphene sheets are given in Figure 4.1 (a, b). The graphene is made in one atom or molecule thickness and its energy band gap is zero. Therefore, it is important material in many areas. Its contribution to increasing efficiency is investigated in the nuclear battery design.

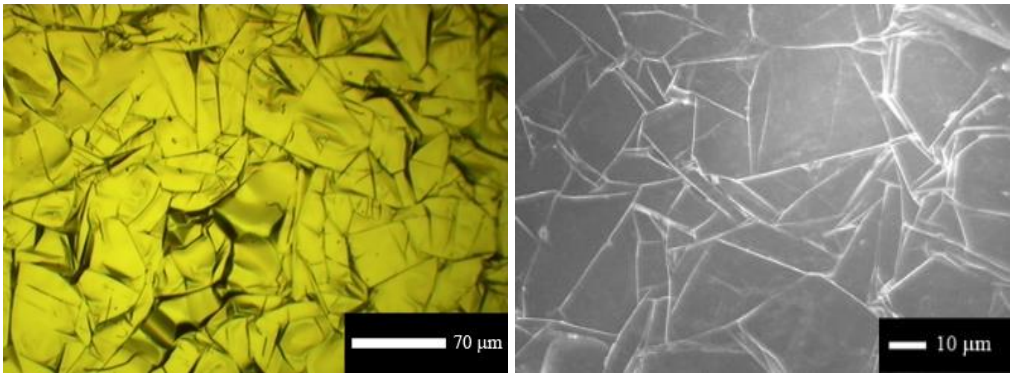

(a) (b)

Figure 4.1 a) Optical image and b) SEM image of the graphene sheet [118].

4.1.1 Preparation of Phosphor Layers

In this study, phosphor layers are manufactured as a thin film form by using ZnS:CuCl and $SrAl_2O_4:Eu^{2+},Dy^{3+}$ inorganic crystalline powder phosphors which are given in Table 4.1, and different substrates such as polycarbonate, polyethylene, and glass. Various methods have been tried in the preparation of phosphor layers:

a) $SrAl_2O_4:Eu^{2+},Dy^{3+}$ phosphor powders are coated on the glass substrate by the spray pyrolysis method and this layer is analyzed by Scanning Electron Microscopy (SEM). SEM image of the phosphor film is given in Figure 4.2.

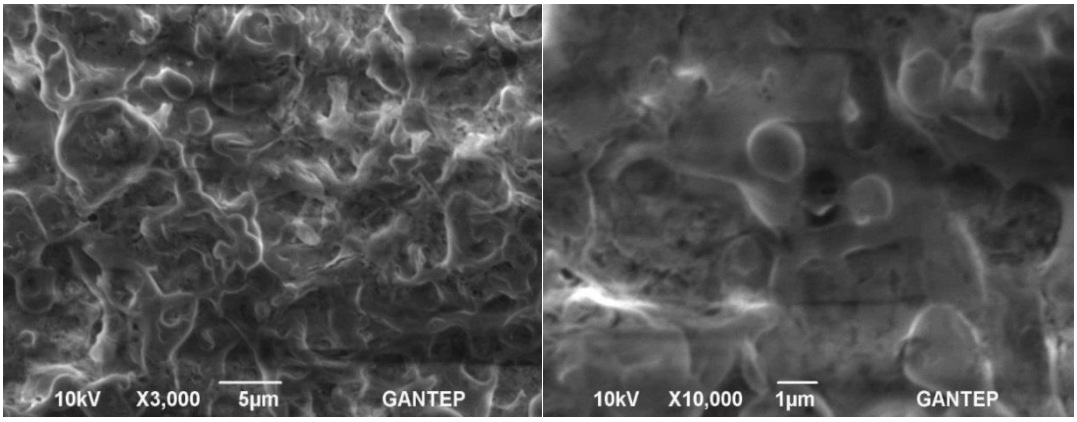

Figure 4.2 SEM image of $SrAl_2O_4:Eu^{2+},Dy^{3+}$ thin film on glass substrate made by spray pyrolysis method.

b) Since other substrates are unsuitable for this method, phosphor powders are dissolved in distilled water or ethyl alcohol and applied onto the substrate and dried.

c) In practical method, phosphor powders are mixed with acrylic adhesive and this mixture is applied as a thin layer onto polycarbonate or polypropylene substrates (Figure 4.3 (a)).

d) In another practical method, the phosphors are deposited on acrylic double-sided adhesive tape substrates with a light transmittance of nearly 95% and PET carrier double-sided adhesive tape substrates with a light transmittance of nearly 90%. The phosphor powders are directly adhered to the transparent adhesive tape with a great viscosity and transparency. This simple and low-cost method is used to produce even and thin phosphor layers consisting of 20 μm-size ZnS:CuCl or 65 μm-size $SrAl_2O_4:Eu^{2+},Dy^{3+}$ phosphor powders and a 0.5 mm-thick adhesion layer (Figure 4.3 (b)).

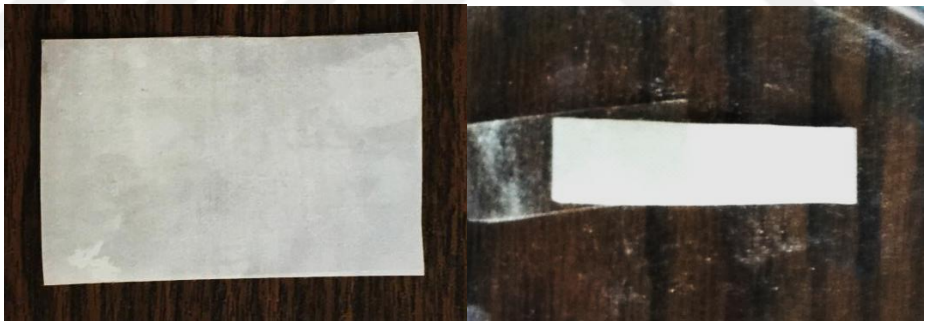

Figure 4.3 a) Phosphor layer prepared with polypropylene. b) Phosphor layer prepared with PET carrier double-sided tape.

The mass of the phosphor powder used in the phosphor layers is determined by precision balance. Accordingly, the thickness of the phosphor layer is calculated and it is ensured that it is in accordance with the optimum thickness calculated in theory. The rule-of-thumb is that the half-value absorber thickness is approximately 1/7 of the maximum range of radiation [119]. Accordingly, the optimum thickness is considered to be approximately 2/7 of the maximum range. The optimum thickness range of ZnS:CuCl and $SrAl_2O_4:Eu^{2+},Dy^{3+}$ phosphor layers are determined as 12

mg/cm^2 and 17 mg/cm^2, respectively for Pm147 beta source. Figure 4.4 shows the change in short-circuit current for different thickness ZnS:CuCl phosphor layers used in the indirect converter battery model.

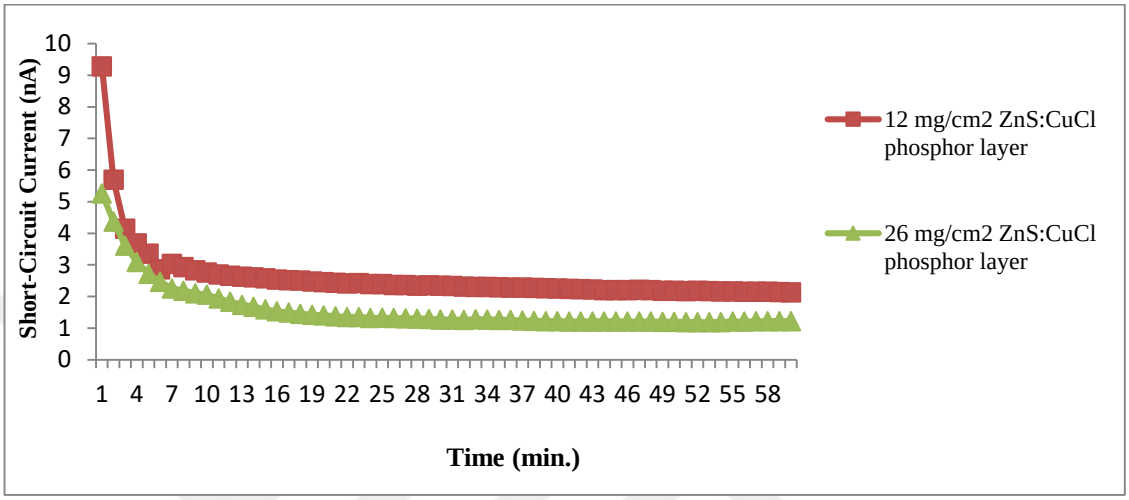

Figure 4.4 Comparison of different mass thicknesses of phosphor layers for indirect conversion nuclear battery model.

4.2 Methods

Theoretical information about direct and indirect energy conversion nuclear battery methods used in experimental studies is given in Chapters 2 and 3. In the direct conversion method, the photovoltaic cells are directly exposed to the prepared beta source and the current-voltage values are measured with ammeter and voltmeter. Measurements of the prototypes are made in a closed box in order to provide isolation from the light environment in the laboratory.

In addition, the effect of graphene is investigated in order to increase efficiency in the direct conversion method. This method is very new in the literature and is an original approach. Theoretically, particles resulting from radioactive decay are slowed down in the graphene layer to reduce kinetic energies, thereby protecting the semiconductor from radiation damage. In the meantime, electrons removed from the nano-film graphene will perform electron-hole production in the semiconductor. Electrons removed from the graphene layer and decelerated radioactive particles will

be directed to the photovoltaic cell. Thus, the energy conversion efficiency can be improved by increasing the number of electrons reaching the photovoltaic cell. In addition, the use of very thin graphene as an electrode may also be a choice for increasing efficiency for betavoltaic batteries [120].

4.3 Design and Structures

For the direct conversion battery models; the beta source and PV cell and also for the indirect conversion battery models; the beta source, the phosphor layer, and the PV cell are arranged and laminated according to Figure 4.5 (a, b). Because of their thin-film structure, phosphor and Pm147 beta sources are combined in a planar structure.

Figure 4.5 (a) shows the betavoltaic battery model and Figure 4.5 (b) shows the beta radioluminescence battery model that we constructed in this study. In addition, to minimize damage and improve efficiency we examined the effect of graphene sheets as shown in Figure 4.5 (c). Theoretically, it is considered that electrons will be captured by transferring particles emitted from radioactive materials onto the thin graphene film and those electrons with lower kinetic energy exiting the radioactive material and graphene will produce excitation in the photovoltaic cell.

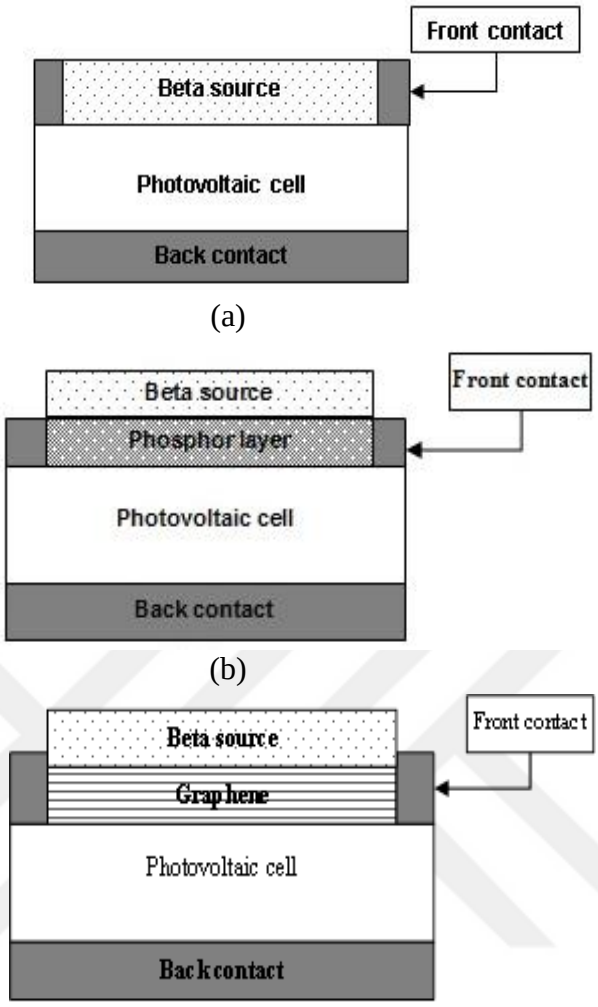

Figure 4.5 a) Direct conversion nuclear battery model, b) indirect conversion nuclear battery model, c) direct conversion nuclear battery model with graphene.

Figure 4.6 shows the prototype of beta direct and indirect nuclear battery models. The battery models are rectangle form with a sandwich-structure and a cross-sectional area of approximately 15 cm^2. In order to reduce the energy loss, the beta source film is directly placed on the surface of the phosphor layer using tape to fix together the beta source and the PV cell, with the phosphor layer in between.

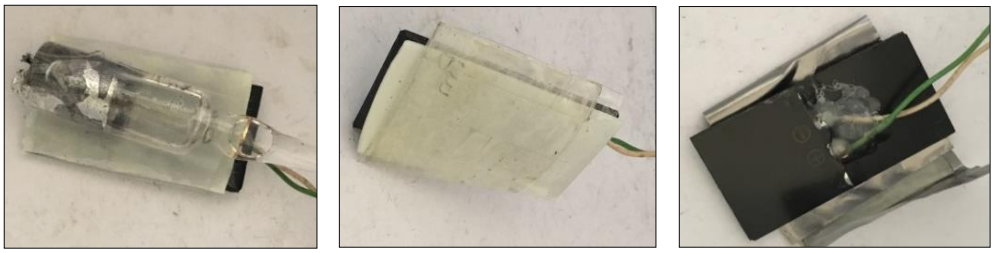

(a) (b) (c)

Figure 4.6 a) Sr90/phosphor layer/photovoltaic cell battery model, b) Pm147/ phosphor layer/photovoltaic cell battery model, and c) Pm147/graphene layer/photovoltaic cell battery model.

4.4 Results

In this study, several types of conversion nuclear batteries are manufactured and tested at normal temperature and pressure values. Short-circuit current (I_{sc}) and open-circuit voltage (V_{oc}) measurements are taken for direct and indirect conversion nuclear battery models in a dark environment and the efficiency (η) values of the batteries are calculated using Eqn. (2.31). The Keithley 485 Picoammeter and Keithley 199 DMM/SCANNER devices are used for current and voltage measurements. The electrical performance outputs obtained for the betavoltaic battery models are given in Table 4.2.

Table 4.2 Electrical performance datas of battery models. Assuming the fill factor (FF) is 0.5 for the photovoltaic cell.

Battery Model	**Isc (nA)**	**Voc (mV)**	**η (%)**
Pm147/PVcell	1.0	1.2	0.101
Sr90/PVcell	2.2	1.21	0.016
Pm147/ZnS:CuCl/PVcell	2.7	1.11	0.252
Pm147/$SrAl_2O_4$:Eu^{2+},Dy^{3+}/PV cell	3.1	1.54	0.401
Sr90/ZnS:CuCl/PVcell	3.4	1.8	0.036
Sr90/$SrAl_2O_4$:Eu^{2+},Dy^{3+}/PV cell	2.4	1.6	0.022
Pm147/Graphene/PVcell	1.1	0.45	0.079

The most efficient battery model is determined as Pm147/$SrAl_2O_4$:Eu^{2+},Dy^{3+}/PV cell. In the direct conversion nuclear battery models, the experimental values demonstrated that battery efficiency approached theoretical calculations for Pm147 beta source. The maximum power is normally higher when the Sr90 beta source is used. But the performance of the battery is lower than expected for Sr90 beta source. This may be due to the beta source which in the glass tube. Further studies, the voltage, and the current values are expected to increase when the liquid Sr90 source is formed into a thin film.

In the indirect conversion nuclear battery models, since emitted photons can reach the photovoltaic cell with the minimum loss, the base of the phosphor layer must have good permeability of the photon. Therefore, polycarbonate and acrylic materials used in this study have high light transmittance. As a result, phosphor layer has improved battery performance. However, the phosphor layer for different beta sources gave different results. The results indicate that combination of the source and phosphors requires choice. Short-circuit current and open-circuit voltage values increase when the phosphor layer is placed between the beta source and the photovoltaic cell as shown in Table 4.2. But after a certain period of time, effect of phosphor layer is decreased due to low beta source activity.

To obtain the effect of time-dependent, different phosphor layers are exposed to beta irradiation for one hour or more. For the different battery models, the changing of the short-circuit current with respect to time is measured and converted into graphics which are shown in Figure 4.7 and Figure 4.8.

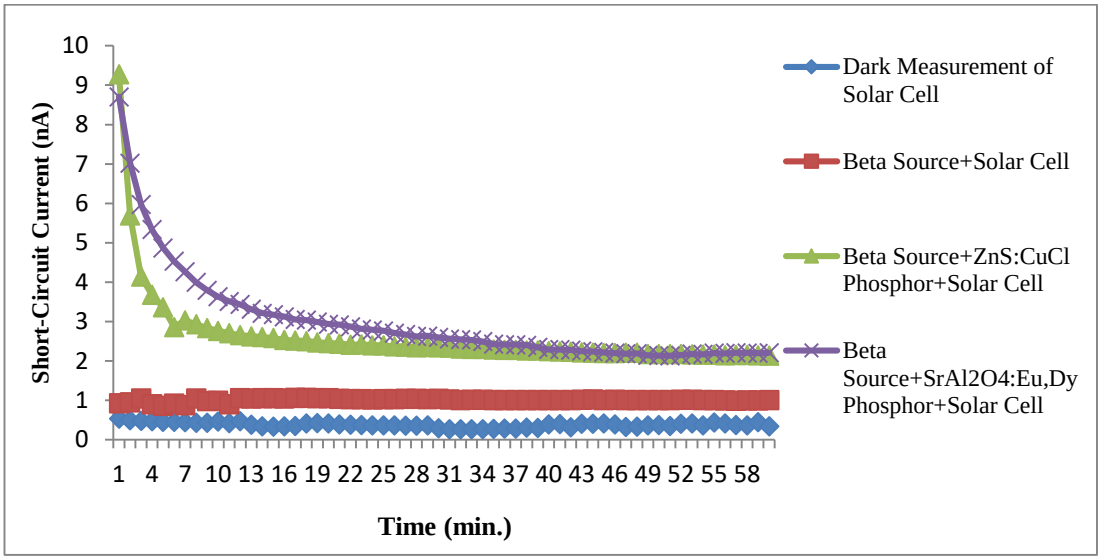

Figure 4.7 The graphs of the short-circuit current with respect to time for the battery models which are made with Pm147 beta source and ZnS:CuCl or $SrAl_2O_4:Eu^{2+},Dy^{3+}$ phosphors (interval 1 minute and the total time is 1 hour).

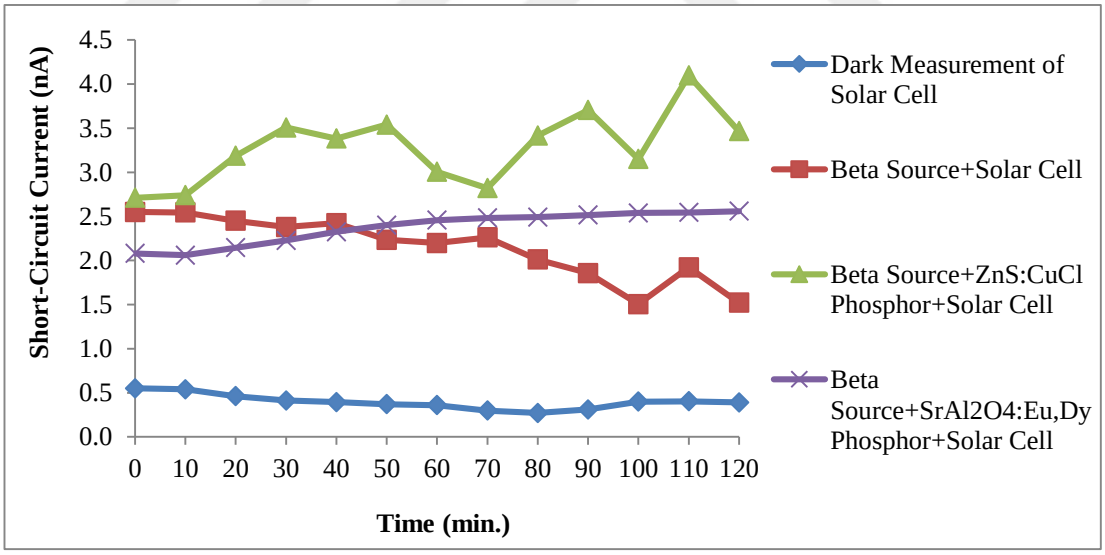

Figure 4.8 The graphs of the short-circuit current with respect to time for the battery models which are made with Sr90 beta source and ZnS:CuCl or $SrAl_2O_4:Eu^{2+},Dy^{3+}$ phosphors (interval 10 minute and the total time is 2 hours).

For the indirect nuclear battery model which is made with Pm147 beta source, although starting values for the current and voltage are high, after a certain time they

are observed to be lower than the initial value. This situation can be occurred due to low activity of Pm147 beta source used in literature. But Sr90 used as a beta source, because of its high energy, phosphor layer increases the short-circuit current after a short time. In addition, placing graphene into the PV cell increases the current value, as shown in Figure 4.9. This indicates that beta particles pull electrons from the graphene.

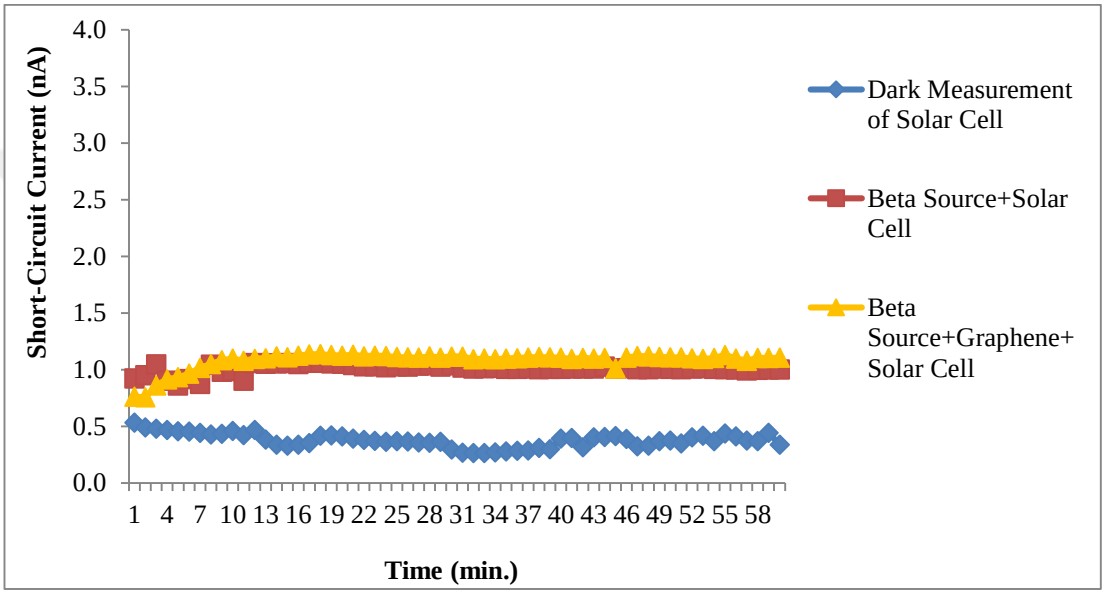

Figure 4.9 The graphs of the short-circuit current with respect to time for the battery models which are made with Pm147 beta source and graphene (interval 1 minute and the total time is 1 hour).

On the other hand, radiation damage hasn't been observed in the phosphor layers and the photovoltaic cells during the test period since activity values of used beta sources are very low. Also, the energy conversion efficiency of the battery models is very low due to various factors limiting the general efficiency of the battery. The low efficiency may have resulted from very low activity. Consequently, improving the purity and activity of the beta source, selecting both high efficiency and transparency phosphor layer and suitable PV cell can increase the energy conversion efficiency of the battery.

CHAPTER 5

MODELING AND SIMULATION OF DIRECT CONVERSION NUCLEAR BATTERIES

In a betavoltaic battery, since the emitted particle energy from the radioisotope is much larger than the band gap of the cell, wider band gap semiconductors give higher efficiency with more radiation tolerance, which potentially allows for the use of higher-energy radioisotope sources [121]. Therefore, it is important to use wide band gap materials, which provide low leakage currents in order to get reasonable achievable power conversion efficiencies [27]. Usually, the efficiency and the band gap width are of positive correlation, but the band gap cannot be adjusted indiscriminately high because the collection of the carriers is difficult due to the high band gap having poor conductivities [21].

In a silicon betavoltaic battery, the diffusion length is longer than the depth at which the electrons are formed, but the lifetime degradation leads to a significant change in the open-circuit voltage. On the other hand, the voltage of the betavoltaic device, which uses a wide band gap semiconductor such as gallium phosphide (GaP) and gallium nitride (GaN), is higher due to the wider band gap [21]. Therefore, GaN and GaP are good candidate semiconductor materials for betavoltaic batteries because of their proper wide band gap and large output voltage [54, 122].

However, for instance, the GaN betavoltaic battery has a lower short-circuit current for the Ni63 with the same activity even if it exhibits a higher open-circuit voltage than silicon betavoltaic [54]. Generally, it has been observed that the collection efficiency (internal quantum efficiency) is low due to the small diffusion lengths in wide band gap semiconductors [77, 123, 124]. The collection efficiency is low if the diffusion length is too small compared with the cell thickness ($L \ll d$). This criterion

means high losses of minority carriers in the bulk. Hence, the obtainable efficiency of the wide band gap betavoltaic cell is smaller than the efficiency of the high-quality silicon betavoltaic cell [77].

For this reason, heterojunction photovoltaic cells may be a good choice to use both wide band gap semiconductors and high collection efficiency. When two different semiconductors are used to form a junction, the junction is called a semiconductor heterojunction. The fact that the two materials used to create the heterojunction have different energy band gap is advantageous in that they absorb the different energetic particles emitted by the radioisotope. The spectral response, equivalently, the quantum efficiency is one of two principal electrical characteristics used to consider cell performance [125]. The p-n heterojunction photovoltaic cell usually has a better short-wavelength response, lower series resistance, and better radiation hardness than a p-n homojunction photovoltaic cell [82]. Heterojunction cells have many similarities and a few differences to Schottky barrier cells. The most important similarity is that the short wavelength photons (or particles) in most cases cause a good photon (particle) energy response by being absorbed in or near the depletion zone of the device. If the band gap energy of material 1 is large, high energy particles will be absorbed inside the depletion region of material 2 where the carrier collection should be very efficient. The most important difference is that the open-circuit voltage can be high without the need for carefully controlled interface layers, such as at the p-n junction [81].

Theoretical calculations and literature review for GaN-based betavoltaic batteries and photovoltaic cells have revealed that the collection efficiency is very low compared to silicon batteries. Lu et al. (2011) calculated the collection efficiency for GaN Schottky betavoltaic battery as 0.29 [126]. Honsberg et al. (2005) calculated the collected current of the GaN betavoltaic battery to be about 1/3 lower than the silicon betavoltaic battery [21]. Similarly, Allen et al. (2010) and Diaz (2011) showed that the internal quantum efficiency for the GaP photovoltaic cell was less than 0.5 [127, 128]. However, in the studies of GaP-Si heterojunction photovoltaic cells, the internal quantum efficiency is greater than 0.9 [129, 130]. On the other hand, the use of heterojunction photovoltaic cells has not been extensively studied in betavoltaic battery studies.

In this chapter, heterojunction photovoltaic cells are analysed to increase collection efficiency and the maximum power in the betavoltaic battery models. A theoretical investigation of the electrical performance has been carried out on the betavoltaic cells modeled using Si, GaN, GaP, GaN-Si and GaP-Si semiconductors for Ni63 or Pm147 beta source. Ni63 and Pm147 are preferred as radioisotope because they are suitable for betavoltaic batteries [21, 98, 126, 131, 132]. By using 1 mCi/cm^2 activity density Ni63 or Pm147 as the beta sources, the electrical performance of the 1 cm^2 area nuclear battery models calculated numerically in Mathematica and Matlab programs by equations given in Chapter 2. In addition, the effects of doping concentration and junction depth on the maximum power are investigated separately for GaN homojunction and GaN-Si heterojunction betavoltaic batteries. Similarly, the effects of junction depth on the maximum power and the collection efficiency are examined for GaP, Si and GaP-Si betavoltaic batteries. Then by optimizing these parameters, maximum collection efficiency, and maximum power are obtained.

5.1 Simulation Calculations of Si, GaP and GaP-Si Betavoltaic Battery Models

5.1.1 GaP Betavoltaic Battery Model

In this study, GaP photovoltaic cell parameters which are taken as a reference in Lu et al. (2013) [133] are used for the betavoltaic battery models. GaP n-p homojunction betavoltaic battery model is shown in Figure 5.1. The parameters used in the Ni63/GaP and Pm147/GaP betavoltaic battery models are shown in Table 5.1. Using these parameters and the equations given in sections 2.2.1 and 2.2.2, collection efficiency, leakage current, short-circuit current, open-circuit voltage, maximum power, and efficiency values are calculated in the Mathematica program. According to the results of the calculation, for the GaP n-p junction, higher collection efficiency is obtained than for the GaP p-n junction. However, the maximum collection efficiency found to be less than 0.58 in the Ni63/GaP n-p betavoltaic battery. In the Pm147/GaP n-p betavoltaic battery, the maximum collection efficiency decreased to 0.2, as shown in Figure 5.2. On the other hand, due to high beta energy, maximum power is higher in the Pm147/GaP betavoltaic battery, as shown in Figure 5.3.

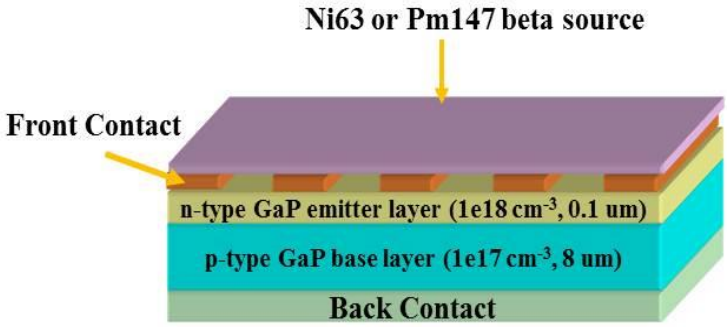

Figure 5.1 Schematic diagram of a GaP n-p homojunction betavoltaic battery model.

Table 5.1 Parameters used in the GaP n-p homojunction betavoltaic battery models.

N_a (cm^3)	N_d (cm^3)	Base layer thickness (µm)	L_n (µm)	L_p (µm)	W (µm)	S_n (cm/s)	S_p (cm/s)
$1x10^{17}$	$1x10^{18}$	8	1	3.5	0.17	$1x10^6$	$1x10^5$

The thickness for the emitter, base and depletion regions of the p-n junction should be consistent with the calculated range (penetration depth) by taking into account the average energy of the beta particle [15]. In particular, the thickness of the emitter region, that is, the junction depth plays an important role in determining the collection efficiency and the maximum power. For different junction depth values, the calculated results show that the maximum power for the Ni63/GaP n-p betavoltaic battery is obtained when the junction depth is 0.1 µm, as shown in Figure 5.3. Because of its low energy, small junction depth values for the Ni63 beta source cause higher efficiency. As shown in Figure 5.3, since the energy of the Pm147 beta source is higher, the optimum junction depth for the Pm147/GaP n-p betavoltaic battery is between 1 and 3 µm.

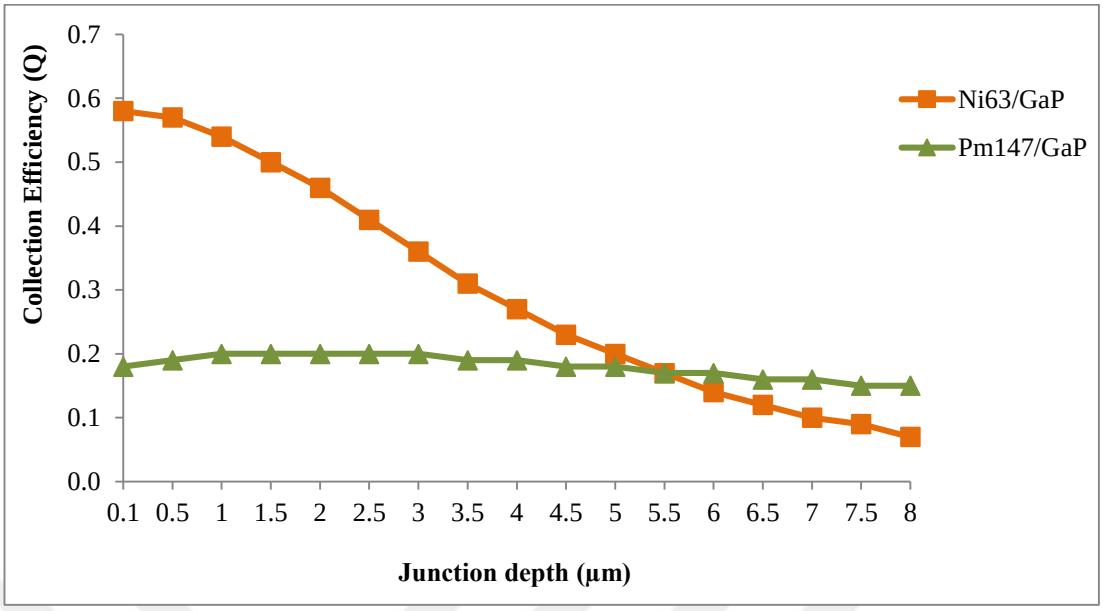

Figure 5.2 Collection efficiency versus the junction depth in the Ni63/GaP and Pm147/GaP n-p betavoltaic battery models.

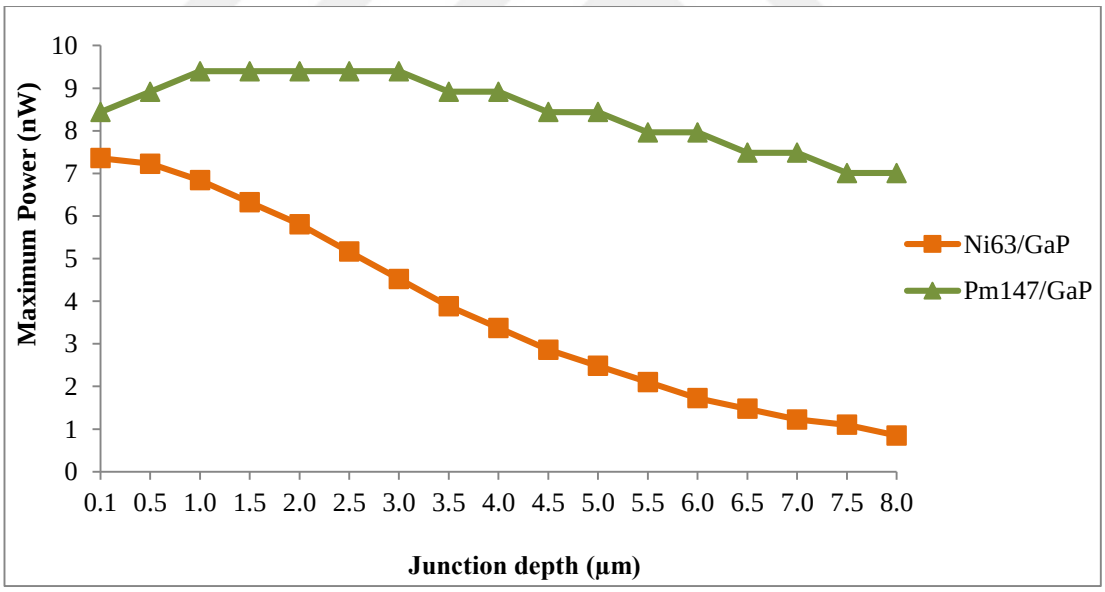

Figure 5.3 Maximum power versus the junction depth in the Ni63/GaP and Pm147/GaP n-p betavoltaic battery models.

For the Pm147 beta source, the GaP betavoltaic battery has advantages due to wide band gap and radiation hardness, but it does not have the expected high power output because of its low diffusion lengths despite the larger junction depth requirement.

Therefore the Ni63 beta source appears to be more suitable for the GaP semiconductor.

5.1.2 Si Betavoltaic Battery Model

Electron and hole diffusion lengths and diffusion coefficients of silicon utilized in the model are calculated using the formulas given in Tang's study [134], and these results are given in Table 5.2. The Si n-p junction diode with the same doping concentrations is used to compare with the GaP betavoltaic battery model. Due to the high diffusion length, the base layer thickness of the silicon n-p junction is taken as 160 μm by regarding the practical considerations. Depletion region, collection efficiency, and maximum power output are calculated for different junction depth values according to these parameters.

Table 5.2 Parameters used in Si n-p homojunction betavoltaic battery models.

N_a (cm^3)	N_d (cm^3)	Base layer thickness (μm)	L_n (μm)	L_p (μm)	W (μm)	S_n (cm/s)	S_p (cm/s)
$1x10^{17}$	$1x10^{18}$	160	27.9	75.5	0.11	$1x10^3$	$1x10^3$

The maximum collection efficiency for the Ni63/Si n-p betavoltaic battery reaches up to 95% in the 1.0 μm junction depth due to its high diffusion length and gradually decreases after 5.0 μm junction depth. In the Pm147/Si n-p betavoltaic battery, the optimum junction depth is higher than 10 μm due to the higher penetration depth. After a 12 μm junction depth, the collection efficiency decreases slowly. The graphs showing the relationship between the collection efficiency and the junction depth for these battery models are given in Figure 5.4. The relationships between the maximum power and the junction depth for Ni63/Si and Pm147/Si n-p betavoltaic battery models are examined and the results are shown in Figure 5.5. When the Pm147 beta source is used, the power output is increased by more than 3 times, although the collection efficiency is lower. Thus Pm147 is seen as a suitable beta source for Si semiconductor with high diffusion lengths as it increases the output power significantly. However, in this betavoltaic model with the higher power, the

radiation damage caused by the low band gap reduces battery efficiency in a short time.

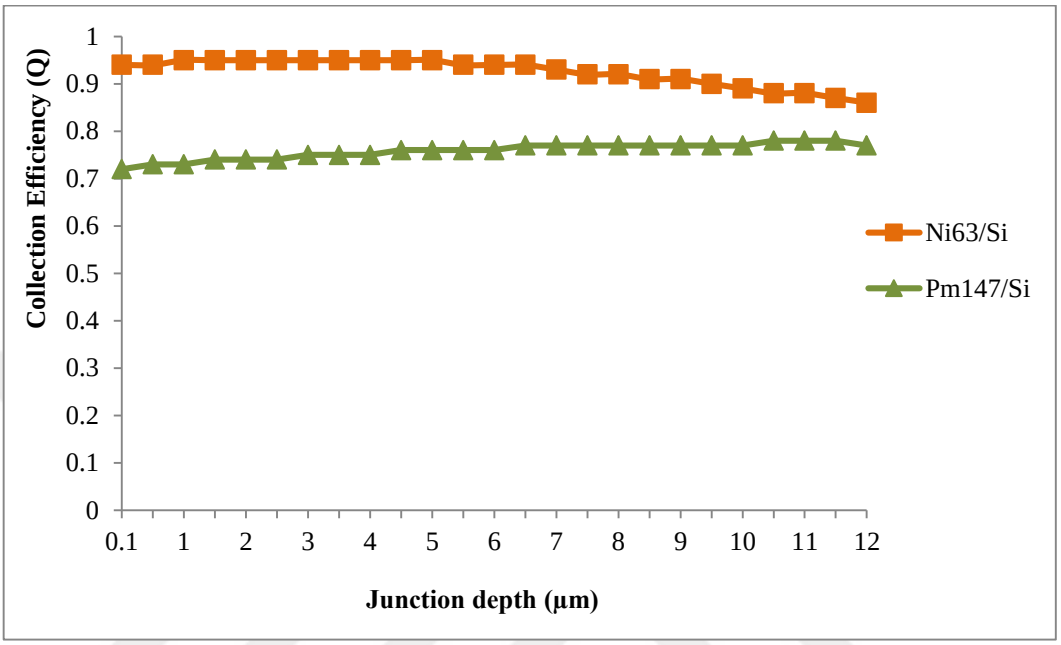

Figure 5.4 Collection efficiency versus the junction depth in the Ni63/Si and Pm147/Si n-p betavoltaic battery models.

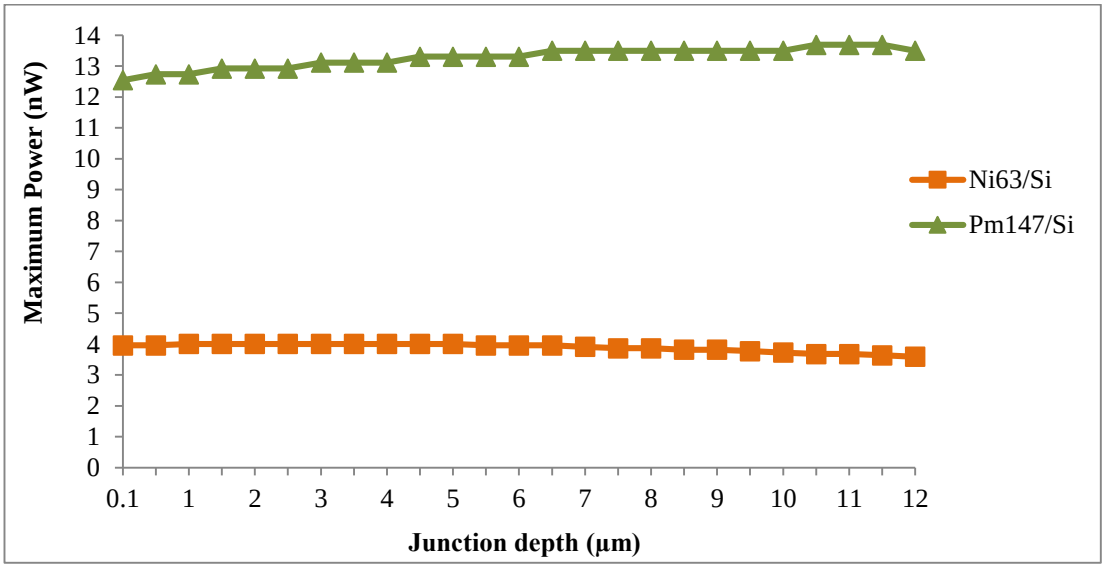

Figure 5.5 Maximum power versus the junction depth in the Ni63/Si and Pm147/Si n-p betavoltaic battery models.

5.1.3 GaP-Si Heterojunction Betavoltaic Battery Model

When GaP semiconductors are used, it has been found that the collection efficiency values are not at a high level due to the low diffusion lengths. Theoretical analyses have been made for the heterojunction photovoltaic cell used to increase efficiency. The diffusion length and the diffusion coefficient parameters corresponding to N_a, N_d values are calculated separately for p-type and n-type of GaP and Si. GaP to take advantage of the wide band gap in the first layer; and silicon with high diffusion lengths in the second layer are preferred. The design of the GaP-Si n-p heterojunction betavoltaic battery model is shown in Figure 5.6.

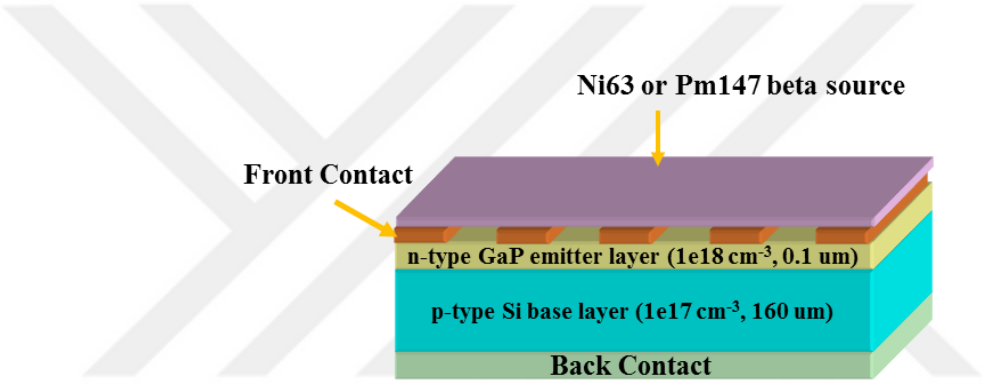

Figure 5.6 Designed 1 cm^2 area device structure of GaP-Si n-p heterojunction betavoltaic battery.

The parameters used in GaP-Si n-p heterojunction betavoltaic battery models are given in Table 5.3. As a result of theoretical analyses, it has been determined that the collection efficiency and depletion region thickness are higher in the GaP-Si heterojunction betavoltaic batteries. When the GaP-Si heterojunction is used in the betavoltaic battery, there is a serious increase in the maximum power output. Considering that the largest contribution to the collection efficiency is made by the base layer, the use of n-type Si instead of n-type GaP with low carrier mobility [135] and diffusion coefficient parameters provides a great advantage.

Table 5.3 Parameters used in GaP-Si n-p heterojunction betavoltaic battery models.

N_a (cm^3)	N_d (cm^3)	Base layer thickness (µm)	L_n (µm)	L_p (µm)	W (µm)	S_n (cm/s)	S_p (cm/s)
$1x10^{17}$	$1x10^{18}$	160	1	75.5	0.20	$1x10^{6}$	$1x10^{3}$

As shown in Figure 5.7, the collection efficiency for the Ni63/GaP-Si n-p betavoltaic battery is 0.93, which decreases as junction depth increases due to low energy of Ni63. In the Pm147/GaP-Si n-p betavoltaic battery, the collection efficiency, which is 0.73 in 0.1 junction depth, decreases more slowly as the junction depth increases. The low collection efficiency values of the GaP betavoltaic batteries are significantly increased in the use of GaP-Si heterojunction. Figure 5.8 displays the effect of thickness of n-type GaP (junction depth) on the maximum power. The emitter thickness is varied from 0.1 µm to 8 µm to determine the effect of the junction depth on the maximum power. The optimum junction depth of the betavoltaic battery for GaP-Si heterojunction is found to be as low as 0.1 µm. While the maximum power for Ni63/GaP-Si n-p betavoltaic battery is 19.03 nW, the maximum power reaches 55.20 nW with the use of Pm147 beta source. This result shows that Pm147 beta source is a good choice for the GaP-Si betavoltaic batteries.

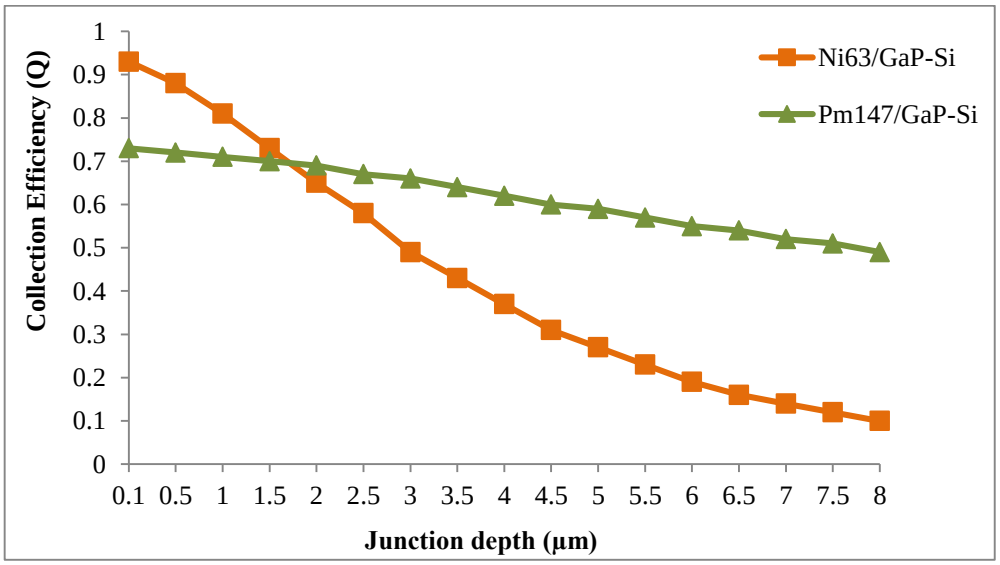

Figure 5.7 Collection efficiency versus the junction depth in the Ni63/GaP-Si and Pm147/GaP-Si n-p betavoltaic battery models.

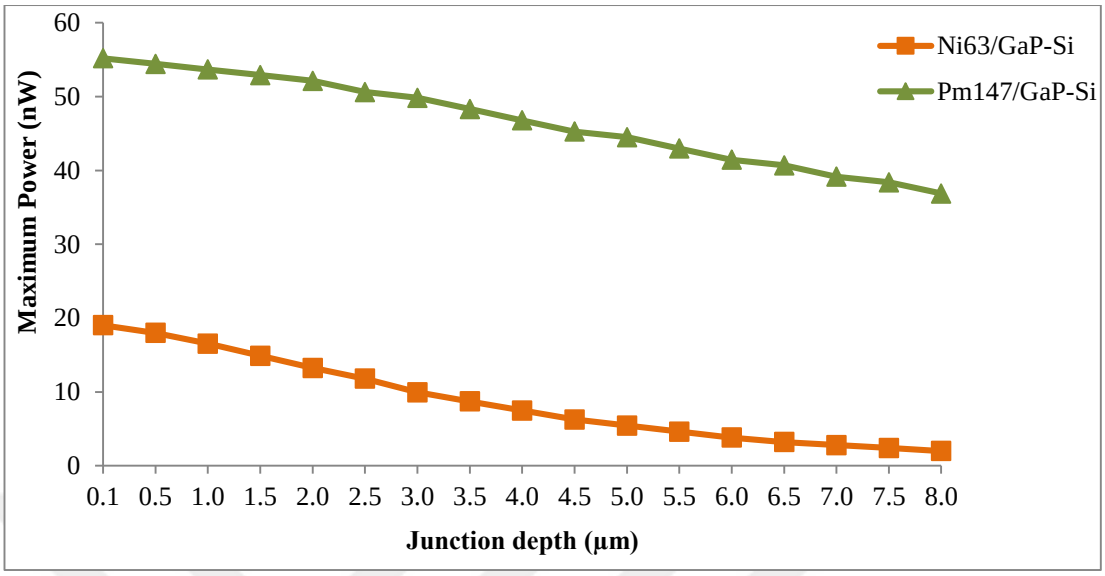

Figure 5.8 Relationships between the maximum power and junction depth for Ni63/GaP-Si and Pm147/GaP-Si n-p betavoltaic battery models.

The electron-hole pairs produced in the depletion region, as well as within a diffusion length adjacent to depletion region, is also efficient electron-hole pairs. They can go to the depletion region and conduce to energy production. Therefore, minority carrier diffusion length is an important parameter affecting short-circuit current and collection efficiency in the betavoltaic battery. Based on this, in this study, it is aimed to create a high-efficiency betavoltaic battery by using GaP-Si heterojunction which utilizes the wide band gap and radiation hardness of GaP and high diffusion length values of silicon. The doping concentration should be chosen correctly for the performance of the betavoltaic battery since it has a significant effect on the diffusion coefficient, lifetime, and diffusion length of carriers [136]. For this reason, higher efficiency can be achieved for GaP-Si betavoltaic battery when the doping concentrations are optimized.

5.1.4 Performance Comparison of these Models

The electrical performance of the ideal devices of Si, GaP and GaP-Si betavoltaic batteries is obtained using Eqn. (2.11) – Eqn. (2.42) and is given in Table 5.4. In order to compare the results, all the I-V characteristic curves are drawn in the same

graph as shown in Figure 5.9. In the ideality factor (n) = 1 condition, the leakage currents are theoretically calculated as $9.91x10^{-7}$ μA, $5.54x10^{-25}$ μA, $3.69x10^{-37}$ μA for Si, GaP and GaP-Si, respectively.

According to doping concentrations of $N_a=1x10^{17}$ cm^{-3}, $N_d=1x10^{18}$ cm^{-3} and the junction depth of 0.1 μm, the maximum power of Ni63/GaP-Si n-p betavoltaic battery is about 19.03 nW corresponding to a fill factor of 0.93, an open-circuit voltage of 2.05 V, a short-circuit current of 10.0 nA and the energy conversion efficiency of about 18.91%. For the Pm147/GaP-Si n-p betavoltaic battery, the maximum power of about 55.20 nW, a fill factor of 0.93, an open-circuit voltage of 2.07 V, a short-circuit current of 28.6 nA and the energy conversion efficiency of about 15.04% are calculated under the same conditions. Nevertheless, it is seen that the electrical performance outputs of Si and GaP are lower in Table 5.4. The obtained results showed that the use of heterojunction is a suitable method to increase the efficiency of betavoltaic batteries.

Table 5.4 Electrical performance results for 1 mCi/cm^2 n-p betavoltaic battery models when junction depth values are optimum.

	Q	**I_{sc} (μA)**	**V_{oc} (mV)**	**FF**	**P_{max} (nW)**	**Efficiency (η) (%)**
Ni63/Si	0.95	0.0224	258.73	0.69	4.00	3.98
Ni63/GaP	0.58	0.0062	1310.01	0.90	7.36	7.31
Ni63/GaP-Si	0.93	0.0100	2045.56	0.93	19.03	18.91
Pm147/Si	0.78	0.0672	287.00	0.71	13.69	3.73
Pm147/GaP	0.20	0.0078	1315.93	0.91	9.40	2.56
Pm147/GaP-Si	0.73	0.0286	2072.69	0.93	55.20	15.04

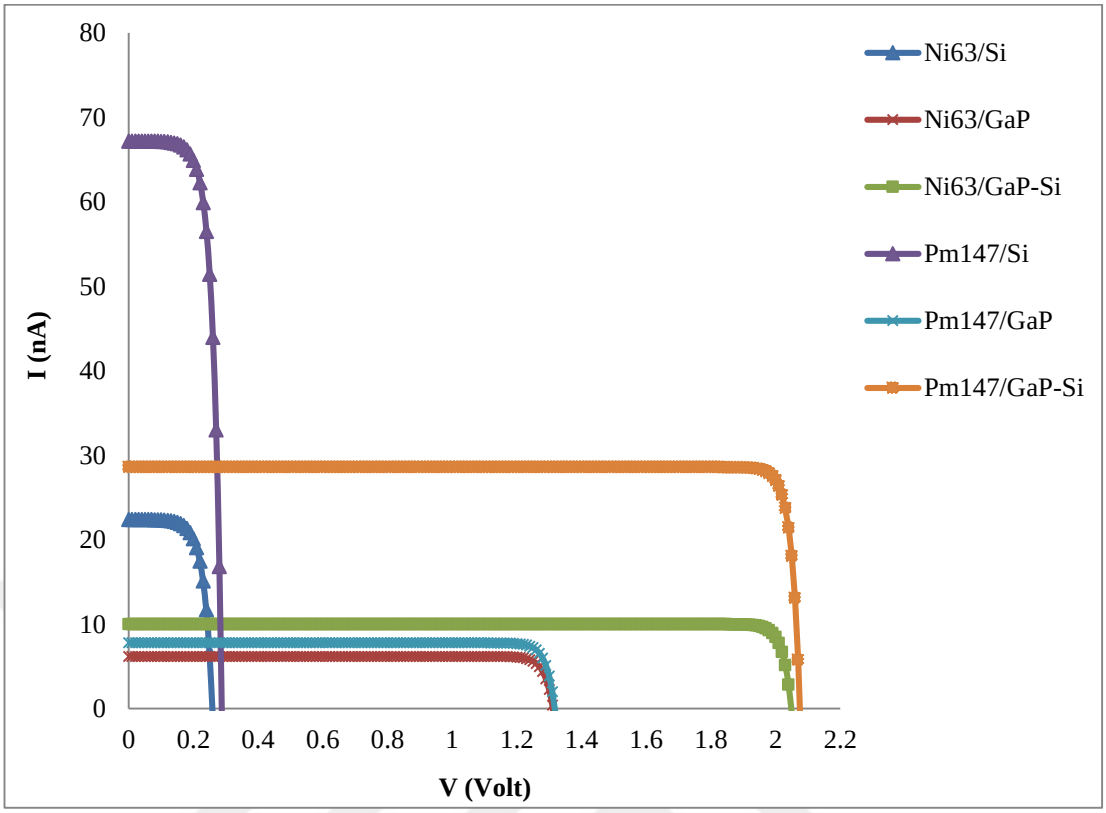

Figure 5.9 Theoretical I–V characteristics of Si, GaP and GaP-Si betavoltaic batteries under 1 mCi/cm^2 Ni63 and Pm147 beta-radiation.

Figure 5.9 shows a significant increase in the voltage values of the betavoltaic battery when using the wide band gap and heterojunction semiconductors. On the other hand, when the narrow band gap Si semiconductor is used, the voltage values of the batteries are low but there is a remarkable increase in the current values. When the Pm147 beta source is used, there is a significant increase, especially in current values since the high energy particles produce a greater number of e-h pairs.

5.2 Simulation Calculations of GaN and GaN-Si Betavoltaic Battery Models

5.2.1 GaN Betavoltaic Battery Model

In this model, diffusion length of p-type and n-type, depletion region and collection efficiency values are calculated for Ni63/GaN betavoltaic battery using parameters given for p-GaN and n-GaN in Kumakura's et al. (2005) study [137]. As a result, the collection efficiency values are found to be less than 0.5 in GaN p-n betavoltaic batteries, as given in Table 5.5.

As presented in Figure 5.10, for different junction depth values the calculated results show that the maximum power for the Ni63/GaN p-n betavoltaic battery is obtained when the junction depth is 2 μm for $5x10^{16}$ cm^{-3} p-type doping concentration. However, considering the effect of different N_a values on the maximum power it is seen that optimum junction depth (emitter thickness) decreases as N_a value increase. The effect of n-type doping concentration (N_d) exchange on the junction depth is found to be less.

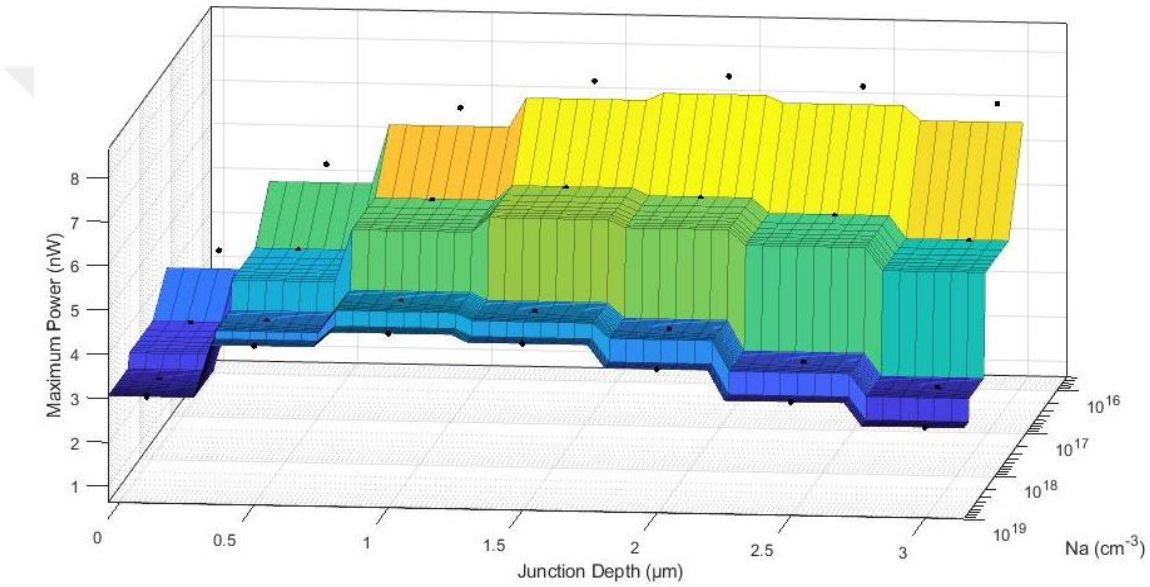

Figure 5.10 Maximum power versus the junction depth and p-type doping concentration (N_a) in the Ni63/GaN p-n betavoltaic battery when N_d is $4x10^{17}$ cm^{-3}.

Table 5.5 shows the parameters used for the Ni63/GaN p-n betavoltaic battery model and the corresponding collection efficiency results. Since the mobility and lifetime of GaN decrease at high doping concentrations [136, 137] the minority carrier diffusion length and the depletion region decrease with increasing p-type doping concentration (N_a) and n-type doping concentration (N_d), so the collection efficiency decreases with increase in doping concentration. As a result, lower doping concentration generally causes larger collection efficiency and the maximum power. As shown in Figure 5.11, the effect of doping concentration of p-type on the maximum power is

found to be great in the Ni63/GaN betavoltaic battery model. The effect of doping concentration of n-type is lower.

Table 5.5 Collection efficiency (Q) results for Ni63/GaN p-n betavoltaic battery. Junction depths are taken as 1.5 μm.

N_a (cm^{-3})	N_d (cm^{-3})	L_p (μm)	L_n (μm)	W (μm)	Q
$5x10^{16}$	$4x10^{17}$	3.24	0.23	0.27	0.49
$4x10^{17}$	$4x10^{17}$	1.88	0.23	0.13	0.39
$4x10^{18}$	$4x10^{17}$	0.93	0.23	0.10	0.29
$1x10^{19}$	$4x10^{17}$	0.76	0.23	0.09	0.26
$3x10^{19}$	$4x10^{17}$	0.22	0.23	0.09	0.13
$5x10^{16}$	$4x10^{18}$	3.24	0.20	0.26	0.48
$4x10^{17}$	$4x10^{18}$	1.88	0.20	0.10	0.37
$4x10^{18}$	$4x10^{18}$	0.93	0.20	0.04	0.27
$1x10^{19}$	$4x10^{18}$	0.76	0.20	0.03	0.24
$3x10^{19}$	$4x10^{18}$	0.22	0.20	0.03	0.11

At the present time, metal-organic chemical-vapor deposition (MOCVD) is the primary method for GaN growth. In this method, there are various problems in the growth of GaN as a thick high-quality layer. Furthermore, the hole concentration of MOCVD p-GaN is in the limited range of $1–5 \times 10^{17}$ cm^{-3} [138]. Due to these limitations, the radiation generated electron-hole pairs cannot be effectively collected because of the low width of the depletion region of the GaN p-n junction [138] and the low diffusion lengths [124]. For this reason, in order to eliminate these problems, some researchers have focused on the use of Schottky or p-i-n junction for GaN betavoltaic batteries [54]. In this study, we preferred GaN-Si heterojunction to increase the depletion region and diffusion length parameters.

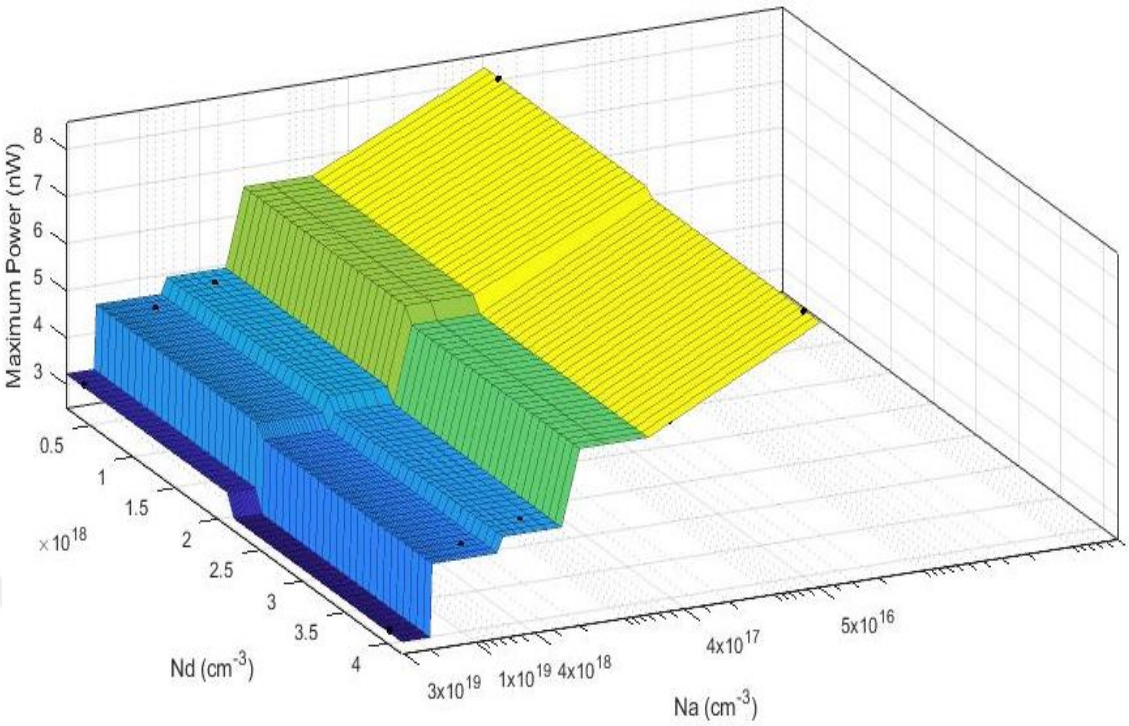

Figure 5.11 Maximum power versus doping concentrations (N_a and N_d) for Ni63/GaN p-n betavoltaic battery.

5.2.2 GaN-Si Heterojunction Betavoltaic Battery Model

When GaN semiconductors are used, it has been found that the collection efficiency values are not at the high level even in the case of lightly doping due to the low diffusion lengths. Theoretical analyses have been made for the heterojunction photovoltaic cell used to increase efficiency. The diffusion length and the diffusion coefficient parameters corresponding to N_a, N_d values are calculated separately for p-type and n-type of GaN and Si. GaN to take advantage of the wide band gap in the first layer; and silicon with high diffusion lengths in the second layer are preferred in this model, as shown in Figure 5.12.

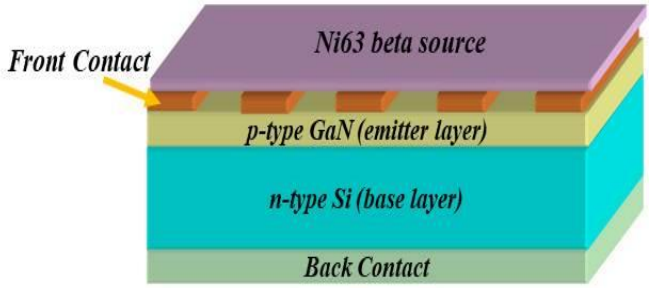

Figure 5.12 Designed 1 cm^2 area device structure of Ni63/GaN-Si p-n heterojunction betavoltaic battery.

As seen in Table 5.6, when the GaN-Si heterojunction is used in the betavoltaic battery, there is a serious increase in the collection efficiency values. Considering that the largest contribution to the collection efficiency is made by the base layer, the use of n-type Si instead of n-type GaN with low carrier mobility [139] and diffusion coefficient parameters provides a great advantage.

In the calculation results as given in Table 5.6, it has been determined that the collection efficiency and depletion region thickness are higher when the lightly-doped p-type GaN and n-type silicon are used in Ni63/GaN-Si heterojunction betavoltaic battery. At the same time, Figure 5.13 shows that the maximum power increases significantly at low n-type concentrations. Although the effect of p-type concentration is not significant, it has been found that there is a small increase in the maximum power due to the decrease in the leakage current at higher concentrations and the corresponding increase in the open-circuit voltage.

Table 5.6 Collection efficiency (Q) results for Ni63/GaN-Si p-n betavoltaic battery. Junction depths are taken as 0.5 μm.

N_a (cm^{-3})	N_d (cm^{-3})	L_p (μm)	L_n (μm)	W (μm)	Q
$5x10^{16}$	$4x10^{16}$	3.24	200.01	0.45	0.96
$4x10^{17}$	$4x10^{16}$	1.88	200.01	0.37	0.94
$4x10^{18}$	$4x10^{16}$	0.93	200.01	0.37	0.91
$1x10^{19}$	$4x10^{16}$	0.76	200.01	0.37	0.90
$3x10^{19}$	$4x10^{16}$	0.22	200.01	0.37	0.84
$5x10^{16}$	$4x10^{17}$	3.24	54.40	0.30	0.92
$4x10^{17}$	$4x10^{17}$	1.88	54.40	0.15	0.89
$4x10^{18}$	$4x10^{17}$	0.93	54.40	0.12	0.86
$1x10^{19}$	$4x10^{17}$	0.76	54.40	0.12	0.85
$3x10^{19}$	$4x10^{17}$	0.22	54.40	0.12	0.79
$5x10^{16}$	$4x10^{18}$	3.24	8.65	0.29	0.72
$4x10^{17}$	$4x10^{18}$	1.88	8.65	0.11	0.68
$4x10^{18}$	$4x10^{18}$	0.93	8.65	0.05	0.63
$1x10^{19}$	$4x10^{18}$	0.76	8.65	0.04	0.63
$3x10^{19}$	$4x10^{18}$	0.22	8.65	0.04	0.57
$5x10^{16}$	$4x10^{19}$	3.24	1.04	0.29	0.41
$4x10^{17}$	$4x10^{19}$	1.88	1.04	0.11	0.34
$4x10^{18}$	$4x10^{19}$	0.93	1.04	0.04	0.29
$1x10^{19}$	$4x10^{19}$	0.76	1.04	0.02	0.27
$3x10^{19}$	$4x10^{19}$	0.22	1.04	0.02	0.21

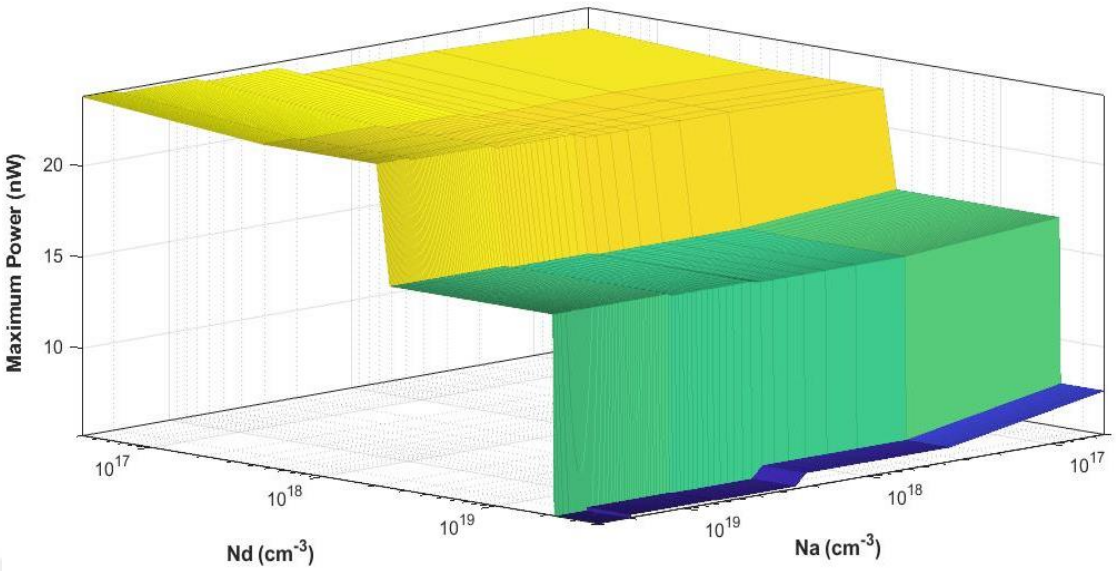

Figure 5.13 Relationships between the maximum power and p-type and n-type doping concentrations for Ni63/GaN-Si p-n betavoltaic battery.

The e-h pairs produced in the n-type Si layer with high diffusion length and the depletion region thickness are increased especially at low doping concentrations, so that the optimum junction depth is lower than that of the homojunction battery. Figure 5.14 shows the effect of thickness of p-type GaN with the change of N_d basis on the maximum power. The emitter thickness is varied from 0.1 μm to 3 μm to determine the effect of the junction depth on collection efficiency and the maximum power. The optimum junction depth of the betavoltaic battery for GaN-Si p-n heterojunction is found to be as low as 0.1 μm in the case of using low-doped silicon n-type material. However, in the case of using highly-doped silicon n-type material, it is seen that there is a slight increase in the optimum junction depth in Figure 5.14. The effect of p-type doping concentration (N_a) exchange on the junction depth is found to be lower.

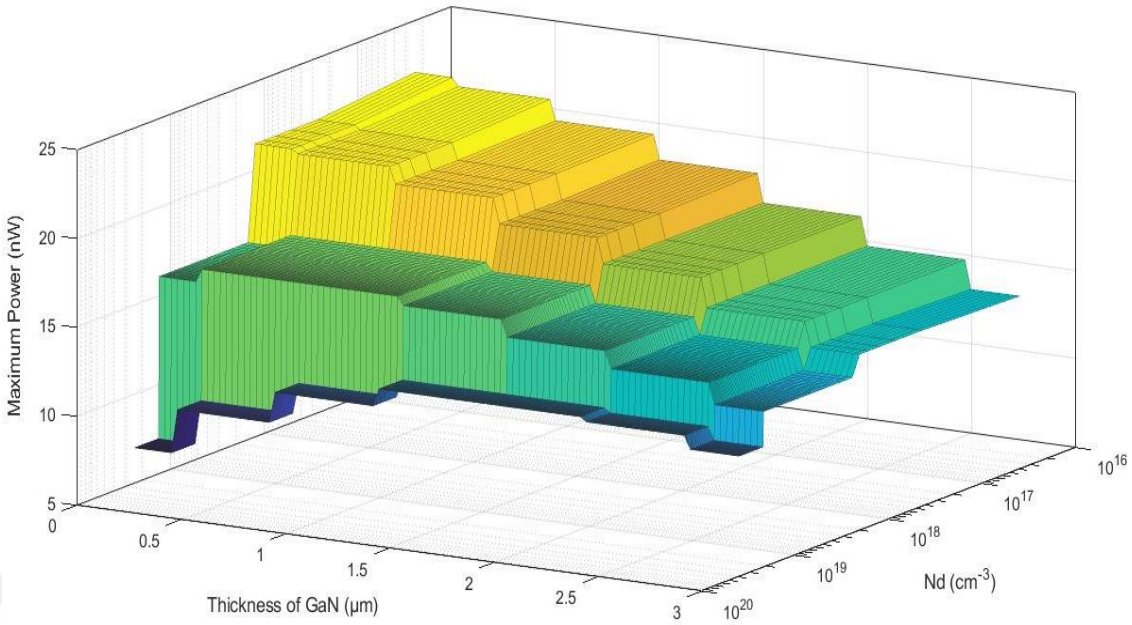

Figure 5.14 Relationships between the maximum power and p-type doping concentration and junction depth for Ni63/GaN-Si p-n betavoltaic battery when N_a is $5x10^{16}$ cm^{-3}.

When considering the effect of doping concentrations on maximum power and energy conversion efficiency, the optimum values are found as $N_a = 4x10^{17}$ cm^{-3} and $N_d = 4x10^{16}$ cm^{-3} for the optimum junction depth of 0.1 μm. In this design, while the collection efficiency is 97%, the open-circuit voltage increases due to a small drop in leakage current by increasing energy conversion efficiency. The leakage currents are theoretically calculated as $1.11x10^{-44}$ μA, $2.89x10^{-61}$ μA for GaN and GaN-Si, respectively. It is expected that these values are too small for the ideality factor (n) = 1 condition.

5.2.3 Performance Comparison of these Models

As given in Table 5.7, the electrical performance of the ideal devices of Ni63/GaN and Ni63/GaN-Si betavoltaic batteries is obtained theoretically by Eqn. (2.11) – Eqn. (2.42) and the I-V curves shown in Figure 5.15 can be drawn. According to doping concentrations of $N_a=4x10^{17}$ cm^{-3}, $N_d=4x10^{16}$ cm^{-3} and the junction depth of 0.1 μm, the maximum power of GaN-Si p-n betavoltaic battery is about 22.90 nW corresponding to a fill factor of 0.96, an open-circuit voltage of 3.47 V, a short-circuit current of 6.9 nA and the energy conversion efficiency of about 22.75%.

Whereas, the maximum power and efficiency of the GaN p-n betavoltaic battery are calculated to be 8.30 nW and 8.25%, respectively, even at optimized 2 μm junction depth and $N_a = 5x10^{16}$ cm^{-3}, $N_d = 4x10^{17}$ cm^{-3}.

Table 5.7 Electrical performance results for 1 mCi/cm^2 Ni63/GaN and Ni63/GaN-Si p-n betavoltaic batteries when doping concentration and junction depth values are optimum.

	Q	**I_{sc} (μA)**	**V_{oc} (mV)**	**FF**	**P_{max} (nW)**	**Efficiency (η) (%)**
Ni63/GaN	0.5	0.0035	2465.63	0.95	8.30	8.25
Ni63/GaN-Si	0.97	0.0069	3467.96	0.96	22.90	22.75

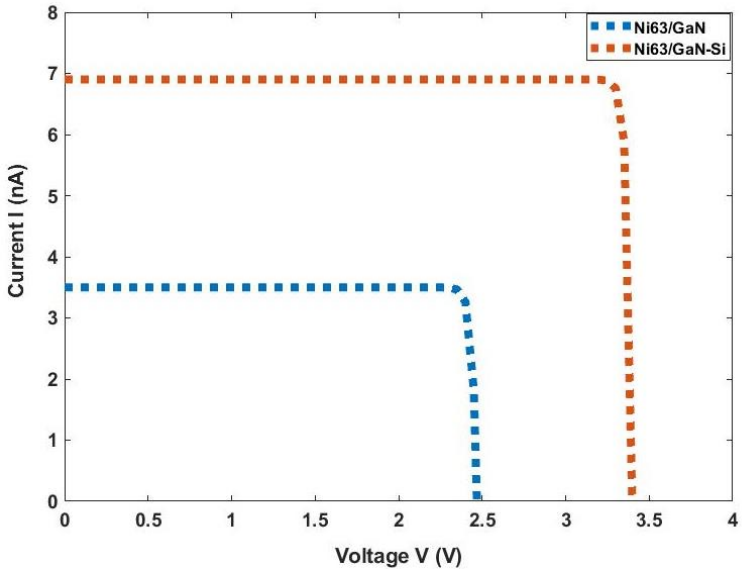

Figure 5.15 Theoretical I-V characteristics of GaN and GaN-Si battery under 1 mCi/cm^2 Ni63 beta-radiation.

As a result of simulation calculations, it is seen that current and voltage values are increased by using GaN-Si p-n heterojunction semiconductor and thus the efficiency of the betavoltaic battery is improved.

CHAPTER 6

CONCLUSIONS

In recent years, significant developments have been experienced in new generation materials, semiconductors, and nano-technology. Wide band gap semiconductors, which have the advantages of radiation resistance and high carrier mobility, have increased the interest in research for nuclear batteries. However, the desired efficiency has not been achieved yet and the expected results have not been achieved in direct and indirect conversion nuclear batteries. Nevertheless, in light of technological advances, efficiency can be improved by making changes and improvements in nuclear battery designs.

In this thesis, the progress of direct and indirect conversion nuclear batteries is investigated experimentally and theoretically. The theoretical basis of the operation principles of nuclear battery systems and the parameters affecting the efficiency are analyzed and the contribution of these parameters to the efficiency is determined by experimental and theoretical models. The results showed that the efficiency of nuclear batteries can be increased by optimization of the parameters.

In the experimental study, different types of conversion nuclear batteries are designed and tested at normal temperature and pressure values. In prototypes, Pm147 and Sr90 beta sources and Si photovoltaic cells, which are frequently used in the literature for nuclear battery applications, are preferred. ZnS:CuCl and $SrAl_2O_4:Eu^{2+},Dy^{3+}$ are selected as the most suitable phosphors for indirect conversion. The most efficient battery model is determined as Pm147/ $SrAl_2O_4:Eu^{2+},Dy^{3+}$/PV cell. The performance of the battery is lower than the expected values if the Sr90 is used as a beta source. This may be due to the beta source which in the glass tube. Further studies, the voltage, and the current values are

expected to increase when the liquid Sr90 source is formed into a thin film. In the indirect conversion nuclear battery models, polycarbonate and acrylic materials used in this study has a high light transmittance. As a result, phosphor layer has improved battery performance. However, the phosphor layer for different beta sources gave different results. The results indicate that selection for the combination of the source and phosphors is very important. In addition, radiation damage hasn't been observed in the phosphor layers and the PV cell during the test period since activity values of used beta sources are very low. Also, the energy conversion efficiency of the battery models is very low because of varied factors. The low efficiency may have caused by very low activity. Consequently, heightening the activity of the source, selecting high efficiency and suitable phosphor and PV cell can advance the performance of the battery.

One of the most important principles for determining the efficiency of nuclear batteries is that the radiation source matches the scale of the transducer used for energy conversion. Therefore, the optimization of the transducer is very important. Battery performance can be improved by using different semiconductor types. In order to achieve achievable power conversion efficiencies, it is important to turn to wide band gap semiconductor materials that provide low leakage currents. However, the use of wide band gap semiconductors has some advantages and disadvantages. For wide band gap semiconductors, it is difficult to obtain long diffusion lengths and a large depletion region in which electron-hole pairs are collected. Despite, wide band gap semiconductors produce higher open-circuit voltage, power, and efficiency. Moreover, they have high radiation resistance.

In this study, silicon as a narrow band gap semiconductor and GaP or GaN as a wide band gap semiconductor are used for the theoretical design of betavoltaic batteries. For battery design, it is important to analyze the energy accumulation and the depth of penetration of the radioactive particles, in the semiconductors. In wide band gap semiconductors such as GaN and GaP, the energy required to form an electron-hole is considerably greater than the silicon semiconductor. Thus, the number of electron-hole pairs determining the current is much greater in silicon. Because of this effect, the short-circuit current in the silicon is calculated higher. However, since the leakage current in the silicon is much higher than in wide band gap semiconductors,

the open-circuit voltage is quite low for silicon. On the other hand, even though the short-circuit current is low for wide band gap semiconductors, they can perform better due to the high open-circuit voltage.

Given the benefits of wide and narrow band gap semiconductors for betavoltaic batteries, the use of GaN-Si and GaP-Si heterojunction photovoltaic cells is predicted to be suitable for increased efficiency. For this reason, the advantages of both narrow and wide band gap semiconductors have been utilized with the heterojunction model developed in the study. In the literature, the use of heterojunction semiconductor in betavoltaic batteries is insufficient. In order to fill this deficiency, a theoretical model is developed for heterojunction betavoltaic batteries and analyzes are made. In the theoretical analysis, the collection efficiency and maximum power calculations are performed in battery models formed with both homojunction and heterojunction semiconductors. Semiconductor parameters are analyzed and optimized to improve the collection efficiency in the semiconductor transducer. By optimizing the semiconductor design parameters, the battery efficiency is further increased.

The collection efficiencies of the base, emitter, and depletion layers are also determined separately using numerical solutions for homojunction and heterojunction betavoltaic batteries. The thicknesses and the doping concentrations of emitter, depletion region and base regions of the cell directly affect these parameters. The electrical performance analysis results show that the junction depth of the betavoltaic battery should be determined according to the diffusion length of the semiconductor. In addition, low doping concentration and high diffusion length are the most important factors that increase the performance of the battery. In this thesis, the electrical performance outputs of Pm147/Si, Pm147/GaP, Ni63/Si, Ni63/GaP, Ni63/GaN homojunction, and Pm147/GaP-Si, Ni63/GaP-Si, Ni63/GaN-Si heterojunction betavoltaic batteries have been compared and it has been found that the collection efficiency, open-circuit voltage and hence the maximum power increase significantly when heterojunction cell is used.

By optimizing the doping concentration and junction depth, high-efficiency heterojunction betavoltaic micro-battery can be achieved. The maximum powers are calculated as 19.03 nW/cm^2 and 55.20 nW/cm^2, in case of using 1 mCi Ni63 and

Pm147 beta source, respectively and using GaP-Si heterojunction with the junction depth of 0.1 μm and doping concentrations of N_a= $4x10^{17}$ cm^{-3} and N_d= $4x10^{16}$ cm^{-3} in the emitter and the base region, respectively. Also, the maximum power is calculated as 22.90 nW/cm^2 in case of using 1 mCi Ni63 beta source and GaN-Si heterojunction with junction depth of 0.1 μm and doping concentrations of N_a= $4x10^{17}$ cm^{-3} and N_d= $4x10^{16}$ cm^{-3} in the emitter and the base region, respectively.

In the coming years, multi-layered heterojunction structures and heterojunction cells can be used for betavoltaic battery studies. Theoretical performance analysis can also be performed for different heterojunction betavoltaic cells using the method developed in this thesis.

This work is supported by Gaziantep University Scientific Research Projects Governing Unit (BAPYB), through project MF.14.15.

REFERENCES

[1] Manasse, F., Pinajian, J., Tse, A. (1976). Schottky barrier betavoltaic battery. *IEEE Transactions on Nuclear Science*. **23(1)**, 860-870.

[2] Wacharasindhu, T. (2012). Composite-semiconductor-based micro power source (PhD Thesis), University of Missouri-Columbia.

[3] Duggirala, R., Lal, A., Radhakrishnan, S. (2010). Radioisotope thin-film powered microsystems. Vol: 6. New York: Springer.

[4] Shultis, J. K., Faw, R. E. (2007). Fundamentals of nuclear science and engineering. 2nd(Second) edition. CRC Press.

[5] Mahato, A., et al. (2018). Nuclear battery. *International Journal of Latest Engineering and Management Research (IJLEMR)*. **3(4)**, 71-76.

[6] Liu, Y., et al. (2014). Optimization and temperature effects on sandwich betavoltaic microbattery. *Science China Technological Sciences*. **57(1)**, 14-18.

[7] Zuo, G., Zhou, J., Ke, G. (2013). A Simple theoretical model for 63Ni betavoltaic battery. *Applied Radiation and Isotopes*. **82**, 119-125.

[8] Ronen, Y., Hatav, A., Hazenshprung, N. (2004). 242mAm fueled nuclear battery. *Nuclear Instruments and Methods in Physics Research Section A: Accelerators, Spectrometers, Detectors and Associated Equipment*. **531(3)**, 639-644.

[9] Wang, G., et al. (2010). The effect of temperature changes on electrical performance of the betavoltaic cell. *Applied Radiation and Isotopes*. **68(12)**, 2214-2217.

[10] Moseley, H.G.J., Rutherford, E. (1913). The attainment of high potentials by the use of radium. *Proceedings of the Royal Society of London. Series A, Containing Papers of a Mathematical and Physical Character*. **88**, 471-476.

[11] Revankar, S.T., Adams, T.E. (2014). Advances in betavoltaic power sources. *J. Energy Power Sources*. **1(6)**, 321-329.

[12] Shinn, E., et al. (2013). Nuclear energy conversion with stacks of graphene nanocapacitors. *Complexity*. **18(3)**, 24-27.

[13] Ronen, Y. (2010). Some remarks on the fissile isotopes. *Annals of Nuclear Energy*. **37(12)**, 1783-1784.

[14] Lao, R. (2011). A modular design for nuclear battery technology (Thesis), California Polytechnic State University.

[15] Prelas, M.A., et al. (2014). A review of nuclear batteries. *Progress in Nuclear Energy*. **75**, 117-148.

[16] Kavetskiy, A., et al. (2009). Promethium-147 capacitor. *Applied Radiation and Isotopes*. **67(6)**, 1057-1062.

[17] Mohamadian, M., Feghhi, S., Afarideh, H. (2007). Conceptual design of GaN betavoltaic battery using in cardiac pacemaker. *Proc. 13th Int. Conf. Emerg. Nucl. Energy Syst.(ICENES)*. 1-7.

[18] Bower, K.E., et al. (2002). Polymers, phosphors, and voltaics for radioisotope microbatteries. Boca Raton: CRC press.

[19] Min, G., Rowe, D. (1995). Peltier devices as generators, CRC Handbook of thermoelectrics Chap. 38. London: CRC Press.

[20] Yakubova, G.N. (2010). Nuclear batteries with tritium and promethium-147 radioactive sources (PhD Thesis), University of Illinois at Urbana-Champaign.

[21] Honsberg, C., et al. (2005). GaN betavoltaic energy converters. *Proc. 31st IEEE Photovoltaic Specialists Conference*. **31(1)**, 102-105.

[22] Ronen, Y., Shwageraus, E. (2000). Ultra-thin 242mAm fuel elements in nuclear reactors. *Nuclear Instruments and Methods in Physics Research Section A: Accelerators, Spectrometers, Detectors and Associated Equipment*. 455(2), 442-451.

[23] Corliss, W.R., Harvey, D.G. (1964). Radioisotopic power generation. Prentice-Hall.

[24] Mane, N.S., Hargude, N.V., Patil, V.P. (2016). Atomic batteries: A compact and long life power source. *International Journal of Innovative Research in Science and Engineering*, **2(3)**, 144-147.

[25] Khan, M.R.A. (2015). Design and characterization of pin devices for betavoltaic microbatteries on gallium nitride (Master Thesis), University of Maryland.

[26] Liu, B. (2008). Nuclear micro-engineering using tritium (PhD Thesis), University of Pittsburgh.

[27] Chandrashekhar, M. (2007). Demonstration of a 4H SiC betavoltaic cell (PhD Thesis), Cornell University.

[28] Cabauy, P., et al. (2010). Micropower betavoltaic hybrid sources. *44th Power Sources Conference*. 14-17.

[29] Rappaport, P. (1954). The Electron-Voltaic Effect in p-n Junctions Induced by Beta-Particle Bombardment. *Physical Review*. **93(1)**, 246-247.

[30] Olsen, L.C. (1973). Betavoltaic energy conversion. *Energy Conversion*. **13(4)**, 117-127.

[31] Liu, P., Chang, Y., Zhang, J. (2014). Single-walled carbon nanotube film-silicon heterojunction radioisotope betavoltaic microbatteries. *Journal of Micromechanics and Microengineering*. **24(5)**, 055026.

[32] Cress, C.D. (2008). Effects of ionizing radiation on nanomaterials and III-V semiconductor devices (PhD Thesis), Rochester Institute of Technology.

[33] Xu, Z.-H., et al. (2014). Development of a beta radioluminescence nuclear battery. *Nuclear Science and Techniques*. **25**, 040603.

[34] Hong, L., et al. (2014). Parameter optimization and experiment verification for a beta radioluminescence nuclear battery. *Journal of Radioanalytical and Nuclear Chemistry*. **302(1)**, 701-707.

[35] Kumar, S. (2015). Atomic batteries: Energy from radioactivity. *Research Article, J Nucl Ene Sci Power Generat Technol.* **5(1)**.

[36] Walton, R., et al. (2013). Radioisotopic battery and capacitor system for powering Wireless Sensor Networks. *Sensors and Actuators A: Physical*. **203**, 405-412.

[37] Furlong, R.R., Wahlquist, E.J. (1999). US space missions using radioisotope power systems. *Nuclear news*. **42**, 26-35.

[38] Schmidt, G., Dudzinski, L., Sutliff, T. (2011). Radioisotope power: A key technology for deep space exploration. *6th International Energy Conversion Engineering Conference (IECEC)*. 5640.

[39] Ang, Y.A. (2017). Prediction and analytics of operating parameters on thermoelectric generator energy generation (PhD Thesis), University of Newcastle.

[40] Yao, S., et al. (2012). Design and simulation of betavoltaic battery using large-grain polysilicon. *Applied Radiation and isotopes*. **70(10)**, 2388-2394.

[41] Litz, M. (2014). Isotope beta-battery approaches for long-lived sensors: Technology review (Report). Army Research Lab Adelphi MD Sensors and Electron Devices Directorate.

[42] Klein, C.A. (1968). Bandgap dependence and related features of radiation ionization energies in semiconductors. *Journal of Applied Physics*. **39(4)**, 2029-2038.

[43] CityLabs. from https://citylabs.net/products/. 2019.

[44] Widetronix. from http://www.widetronix.com/. 2019.

[45] Sychov, M., et al. (2008). Alpha indirect conversion radioisotope power source. *Applied Radiation and Isotopes*. **66(2)**, 173-177.

[46] Prelas, M., et al. (1993). Diamond photovoltaic energy conversion. *Second international conference on the application of diamond films and related materials. MY Tokyo*. 5-12.

[47] Prelas, M., et al. (1995). Wide band-gap photovoltaics. Wide Band Gap Electronic Materials. 463-474. Springer.

[48] Walko, R., et al. (1990). Electronic and photonic power applications (Report). Sandia National Labs., Albuquerque, NM (USA).

[49] Sims, P.E., DiNetta, L.C., Barnett, A.M. (1994). High efficiency GaP power conversion for betavoltaic applications. *Proceedings of the 13th Space Photovoltaic Research and Technology Conference (SPRAT 13) in NASA, Lewis Research Center*, 373-382.

[50] Hong, L., et al. (2014). Radioluminescent nuclear batteries with different phosphor layers. *Nuclear Instruments and Methods in Physics Research Section B: Beam Interactions with Materials and Atoms*. **338**, 112-118.

[51] Rivenburg, H.C., et al. (1995). Power source using a photovoltaic array and self-luminous microspheres. U.S. Patent No: US5443657A. United States: Google Patents.

[52] Dixon, J., et al. (2016). Evaluation of a Silicon 90 Sr Betavoltaic Power Source. *Scientific reports*. **6**, 38182.

[53] Martin, J.E. (2000). Physics for radiation protection. Wiley Online Library.

[54] Alam, T.R., Pierson, M.A. (2016). Principles of betavoltaic battery design. *J. Energy Power Sources*. **3(1)**, 11-41.

[55] Venverloo, L.A.J. (1971). Practical measuring techniques for beta radiation. Macmillan International Higher Education.

[56] Strautman, L., Gumarova, S., Sarsekenova, V. (2017). Introduction to the world of nuclear physics. Litres.

[57] Lowenthal, G., Airey, P. (2001). Practical applications of radioactivity and nuclear radiations. Cambridge University press.

[58] (2019). Fundamental Radiation Concepts (Chapter 2). Radiation Safety Short Course (RSSC) Study Guide. University of Florida.

[59] Wray, J. (2004). Silicon strip detector efficiency using a purpose built particle telescope. *Univ. of California, Santa Cruz*.

[60] Ntlamele, S. (2010). Dosimetry of the Teflon encased strontium eye applicator (Master Thesis), University of Limpopo (Medunsa Campus).

[61] Carron, N.J. (2006). An Introduction to the Passage of Energetic Particles through Matter. CRC Press.

[62] Prelas, M., et al. (2016). Nuclear batteries and radioisotopes. Springer.

[63] Siegbahn, K. (1968). Alpha-beta-and gamma-ray spectroscopy. Vol:1. North-Holland Publishing Company.

[64] Loveland, W.D., Morrissey, D.J., Seaborg, G.T. (2017). Modern nuclear chemistry. Second Edition. Wiley Online Library.

[65] Turner, J.E. (2005). Interaction of ionizing radiation with matter. *Health Physics*. **88(6)**, 520-544.

[66] Gümüş, H. (2019). Stopping power and range calculations of electrons for some human body tissues. *ALKÜ Fen Bilimleri Dergisi*. 93-100.

[67] ICRU. (1970). Report No: 16 International Commission on Radiation Units and Measurements

[68] Katz, L., Penfold, A.S. (1952). Range-energy relations for electrons and the determination of beta-ray end-point energies by absorption. *Reviews of Modern Physics*. **24(1)**, 28.

[69] Harrison, S. (2013). Betavoltaic devices. Stanford University. http://large.stanford.edu/courses/2013/ph241/harrison2/

[70] Shur, M. (1990). Physics of semiconductor devices. Upper Saddle River: Prentice Hall.

[71] Duggirala, R., Tin, S., Lal, A. (2007). 3D silicon betavoltaics microfabricated using a self-aligned process for 5 milliwatt/cc average, 5 year lifetime microbatteries. *TRANSDUCERS 2007-2007 International Solid-State Sensors, Actuators and Microsystems Conference*. 279-282.

[72] Keeffe, R. (1973). Direct Energy Conversion Using the Beta-Voltaic Effect in Epitaxial Silicon PN Junction Devices. (Master Thesis), University of McMaster University.

[73] Nejad, G.R.G., Rahmani, F., Abaeiani, G.R. (2014). Design and optimization of beta-cell temperature sensor based on 63Ni–Si. *Applied Radiation and Isotopes*. **86**, 46-51.

[74] Olsen, L.C. (1993). Review of betavoltaic energy conversion. *NASA TechDoc 19940006935*.

[75] Mueller, T. (2009). Heterojunction solar cells (a-Si/c-Si): investigations on PECV deposited hydrogenated silicon alloys for use as high-quality surface passivation and emitter/BSF. Logos Verlag Berlin GmbH.

[76] Da-Yong, Q., et al. (2008). Demonstration of a 4H SiC betavoltaic nuclear battery based on Schottky barrier diode. *Chinese Physics Letters*. **25(10)**, 3798.

[77] Sachenko, A., et al. (2015). Efficiency analysis of betavoltaic elements. *Solid-State Electronics*. **111**, 147-152.

[78] Olsen, L. (1972). Beta irradiation of silicon junction devices: Effects on diffusion length. *IEEE Transactions on Nuclear Science*. **19(6)**, 375-381.

[79] Pfann, W., Roosbroeck, W. V. (1954). Radioactive and photoelectric p-n junction power sources. *Journal of Applied Physics*. **25(11)**, 1422-1434.

[80] Liu, Y.P., et al. (2014). Energy deposition, parameter optimization, and performance analysis of space radiation voltaic batteries. *Nucl. Sci. Techn.* **25(s1)**, 23-26.

[81] Hovel, H.J. (1975). Semiconductors and semimetals. Vol. 11. Solar cells.

[82] Li, S.S. (2012). Semiconductor physical electronics. Springer Science & Business Media.

[83] Schroder, D.K. (2006). Semiconductor material and device characterization. John Wiley & Sons.

[84] Bao, R., Brand, P.J., Chrisey, D.B. (2012). Betavoltaic performance of radiation-hardened high-efficiency Si space solar cells. *IEEE Transactions on Electron Devices*. **59(5)**, 1286-1294.

[85] San, H., et al. (2013). Design and simulation of GaN based Schottky betavoltaic nuclear micro-battery. *Applied Radiation and Isotopes*. **80**, 17-22.

[86] Green, M.A. (1981). Solar cell fill factors-general graph and empirical expressions. *Solid State Electronics*. **24**, 788.

[87] Chen, C., Chang, Y., Zhang, J. (2012). A novel betavoltaic microbattery based on SWNTs thin film-silicon heterojunction. *2012 IEEE 25th International Conference on Micro Electro Mechanical Systems (MEMS)*. 1197-1200.

[88] Ferrara, M. (2009). Electroluminescence of a-Si/c-Si Heterojunction Solar Cells after High Energy Irradiation (PhD Thesis), University of Hagen.

[89] Colinge, J.-P., Colinge, C.A. (2005). Physics of semiconductor devices. Springer Science & Business Media.

[90] Milnes, A.G., Feucht, D.L. (1972). Heterojunctions and metal semiconductor junctions. Academic Press.

[91] Wacharasindhu, T., et al. (2009). Encapsulated radioisotope for efficiency improvement of nuclear microbattery. *Power MEMS 2009*. 193–196.

[92] Uhm, Y.R., et al. (2016). Study of a betavoltaic battery using electroplated nickel-63 on nickel foil as a power source. *Nuclear Engineering and Technology*. **48(3)**, 773-777.

[93] Theirrattanakul, S., Prelas, M. (2017). A methodology for efficiency optimization of betavoltaic cell design using an isotropic planar source having an energy dependent beta particle distribution. *Applied Radiation and Isotopes*. **127**, 41-46.

[94] Choi, B.G., et al. (2015). Ni-63 radioisotope betavoltaic cells based on vertical electrodes and pn junctions. *2015 IEEE 15th International Conference on Nanotechnology (IEEE-NANO)*. 889-892.

[95] Wu, K., Dai, C., Guo, H. (2011). A theoretical study on silicon betavoltaics using Ni-63. *2011 6th IEEE International Conference on Nano/Micro Engineered and Molecular Systems*. 724-727.

[96] Sachenko, A., et al. (2015). Analysis of the attainable efficiency of a direct-bandgap betavoltaic element. *Journal of Physics D: Applied Physics*. **48(45)**, 455101.

[97] Patrick, E.E., et al. (2015). Simulation of Radiation Effects in AlGaN/GaN HEMTs. *ECS Journal of Solid State Science and Technology*. **4(3)**, Q21-Q25.

[98] Flicker, H., Loferski, J., Elleman, T. (1964). Construction of a promethium-147 atomic battery. *IEEE Transactions on Electron Devices*. **11(1)**, 2-8.

[99] Xu, Z.-H., et al. (2015). Structural effects of ZnS: Cu phosphor layers on beta radioluminescence nuclear battery. *Journal of Radioanalytical and Nuclear Chemistry*. **303(3)**, 2313-2320.

[100] Nsimama, P.D. (2010). Characterization of $SrAl_2O_4$:Eu^{2+},Dy^{3+} nano thin films prepared by pulsed laser deposition (PhD Thesis), University of the Free State.

[101] Ravi, S., et al. (2001). Salient features in the preparation of promethium-147 activated zinc sulphide phosphor light sources. *Journal of radioanalytical and nuclear chemistry*. **250(3)**, 565-568.

[102] Weeden-Wright, S.L. (2012). Radiation induced effects on phosphor powder photoluminescence (PhD Thesis), Vanderbilt University.

[103] Watts, H., Oestreich, M., Robinson, R. (1963). A nuclear-photon energy conversion study. Iit Research Inst Chicago Il.

[104] Hillie, K.T. (2001). Degradation of ZnS: Cu, Au, Al phosphor powder and thin films under prolonged electron bombardment (PhD Thesis), University of the Free State.

[105] Gollub, S.L. (2015). Systematic Investigation of defect-mediated photoluminescence through radiation-induced displacement damage (PhD Thesis). Vanderbilt University.

[106] Clabau, F., et al. (2007). On the phosphorescence mechanism in $SrAl_2O_4$: Eu^{2+} and its codoped derivatives. *Solid State Sciences*. **9(7)**, 608-612.

[107] Stan, C.S., et al. (2010). Phosphorescent composites based on polyethyleneterephtalate. *Materiale Plastice*. **47(3)**, 324.

[108] Kowatari, M., et al. (2002). The temperature dependence of luminescence from a long-lasting phosphor exposed to ionizing radiation. *Nuclear Instruments and Methods in Physics Research Section A: Accelerators, Spectrometers, Detectors and Associated Equipment*. **480(2)**, 431-439.

[109] Golob, B. 2019. Scintillation detectors. Lecture 4. from http://www-f9.ijs.si/~golob/sola/seminar/scintilatorji/Lecture4.pdf.

[110] Yen, W.M., Shionoya, S., Yamamoto, H. (2007). Phosphor handbook. Second Edition. CRC press.

[111] Ronda, C.R. (2007). Luminescence: from theory to applications. John Wiley & Sons.

[112] Leipzig, U. 2019. The Ionoluminescence Method. from https://bloch.physgeo.uni-leipzig.de/en/aqs/research/methods/ion-beam-analysis/il/.

[113] Lecoq, P., Gektin, A., Korzhik, M. (2016). Inorganic scintillators for detector systems: physical principles and crystal engineering. Springer.

[114] Sebastian, J.S. (1998). Degradation of ZnS phosphors during electron beam bombardment (PhD Thesis), University of Florida.

[115] Cress, C.D., et al. (2008). Alpha-particle-induced luminescence of rare-earth-doped Y2O3 nanophosphors. *Journal of Solid State Chemistry*. **181(8)**, 2041-2045.

[116] Bem, B.D. (2010). Thermal, structural and luminescent properties of long after-glow MAlxOy: Eu^{2+}, Dy^{3+}(M: Sr, Ba) phosphors (PhD Thesis), University of the Free State.

[117] Han, S.-D., et al. (2008). Preparation and characterization of long persistence strontium aluminate phosphor. *Journal of luminescence*. **128(3)**, 301-305.

[118] Graphene-Supermarket. from https://graphene-supermarket.com/Conductive-Graphene-Sheets.html. 2017.

[119] Wang, Y. (1969). Handbook of radioactive nuclides. The Chemical Rubber Company.

[120] Li, F., et al. (2014). GaN PIN betavoltaic nuclear batteries. *Science China Technological Sciences*. **57(1)**, 25-28.

[121] Son, K.a., et al. (2010). GaN-based high temperature and radiation-hard electronics for harsh environments. *Nanoscience and Nanotechnology Letters*. **2(2)**, 89-95.

[122] Wagner, D., Novog, D., LaPierre, R. (2019). Simulation and optimization of current generation in gallium phosphide nanowire betavoltaic devices. *Journal of Applied Physics*. **125(16)**, 165704.

[123] Zhang, L., et al. (2018). Model and optimal design of 147Pm SiC-based betavoltaic cell. *Superlattices and Microstructures*. **123**, 60-70.

[124] Krasnov, A., et al. (2015). Optimization of energy conversion efficiency betavoltaic element based on silicon. *Journal of Nano- and Electronic Physics*. **7(4)**, 04004.

[125] Kittidachachan, P., et al. (2007). A detailed study of p–n junction solar cells by means of collection efficiency. *Solar energy materials and solar cells*. **91(2-3)**, 160-166.

[126] Lu, M., et al. (2011). Gallium Nitride Schottky betavoltaic nuclear batteries. *Energy Conversion and Management*. **52(4)**, 1955-1958.

[127] Allen, C.R., Jeon, J.-H., Woodall, J.M. (2010). Simulation assisted design of a gallium phosphide n–p photovoltaic junction. *Solar Energy Materials and Solar Cells*. **94(5)**, 865-868.

[128] Diaz, M. (2011). Design, fabrication, characterization, and analysis of wide band gap gallium phosphide solar cells and gallium phosphide on silicon (Master Thesis), University of Delaware.

[129] Feifel, M., et al. (2017). MOVPE grown gallium phosphide–silicon heterojunction solar cells. *IEEE Journal of Photovoltaics*. **7(2)**, 502-507.

[130] Zhang, C. (2017). Gallium Phosphide Integrated with Silicon Heterojunction Solar Cells (PhD Thesis), Arizona State University.

[131] Zai-Jun, C., et al. (2011). Demonstration of a high open-circuit voltage GaN betavoltaic microbattery. *Chinese Physics Letters*. **28(7)**, 078401.

[132] Wang, G.Q., et al. (2014). Demonstration of Pm-147 GaN betavoltaic cells. *Nuclear Science and Techniques*. **25(2),** 020403.

[133] Lu, X., et al. (2013). Improving GaP solar cell performance by passivating the surface using AlxGa1-xP epi-layer. *IEEE Journal of the Electron Devices Society*. **1(5)**, 111-116.

[134] Tang, X., et al. (2012). Optimization design and analysis of Si-63 Ni betavoltaic battery. *Science China Technological Sciences*. **55(4)**, 990-996.

[135] Millán, J. (2007). Wide band-gap power semiconductor devices. *IET Circuits, Devices & Systems*. **1(5)**, 372-379.

[136] Mnatsakanov, T.T., et al. (2003). Carrier mobility model for GaN. *Solid-State Electronics*. **47(1)**, 111-115.

[137] Kumakura, K., et al. (2005). Minority carrier diffusion length in GaN: Dislocation density and doping concentration dependence. *Applied Physics Letters*. **86(5)**, 052105.

[138] Cheng, Z., et al. (2012). A high open-circuit voltage gallium nitride betavoltaic microbattery. *Journal of Micromechanics and Microengineering*. **22(7)**, 074011.

[139] Wang, J., et al. (2015). Review of using gallium nitride for ionizing radiation detection. *Applied Physics Reviews*. **2(3)**, 031102.

CURRICULUM VITAE

PERSONAL INFORMATION

Surname, Name	**:** Kavak Yürük, Reyyan
Nationality	**:** Turkish (T.C.)
Date and Place of Birth	**:** 30 June 1981, Siirt/Kurtalan
Marital Status	**:** Married
Phone	**:** +90 5069466346
E-mail	**:** reyyankavak@gmail.com

EDUCATION

Degree	Institution	Year of Graduation
MSc	Bahçeşehir University, Graduate School of Natural & Applied Sciences, Urban Systems and Transportation Management	2010
MSc	Gazi University, Faculty of Education, Physics Teaching Education	2006
BSc	Ankara University, Faculty of Science, Physics	2004

WORK EXPERIENCE

Year	Place	Enrollment
2018-	Mardin Artuklu University Central Research Laboratory	Instructor
2009-2018	Mardin Artuklu University	Academic Expert
2007-2009	Istanbul Metropolitan Municipality Directorate of City Lighting and Energy	Physicist and Energy Management Specialist
2005-2006	Goldsoft Software Company /Ankara	Software Developer
2004-2005	Mikrobim Software Company /Ankara	Programmer

FOREIGN LANGUAGES

English - Upper Intermediate

PUBLICATIONS (SCI &SCI-EXPANDED & SSCI & Arts and Humanities)

Kavak Yürük, R. and Tütüncüler, H. (2019). Theoretical Investigation of High-Efficiency GaN-Si Heterojunction Betavoltaic Battery. *Canadian Journal of Physics,* **97(9)**, 1031-1038. doi:10.1139/cjp-2018-0579.

Yürük, R. K., & Tütüncüler, H. (2017). Investigation of the Effect of Beta Source and Phosphors on Photovoltaic Cells. *AIP Conference Proceedings.* **1815(1)**, 040002. AIP Publishing. doi:10.1063/1.4976371.

CONFERENCES AND CONGRESS

Kavak Yürük, R. and Tütüncüler, H. (2016). Investigation of the Effect of Beta Source and Phosphors on Photovoltaic Cells. *The Turkish Physical Society 32nd International Physics Congress* (TPS32), Oral Paper Presentation (Publication No: 4586710).

Koç, R., Tütüncüler, H., Kavak Yürük, R., Özkeçeci, S. (2014). Radyoaktif Bozunma Enerjisinin Elektrik Enerjisine Dönüştürülmesi (Poster Sunumu), *Enerji Teknolojileri Ar-Ge Proje Pazarı*, Gaziantep.

Garip, M., Kavak, R. (2009). İstanbul Büyükşehir Belediyesi Enerji Etüt Çalışması. *3. Enerji Verimliliği ve Kalitesi Sempozyumu*, Kocaeli.